



SAPIENZA
UNIVERSITÀ DI ROMA

Department of Computer, Control and Management Engineering
University of Rome La Sapienza

Ph.D. Program in
Automatic control, Bioengineering and Operations Research

Curriculum: **BIOENGINEERING**

XXXII Cycle

The structural and functional multilayer modular organization of the human brain

Maria Grazia Puxeddu

Advisor

Laura Astolfi, Ph.D.

Ph.D. program coordinator

Giuseppe Oriolo, Ph.D.

Co-advisor

Manuela Petti, Ph.D.

External reviewers

Christian-G. Bénar, Ph.D.

Richard F. Betzel, Ph.D.

Academic Year 2019/2020

Tables of contents

Introduction	1
Hints of brain connectivity and graph theoretical analysis	5
i. Structural and functional brain connectivity	5
ii. Network science applied to brain imaging	8
iii. The modular structure of brain networks	9
SECTION I - Comparison among multilayer community detection algorithms and application to EEG-based functional connectivity	13
1.1. Introduction	13
1.2. Methods	18
1.2.1. Benchmark networks generation	18
1.2.2. Simulation studies for algorithms comparison	21
1.2.3. Multilayer community detection on EEG brain networks	26
1.3. Results	27
1.3.1. Simulation studies for algorithms comparison	27
1.3.2. Multilayer community detection on EEG brain networks	35
1.4. Discussion	37
1.5. Conclusion	41
1.6. Supplementary material	42
1.6.1. Comparative analysis on networks with evolving community structure and increasing or decreasing clusters number	42
1.6.2. Comparative analysis on networks with lower graph density	47
1.6.3. Preliminary investigation on the temporal resolution parameter in the multilayer modularity optimization algorithm, genlouvain	52
1.6.4. Preliminary investigation on the trade-off parameter in the multi-objective function optimization algorithm, FacetNet	57
SECTION II - The modular organization of the human brain networks across the lifespan	62
2.1. Introduction	62
2.2. Methods	64
2.2.1. Experimental dataset and data processing	64
2.2.2. Multilayer network construction	65
2.2.3. Multilayer and multiscale community detection	67

2.2.4. Analysis of the communities.....	68
2.3. Results	71
2.3.1. Statistics of the multilayer multiscale modularity maximization.....	71
2.3.2. Age-related changes of the modular structure.....	74
2.4. Discussion.....	81
2.5. Conclusion.....	87

SECTION III - The modular organization of the human brain networks across functional and structural connectivity and across subjects 88

3.1. Introduction.....	88
3.2. Methods	90
3.2.1. Experimental dataset and data processing	90
3.2.2. Multi-modal multi-subject community detection.....	92
3.2.3. Analysis of the communities.....	94
3.2.4. Correlation with behavioral assessments.....	97
3.3. Results	99
3.3.1. Preliminary analysis of the communities.....	100
3.3.2. Modes of variability between and within modality	103
3.3.3. Variability between and within modalities at specific scales.....	106
3.3.4. Correlation with behavioral assessments.....	111
3.4. Discussion.....	115
3.4.1. Relationship between structural and functional modular structure across subjects	115
3.4.2. Methodological innovations of the multilayer framework	117
3.4.3. Limitation and future advancements	118
3.5. Conclusion.....	119

Conclusion..... 120

Bibliography..... 123

List of publications

Scientific Curriculum

Introduction

The human brain is an embedded complex system whose functions cannot be reduced to the processes of its fundamental units. Rather, brain functioning emerges as a consequence of complex patterns of interactions involving all its parts at different levels, from neuron cells to larger brain areas.

The past years have been characterized by exponential growth in the field of neuroimaging techniques. Hence the availability of large datasets that characterize brain interactions patterns (Jirsa and McIntosh, 2007), crossing different domains and time-scales, or associated with task-evoked brain activity. The need for robust methods to interpret and manage the increasing complexity and size of these data nicely met the rise of network science (Börner et al., 2007; Newman, 2010). Indeed, the intersection of these disciplines led to the modeling of the brain as a network, in which a number of nodes (subcortical, cortical or scalp regions) interact each other through a set of edges (structural or functional connections) (Bullmore and Sporns, 2009; Sporns, 2014). Thus, the parallel recording of the interactions of many neuronal groups results in datasets forming, under a mathematical/physics point of view, a complex network. Once the brain network has been estimated, its emerging or topological properties can be measured through a rich collection of metrics developed in the field of network science and rooted in the mathematical branch of graph theory (Bullmore and Bassett, 2011). In this context was born the *network neuroscience* (Bassett and Sporns, 2017), an ascending discipline aimed to map, synthesize, analyze, interpret and model neurobiological data. Nowadays, network neuroscience forms the backbone of our way to comprehend the brain structure and function as a complex system.

Several measures of the graph theory have been extensively applied to the structural and functional brain networks, in order to investigate their topological properties. In the first instance, neuroscientists exploited local and global measures to assess the importance of single brain regions (nodes) or properties of the network as a whole, respectively, revealing non-random attributes. These measures included for example degree centrality,

betweenness centrality, path length, clustering coefficient, and efficiency. However, local and global measures might not paint the whole picture of the brain functioning, so that more recently a new focus has been on the mesoscale (intermediate) level. Here we can observe how the brain network's elements organize themselves in modules that adopt different configurations basing on the type of connectivity, the brain state, and the external environment. In the network science, modules are groups of nodes internally strongly interconnected, but weakly coupled with the other nodes of the network. By supporting balanced mechanisms of integration and segregation within and between different brain areas (Sporns, 2013), modules constitute the building blocks underpinning brain network's organization. Thus, decomposing the brain network to identify its modular structure has become crucial to gain new insights into brain cortical organization as well as cognitive functions (Fox and Friston, 2012; Tononi et al., 1994).

The network-based modeling and analysis have profoundly contributed to deepening our understanding of brain functioning. Many times, modules have been detected in single networks, extracting useful information on single subjects, time-points, tasks, disease or connectivity patterns. Yet, there is a long way to go in the inferences *across* brain networks. Indeed, the patterns of human brain connectivity intrinsically evolve across several domains. Brian networks can change their topology, for example, in time in ranges spanning from milliseconds (thanks to high temporal resolution acquisition techniques based on EEG/MEG) to years (e.g. in lifespan studies). Connectivity patterns might also vary across the frequencies in which the collected signals can be decomposed, across different tasks, from subject to subject, across different acquisition modality, and in turn also the modular structure would mutate. For a long time, two easy strategies adopted to manage this amount of information consisted of aggregating or discarding data, to obtain a single network instance. However, such strategies could be misleading or could lead to poorly accurate or reliable results. The mathematical formalism of multilayer networks addresses this issue (De Domenico, 2017; Kivela et al., 2014; Vaiana and Muldoon, 2018). A multilayer network consists of an ensemble of single-layer networks, each one corresponding and encoding a specific attribute of the system (i.e. different time points,

frequencies, subjects, tasks, connectivity metrics). This formulation combines the simplicity of the classical networks and the flexibility in modeling multimodal data. While many graph measures have been successfully translated from single- to multi-layer networks, principled frameworks are still needed, that could allow to treat and manipulate dependencies in multilayer networks. Overall, the size and complexity of brain data and physiological questions on brain architecture require adequate multilayer frameworks developed upon robust strategies for statistical inference.

In this context takes place this dissertation, which tackles the challenge of uncovering and characterizing modules in multilayer brain networks. It serves a dual purpose. On one side we attempted to broaden our knowledge of the human brain structural and functional organization across different domains, on the other side we enriched the mathematical and statistical methods in the field of multilayer networks.

While the following chapter introduces the principal methods that will be exploited, the main body of this work is composed by three sections, that take the form of journal articles.

In section I, I report a comparative analysis among different algorithms employed to detect modules in multilayer networks. In fact, despite the presence of some common practice, there is still no agreement about which algorithm is the most reliable, and a way to test and compare them all under a variety of conditions is lacking. We tested their ability to recover both steady and dynamic modules configurations, statistically evaluating their performances by means of ad-hoc implemented benchmark graphs. Results seek to provide guidelines about the choice of the more appropriate algorithm according to the different properties of the brain network under exam. To prove the validity of the results, we applied the algorithms to functional brain networks derived from electroencephalographic (EEG) signals in a controlled condition. Despite modular organization has not been really investigated in EEG based brain networks, we believe they are extremely suited to study the evolution of cognitive processes across time, and so through a multilayer framework, given their high temporal resolution.

In section II we investigated the evolution of the brain structural modular organization across the human lifespan. In doing that, we developed an ensemble-based multilayer network approach, a statistical procedure that allowed us to efficiently link changes of structural connectivity patterns to development and aging.

Given the results obtained in section I, where we found the best multilayer community detection algorithm, in section III we extended its formulation to track variations of brain network architecture across two domains simultaneously. In particular, we explored how it changes across subjects and across different types of connectivity (structural and functional).

The studies in sections II and III make use of a freely available dataset, released as part of the Nathan Kline Institute (NKI), Rockland, NY lifespan sample. It includes functional, diffusion-weighted, and structural magnetic resonance imaging (MRI) scans of individuals aged 7-85 years, from which we reconstructed structural and functional networks.

A conclusion summarizing the main contributions of this Ph.D. project, together with their impact and limitation, closes this dissertation. Finally, two chapters are dedicated to a list of the papers and CV originated from this Ph.D. course.

Section I has been carried out in collaboration with the Neuroelectrical Imaging and BCI Lab (NEILab, PI: Donatella Mattia, MD, Ph.D.) at Fondazione Santa Lucia, IRCCS, Rome, Italy. All the data threatened in this section have been collected in this laboratory. Sections II and III were performed in collaboration with the Computational Cognitive Neuroscience Laboratory (PI: Olaf Sporns, Ph.D.) and the Brain Networks and Behavioral Laboratory (PI: Richard Betzel, Ph.D.) of Indiana University, Bloomington, USA.

Hints of brain connectivity and graph theoretical analysis

i. Structural and functional brain connectivity

Brain connectivity refers to patterns of links connecting distinct units of the central nervous system (Jirsa and McIntosh, 2007; McIntosh and Mišić, 2013). Both elements and links can encode different information. Units can stand for single neuronal cells, neural groups, or larger brain regions. Links can be divided in two main classes: (i) links constituted by anatomical connections, such as synapses or fiber tracts pathways between cortical and subcortical grey matter regions, form structural connectivity; (ii) links inferred through statistical or causal dependencies, such as cross-correlation or coherence, form the functional brain connectivity. In this way, structural connectivity refers to anatomical (physical) connections among brain areas, while functional connectivity to their activity or co-activity over time (Friston, 2011), regardless of whether these areas are connected by direct structural links.

Overall, brain connectivity underpins and constrains brain activity, so that reconstructing and analyze it plays a key role in elucidating brain functioning.

In this dissertation the focus will be on human brain connectivity/networks. While animal nervous system can be sometimes studied through invasive techniques, the human brain is mostly investigated with non-invasive imaging methods, like electroencephalography (EEG), magnetoencephalography (MEG), and magnetic resonance imaging (MRI). EEG and MEG capture rapid variations of the electric and magnetic field generated at cortical level and still observable in the scalp surface. MRI applies specific sequences of magnetic field to excite atoms in the brain. Atoms respond altering properties associated to brain activity, such as blood volume and oxygen concentration. Measuring these alterations is then used to estimate structural and functional connections among brain regions. Here we will exploit brain connectivity estimated from EEG and MRI signals.

To reconstruct structural networks we used MRI, that also goes by the name of diffusion weighted imaging (DWI) (Hagmann et al., 2007). DWI exploit the motion of the water molecules in the brain to infer tracts of connections. In a free space water is subjected to Brownian motion that shows no preferential diffusion direction (isotropic motion). In the brain, the presence of myelinated axon bundles constrains the direction of the water motion (anisotropic motion), so that water molecules diffuse preferentially along the bundles' longitudinal axis (Basser et al., 2000; Mori and Zhang, 2006). Exciting atoms through a magnetic field and estimating the directionality of the caused motion, we can reconstruct physical pathways connecting neural elements, commonly called "streamlines". The number of streamlines connecting two regions of the cortex surface will constitute the weight of the link connecting these nodes in the brain network. Different processing strategies adopted to obtain the final structural network will be discussed in the studies in section II and III.

MRI scans can also be used to estimate functional connectivity, basing on the concept that neuronal activity is strictly related to blood flow in the brain vessels (Logothetis et al., 2001). Indeed, sustained activity of neuronal populations require oxygen, which is transported and furnished by the hemoglobin contained in red blood cells. Hence, when active, brain areas will be surrounded by oxygen-rich blood. The quantity of oxygen in the blood affects its ferromagnetic properties, so that applying a magnetic field and observing the response of the blood it is possible to distinguish between oxygen-rich (active) and oxygen-poor (non-active) brain areas. The signal observed is called BOLD (blood-oxygen-level-dependent). Functional connectivity can be then inferred by observing the BOLD signal in different brain areas and identifying in which of them it co-fluctuates, exploiting for example measures of correlation. The correlation coefficients of all the pairs of brain regions will constitute the links of the functional brain network. A more detailed preprocessing of the BOLD signals will be treated in section III.

We estimated functional brain networks also from EEG recordings. EEG measures the spontaneous activity of the brain by capturing, through sensors placed on the scalp, the voltage fluctuations resulting from ionic currents provoked by the synchronous activity

of pyramidal neurons. From these signals we can infer functional connectivity in terms of directed causal information flow between brain areas. The concept of causality is based on Granger's argument (Granger, 1969), that if a signal X_1 "causes" a signal X_2 , then the lagged values of X_1 contain information that help in predicting X_2 above and beyond the information contained in the lagged values of X_2 . Granger causality is statistically implemented through different methods, including Direct Transfer Function (DTF) (Kaminski and Blinowska, 1991), Partial Directed Coherence (PDC) (Baccalá and Sameshima, 2001) and Phase-slope Index (PSI) (Nolte and Mueller, 2010), that can all be applied to EEG signals. In this thesis we used the PDC metric. PDC is a spectral estimator based on multivariate autoregressive models that allow to reconstruct the direction of information flow. It is known to be characterized by high accuracy in the estimation of connectivity patterns, distinguishing between direct and indirect connectivity flows better than other estimators (Astolfi et al., 2007). More details on the estimation of EEG functional connectivity based on PDC will be discussed in section I.

Both MRI and EEG are well established non-invasive neuroimaging methods. Being able to extract connectivity patterns from both type of signals is crucial, since no one technique by itself can adequately address the varied questions of interest in research and clinical applications. EEG signals are suitable to recover highly variable connectivity patterns, due to its high temporal resolution. Moreover, EEG has the great advantage of being a low-cost, portable technique, which allows to collect data from subjects in a variety of tasks and under different clinical conditions. MRI, on the contrary, suffers of temporal resolution and portability in favor of an excellent spatial resolution, that allows reconstructing brain tissue, and consequently connectivity patterns, at the millimeter level. In the first section, we exploited the high temporal resolution of the EEG, to build a temporal multilayer network in which layers represent timestamps, in order to investigate the community detection algorithms in different condition where connectivity patterns suddenly changed or remained stable across several milliseconds. In the second section, we exploited the MRI high spatial resolution to accurately investigate the structural modular organization of the human brain across the lifespan. Finally, in the third section

we exploited MRI signals, to build a new model able to explore the relationship between structural and functional connectivity.

ii. Network science applied to brain imaging

Brain connectivity patterns can be mathematically represented and analyzed in the form of a graph (Bullmore and Sporns, 2009; Bullmore and Bassett, 2011; Fornito et al., 2016). A graph is an abstract representation of a network suitable for every kind of connectivity discussed in the previous paragraphs. It consists of a set of vertices (or nodes) connected each other by means of edges (links, connections). In the following chapter nodes will correspond to small portion of the cortex (voxels) in MRI based studies, or to larger brain areas subtended by the sensors in EEG recording. The links instead, will correspond to streamlines counts (anatomical connectivity), correlation coefficients (functional connectivity inferred from BOLD signals), or causal interactions (functional connectivity inferred from EEG signals).

Mathematically a graph made of N nodes can be represented through an adjacency matrix A in which the entries a_{ij} (with $i, j=1, \dots, N$) assumes a value different from zero only if a link exists connecting node i with node j , and vice versa (Figure 1). The links of the

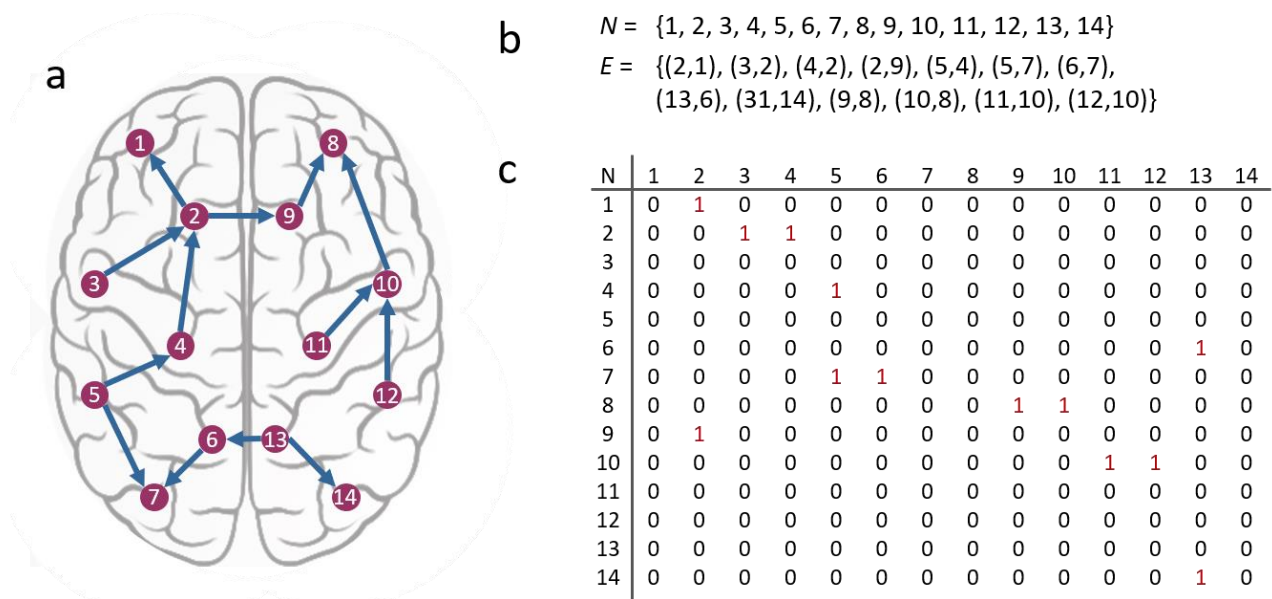


Figure 0.1. Representation of the brain connectivity through a graph (panel a), the list of nodes and edges (panel b), and the relative adjacency matrix (panel c).

graph can be binary or weighted, basing on whether the existence of the link is the only aspect of interest or we are interested in the strength of such connection. Binary and weighted adjacency matrix are made of 0/1 and 0/non-zero entries, respectively. Moreover, links can be directed or undirected basing on whether we know the direction of influences between nodes or it is impossible to determine whether the activity of brain region a influences that of region b or whether it is the other way around. Undirected graphs result in a symmetric adjacency matrix, while this is not necessarily true for the directed one. In this dissertation we will deal with both binary-directed networks (estimated from EEG signals) and weighted-undirected networks (estimated from MRI data).

Modeling connectivity patterns as a network allow us to extract quantitative information from it by means of several indices that can be computed on the graph. Among many others, measures on brain networks many times included the calculation of the node's degree or strength, clustering coefficient, path length, betweenness or eigenvector centrality, efficiency, small-worldness. All these measures capture local or global properties of the networks, inferring on the centrality/importance of single nodes or global topological properties of the network.

iii. The modular structure of brain networks

This thesis focuses on measures lying at an intermediate level, between local and global, where the organization of the nodes within the network can be observed. Community structure (Newman and Girvan, 2004; Porter et al., 2009) fits this level and consists of the organization of the network in groups of nodes (clusters or communities) promoting mechanisms of segregation and integration between brain areas (Sporns, 2013), that shape communication patterns and make the system efficient. Communities in brain networks (Figure 2) usually refer to groups of nodes in which the network itself can be divided, possibly responsible for specific domains of brain functioning.

While many definitions of community exist in network science, brain networks often exhibit assortative communities, composed by groups of nodes internally highly interconnected while poorly connected with the rest of the network. So-called communities are also referred to as modules (Sporns and Betzel, 2016). Modules can be detected in a data-driven way, basing on the topology of the network, and understanding the modules' composition within the brain network could provide important insights into brain function. To date, many studies have been already carried out detecting modules in anatomical and functional brain networks. In one of the firsts (Hagmann et al., 2008) an anatomical modular structure consisting of six modules has been found, and special attention was put on identifying those regions highly connected intra- and inter-modules, known as hubs. Lately (Heuvel and Sporns, 2013, 2011) those hubs have been found to play a key role in shaping information flow. Other efforts were put on identifying the multiscale organization of anatomical brain networks (Betzel et al., 2013; Lohse et al., 2014), revealing the presence of different meaningful community organization corresponding to cluster of different size. Also in functional network the modular structure has been investigated. First it has been showed that the human brain is actually organized into modules of functionally interconnected areas (Laumann et al., 2015; Meunier et al., 2009). Later it has been found that these communities can be associated to cognitive/behavioral function (Power et al., 2011). Beside a qualitative description of the human brain modular organization, more recent efforts were put on revealing its evolution in different domains. Studies characterized modules composition across

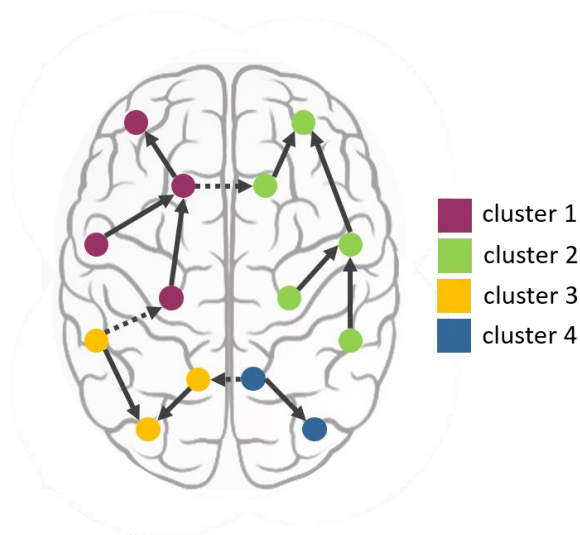


Figure 2. Example of a brain network partitioned into four clusters. The grouping in clusters is indicated through different colors. Intra-clusters and inter-clusters edges are indicated through continuous and dashed arrows, respectively.

cognitive states (Andric and Hasson, 2015; Godwin et al., 2015), during aging (Zuo et al., 2017) (a deeper analysis in section II), or in a learning paradigm (Bassett et al., 2011b). As we will show, multilayer paradigms can be extremely useful in tracking communities in multimodal networks.

There exist different methods to detect community in networks, and through section I we will attempt to provide some guidelines regarding the use of them. In the meanwhile, we want to introduce the popular concept of *modularity* (Q) (Newman, 2006), a quality function used to assess the goodness of a division of the network into modules. Given a network and a partition of it into nodes, modularity estimates the goodness, in terms of assortativity, of this partition with respect to a null model. Its formulation is reported below, in Eq. 1:

$$Q(\gamma) = \sum_{ij} [W_{ij} - \gamma P_{ij}] \delta(\sigma_i \sigma_j) \quad (\text{Eq. 1})$$

Where W_{ij} and P_{ij} are the actual and expected weights of the connection linking nodes i and j . The variable $\sigma_i \in \{1, \dots, K\}$ indicates to which cluster node i belongs, and $\delta(x, y)$ is equal to 1 if $x = y$ and 0 otherwise. The parameter γ represents a spatial resolution weight that, scaling the importance of the null model P_{ij} , rewards partitions with few or many modules. Many possible definitions of null model exist. One of the most common is the configuration model $P_{ij} = \frac{k_i k_j}{2m}$, in which each node's connection strength is preserved but edges are placed in a random fashion.

A multilayer version of Q has been recently introduced (Mucha et al., 2010), in order to qualify assortative communities in multilayer networks. This version allows to incorporate a second channel of connectivity, which in multilayer brain networks can represent for example time or subjects. Its formulation is given by:

$$Q(\gamma, \omega) = \sum_{ijrt} [(W_{ijr} - \gamma P_{ijr}) \delta_{rt} + \omega \delta_{ij}] \delta(\sigma_{ir} \sigma_{jt}) \quad (\text{Eq. 2})$$

Here nodes are linked to themselves across layers through the temporal resolution parameter ω . Its value weights the similarity of the partitions across layers (indicated

through r and t), so that high (low) ω -values reward (non) homogeneous partitioning across layers.

I introduced from the beginning these concepts of modules, modularity and multilayer modularity because they constitute the focus of this Ph.D. project, and will be recurrent over each section.

iv. Validation of network's indices

However, before getting to the heart of the dissertation, I want to highlight that the use of every complex network measure should be accompanied by the design of some null hypothesis. If a null model is properly designed, the statistical comparison of the indices computed on the actual and the null model could provide significant insights on the topological properties of the complex system under exam. Null models are not universally defined. Usually they are built preserving and randomizing different properties, according to the features of interest. In single layer networks, for example, when the focus is on the centrality of the nodes a frequently used null model consists of randomizing edges while preserving the degree-distribution. In absence of a null model, statistical frameworks are needed that ensure the reliability of the obtained measure. The validation of the network's indices through null models or robust statistics also applies to multilayer networks. For example, when the order of the layers is important (i.e. time-varying networks), is a common practice comparing the indices obtained on the real network with those obtained with the multilayer network in which layers are randomly permuted, but networks properties are preserved within each layer. In each of the following section the measures obtained will be either validated through a comparison with respect to a null model, or statistically inferred.

SECTION I

Comparison among multilayer community detection algorithms and application to EEG-based functional connectivity

- 1.1. Introduction
 - 1.2. Methods
 - 1.2.1. Benchmark networks generation
 - 1.2.1.1. Networks with stationary community structure
 - 1.2.1.1. Networks with evolving community structure
 - 1.2.2. Simulation studies for algorithms comparison
 - 1.2.2.1. Stationary community structure
 - 1.2.2.2. Evolving community structure
 - 1.2.3. Multilayer community detection on EEG brain networks
 - 1.3. Results
 - 1.3.1. Simulation studies for algorithms comparison
 - 1.3.1.1. Algorithms comparison on networks with stationary community structure
 - 1.3.1.2. Algorithms comparison on networks with evolving community structure
 - 1.3.2. Multilayer community detection on EEG brain networks
 - 1.4. Discussion
 - 1.5. Conclusion

 - 1.6. Supplementary Material
 - 1.6.1. Comparative analysis on networks with evolving community structure and increasing or decreasing clusters number
 - 1.6.2. Comparative analysis on networks with lower graph density
 - 1.6.3. Preliminary investigation on the temporal resolution parameter in the multilayer modularity optimization algorithm, genlouvain
 - 1.6.4. Preliminary investigation on the trade-off parameter in the multi-objective function optimization algorithm, FacetNet
-

1.1. Introduction

The convergence of network science to the neuroscience field is a recent effort, which has been driven by the growth of two scientific developments. On one side, the number of tools to investigate complex systems has exploded, as more and more complex data from different fields (i.e. social, transport and biological science) have been made available (Boccaletti et al., 2006; Newman, 2003). On the other side, there has been an advancement in the neuroimaging techniques and consequently in the field of brain connectivity (Jirsa and McIntosh, 2007), which allows to model brain structure and function as complex networks of brain areas (nodes) anatomically or causally

interconnected (Sporns, 2011). Thus, network neuroscience (Bassett and Sporns, 2017) is an emerging field that aims to investigate brain organizational principles by means of network science tools.

A feature of networks representing complex systems, included the brain, is the modular structure (Meunier et al., 2010; Newman, 2012a; Porter et al., 2009; Sporns and Betzel, 2016). Modules (or communities, or clusters) are groups of nodes strongly connected which can be related to specific functions of the system. Previous studies pointed out how modular structure represents a mean to reveal non-trivial relationships between topological and functional features of the complex networks (Guimerà and Amaral, 2005). This property of the brain network is located halfway between global and local scale, at a mesoscale level, which is informative of the network's organization (Betzel and Bassett, 2017). Their composition shapes communication patterns of the system and promotes well-balanced mechanisms of integration and segregation between the brain's sub-systems (Betzel et al., 2013; Sporns, 2013; Wig, 2017).

While most of the studies on community detection in brain graphs deal with single layer networks, above all in the electroencephalographic (EEG) applications (Chavez et al., 2010), brain networks are intrinsically multilayer (De Domenico, 2017; Hutchison et al., 2013; Muldoon and Bassett, 2016). There is not a single neuronal connectivity pattern able to represent brain functioning, since brain interactions vary across multiple domains. They evolve in time, across the subject's conditions, tasks, frequency domains (in M/EEG acquisitions), and they can change from subject to subject. Thus, a multilayer framework better accounts for the complexity and diversity of cerebral interactions, resulting more suitable to analyze brain connectivity without either throwing away or combining different information. A multilayer network is a sequence of linked single layer networks, each one encoding specific attributes of the system. This framework allows to integrate multiple channels of connectivity and provide a more natural description of the system, as the nodes (brain areas) can show different sets of interactions in each layer. With this perspective, it is worthwhile to track the modular composition across layers (e.g. in different time points of a task), because changes, as well as stability of the network

structure, could be physiologically meaningful. With this work we aim to identify an optimal way to extract communities in multilayer brain networks, with special focus on those estimated from EEG signals.

Recovering communities in a multilayer network is usually done algorithmically. In fact, networks representing real systems are usually big or with too complex connectivity patterns to detect modules by simple visual inspection, and a range of algorithms have been proposed. Among those freely available we identify three main approaches:

- i) The first one trivially consists of applying a single layer clustering algorithm to each slice of the multilayer network. Previous comparative analysis (Lancichinetti and Fortunato, 2009) have shown how those based on modularity (Girvan and Newman, 2002; Newman and Girvan, 2004) optimization have good performances. In particular (Leicht and Newman, 2008), which from now on we call ModStat (modularity static), performs well in directed EEG brain networks (Puxeddu et al., 2017).
- ii) The second approach is based on the optimization of a multilayer formulation of modularity (Mucha et al., 2010) (Eq. 2). The main implementation of this approach has been given by (Jutla et al., n.d.) and is known as *genlouvain*. This algorithm represents an extension of the classical modularity maximization (Blondel et al., 2008), to which it adds a term that considers the coupling of the nodes across layers. This term is proportional to a resolution parameter, ω , which determines the stability of the network partitioning across the slices.
- iii) The third approach consists of the optimization of a multi-objective function, which aims to maximize both the accuracy of the partitions at each layer and the smoothness across all the layers (Chakrabarti et al., 2006). Two widely used algorithms reflecting this last approach are DynMoga (Folino and Pizzuti, 2014) and FacetNet (Lin et al., 2009, 2008). The former is a genetic algorithm that optimizes modularity and mutual information of consecutive layers. The latter discovers communities iteratively taking into account both the observed data and a probabilistic model given by all the single community structure.

To date, an agreement on which is the most advantageous approach is missing. In the last years, some effort has been made on investigating their behavior on multilayer networks. A conventionally used approach, even in single layer network analysis, consists of testing the algorithms on a real network with known community structure (Lancichinetti and Fortunato, 2009). In (Silva et al., 2016), for example, authors compared the behavior of algorithms based on evolutionary clustering on a high school network, the MIT Social Evolution dataset and the Brazilian Congress network, in which the ground truth is respectively represented by classes, dormitory sectors (Dong et al., 2011) and political alignment of the congressmen based on their party. However, this approach might lack generalization, and the obtained results would be limited to that specific network. Moreover, in the neuroscience field a brain network in which the community structure is known a priori does not exist. Hence, the lack of ground truth for brain communities together with their ubiquity makes it necessary the implementation of benchmark networks, with known community structure and realistic features, where it is possible to test different community detection algorithms. In this work, we propose a toolbox to generate to generate artificial networks with modular structure with manifold features, which reflect in particular those of EEG brain networks. In (Silva et al., 2016) authors also tested the algorithms on a synthetic network. Nevertheless, it is a simple network with few nodes and three clusters, with hardly can be encountered in the neuroscience field. In (Schmidt et al., 2018) authors tested two multilayer clustering approaches on an artificial network with more realistic properties. However, the test made on a single network, as previously said, might lack generalization of the results. On the contrary, the main advantage of our toolbox is its ability to simulate a wide range of conditions. Other already existing tools (Kim and Han, 2009; Lin et al., 2008) are a multilayer version of the Girvan and Newman model (Girvan and Newman, 2002), and they do not allow a deep analysis of the algorithms, as they constrain most of the parameters characterizing the network (e.g. number of nodes, number of clusters, etc.). In (Granell et al., 2015) authors propose a more suitable tool in which a potential user can set some parameters of interest, such as nodes number, clusters number, and the ratio

between intra-clusters and inter-clusters density. However, here we introduce an even more flexible tool, in which several network's features, as number of nodes, graph density, number of clusters, noise level in the community structure (modeled as a random permutation of a certain number of links), and the percentage of nodes changing module at a given layer, can be set. This tool is a multilayer extension of the single layer generator introduced in (Puxeddu et al., 2017). With respect to the previous described tools, we care to have a generator of more-or-less noisy networks, because brain connectivity estimation, not only based on EEG signals, is a process that always produces a certain level of noise in the resulting networks. In the specific case of EEG signals, the noise might depend from different factors, such as physiological/instrumental artifacts (Riita Hari and Aina Puce, 2017) or connectivity estimation methods (Astolfi et al., 2007; He et al., 2019).

Thanks to the proposed benchmark graphs, we performed a comparative analysis of the different multilayer clustering algorithms. Graphs have been generated accounting for a wide range of network features systematically varied in a domain typical of EEG based brain networks. Furthermore, we consider two cases in which the community structure is stationary across the layers and in which it changes dynamically. Both cases are of great interest in the EEG applications. In the former, we aim to get a single partition out from a multilayer network, as it can be useful in case the layers of the network are associated to time points of phenomena supposed stationary, or they represent different subjects of the same category (e.g. healthy or patients) and we want to extract common features. Moreover, as we said, brain networks can be affected by noise, and with this specific case we also want to test the algorithms' ability to recover a stable and accurate partition out of many noisy layers. In the second case, we aim to get variations in the partitioning. This is crucial if the aim is to track the modules' evolution in multilayer networks underlying non-stationary phenomena, or different clinical cohorts. In both cases, stationary and evolving community structure, we statistically evaluated the algorithms' performances under different conditions through analysis of variance (ANOVA). It is important to note that, while we implanted this study in order to properly manage community detection algorithms in multilayer EEG brain networks, the results

that we present have a more general impact. In fact, we simulated a wide range of network features, and many other complex networks might have properties falling into the explored range.

Finally, as a proof of concept, we applied the four approaches to a brain functional multilayer network estimated from EEG signals. Data have been acquired from a healthy subject during resting-state at closed-eyes and open-eyes. We report the differences between the community structure subtending the two phases obtained by using the investigated algorithms, showing accordance with the guidelines provided by the simulation studies.

1.2. Methods

1.2.1. Benchmark networks generation

The tool we developed generates multilayer networks with a defined community structure and consists of an algorithm implemented in Matlab environment (release 2017b). In particular, this toolbox allows a potential user to create networks with either stationary or evolving community structure with features spanning a variety of conditions experimentally observable in EEG based brain networks. In the following paragraphs we describe the implementation of the toolbox for each of the two cases above mentioned.

1.2.1.1. Networks with stationary community structure

The network produced by the toolbox, in this case, presents a stationary community structure, which means that the composition of the clusters across the layers does not change. Here, the variability from a layer to another one is only due to the noise level, so that some links might appear or disappear because of it. In Figure 1.1(a) is shown an example of a 2-layers network generated in this fashion. As mentioned before, the main advantage of using this toolbox is the flexibility it presents. In fact, the users can set several features which will characterize the network: number of nodes (**N**), graph density (**D**),

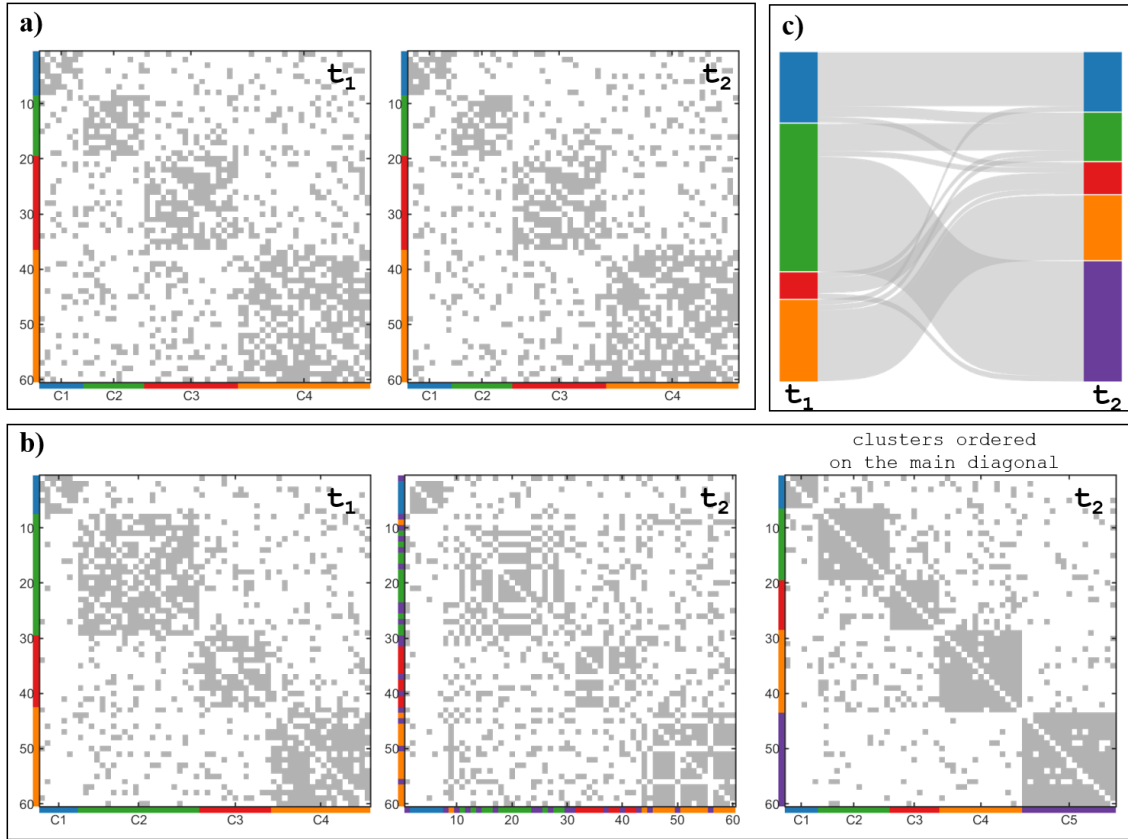


Figure 1.1. Examples of synthetic multilayer networks generated through the toolbox. a) two layers (t_1 and t_2) of a multilayer network with stationary community structure. b) two layers (t_1 and t_2) of a multilayer network with evolving community structure. In the second t_2 the nodes are re-ordered to represent clusters on the main diagonal. c) Sankey diagram of the network generated in panel b.

number of clusters (**CN**) the ratio between intra-clusters and inter-clusters density (**dr**), noise level (**no**) and number of layers (**nL**). The algorithm we present proceeds through two main steps:

- a) Creation of a single layer network (binary and directed) exploiting the algorithm described in (Puxeddu et al., 2017) - we will use this network as base for each layer.
- b) Addition of the percentage of noise (i.e. a percentage of links randomly shifted) set as input to each layer.

With these two steps, we obtain a multilayer network in which each slice has the same imposed community structure obtained in (a), and the variability from a layer to another one is only due to the presence of noise, applied to each network differently with (b). The algorithm used in (a) produces single-layer binary directed networks out of an empty $N \times N$ matrix with the above-listed desired features, and consists in turn of 4 stages:

- a.i) Setting of the size of the communities by randomly choosing CN integers, with the only constraint that their sum is equal to N.
- a.ii) Wiring of the network by randomly filling the empty matrix observing the imposed specifics (about density and ratio between intra-clusters and inter-clusters density).
- a.iii) Checking the absence of isolated nodes inside the clusters, and if present the algorithm rewires the intra-cluster connections.
- a.iv) Ensuring that the internal degree of each node is higher than the external degree (with respect to its cluster) by rewiring.

1.2.1.1. Networks with evolving community structure

In this second case, we want our toolbox to simulate a multilayer network with a community structure that changes nodes' composition across the layers. Also in this case the algorithm in the toolbox starts generating a first layer with (Puxeddu et al., 2017) (with the same stages described above), but then it generates the following slice so that a certain percentage of nodes (**pn**), set as input by the user, changes its allegiances to modules. The algorithm acts only on the connections related to the nodes that change membership, maintaining the rest of the networks as it was originated at the beginning. Similarly, it can also increase or decrease the number of cluster **CN**, moving some nodes into a new community or moving all the nodes belonging to one community in the remaining ones. In this way the user can obtain controlled variations of different entities of the community structure, according to the selected percentage of nodes that must change cluster (**pn**) and to the possible birth or death of communities. In Figure 1.1(b) is reported an example of a 2-layers network with evolving community structure, in which p has been set to 30% and the number of clusters increases through the born of the violet one. We represent this dynamic community structure through the Sankey diagram in Figure 1.1(c).

1.2.2. Simulation studies for algorithms comparison

1.2.2.1. Stationary community structure

The principal aim of this work is to test and compare the multilayer clustering algorithm in both the cases in which community structure is stationary and evolves across the layers. In this paragraph, we present the analysis regarding the first case. We made a simulation study testing the algorithms on the benchmark networks generated through the toolbox described in section 1.2.2.1. We exploited this tool systematically varying the network's features represented by the input parameters. In particular, we explored a range of values for the parameters according to those experimentally detectable in EEG-based functional brain networks. Thus, we generated networks with:

- **N = 60**. In the EEG based networks nodes represent EEG channels. There exist different acquisition systems in which the number of channels usually varies according to the scope of the registration. Configurations from 61 electrodes on are typically used in the research area.
- **D = [0.10, 0.30]**. With these two levels of density, we aim to simulate sparse and dense networks, as connectivity estimation methods can return both.
- **CN = [2, 4, 6]**. We simulate different parsing of the network to have coarser as well as finer communities, made of 30, 15 and 10 nodes, respectively.
- **dr = 2**. We generate networks in which the density inside clusters is twice with respect to the density outside. Namely, the network has a clear community structure. We do this in order to start from a very convenient condition for the algorithms, that we will gradually deteriorate by adding different percentages of noise.
- **no = [10%, 25%, 50%]**. These percentages of noise have been chosen to reproduce networks with different levels of module's sharpness.
- **nL = [2, 10, 50, 100]**. We consider networks with different numbers of layers to see if this factor influences the algorithms' performance. Indeed, we expect multilayer algorithms exploiting a higher dimensionality to mitigate the noise effect.

Then, we run the four algorithm algorithms under analysis [genLouvain, ModStat, DynMoga, FacetNet]. We performed a repeated measures ANOVA to evaluate the effect of the factors $\{\textit{algorithm}, \textit{clusters number}, \textit{noise level}, \textit{number of layers}\}$, with their shown levels, on the performances. We assessed such performances comparing the output of the algorithms with the known community structure through three different indices, which played the role of dependent variables in this statistical analysis. We chose three different indices to evaluate:

- I. *Accuracy*. To evaluate the algorithms' accuracy, we used the Normalized Mutual Information (NMI). It is an index borrowed from the field of Information Theory used to estimate the similarity between two objects. It can assume values from 0 (completely different objects) to 1 (identical objects). It has been already employed in this context to calculate the similarity between two given partitions (Danon et al., 2005), that in our case are the one obtained from the clustering algorithms and the imposed one. We computed the NMI between these two partitions in each layer and then we used the average of all these values as index of accuracy. We will refer to this index as NMI_{acc} .
- II. *Stability*. In networks with stationary community structure is also important to assess how much the clustering algorithms provide a stable partition across all the layers. Thus, we computed the NMI between each layer and the following one, and we computed the average of these values to obtain an index of stability. We name this index as NMI_{stab} .
- III. *Global performance*. We finally wanted an index that summarizes the global performances of the algorithms, considering simultaneously accuracy and stability. We computed this index as the Euclidean distance between two points A and B in the xy plane where the x- and y-axis represent respectively the values of accuracy and stability. A is the point $[x_{(acc)}, y_{(stab)}]$ associated to the actual values of accuracy and stability assumed by the algorithm, and B is the point $[1, 1]$ which represents the optimum (both stability and accuracy reach their highest score, 1). In this way the

Euclidean distance between A and B, which we used as index of global performance, represents the distance from the performance of the algorithms to the optimal possible performance. An example of this index is shown in Figure 1.2(b). We will refer to this index as GS_{ind} , it varies between 0 (optimal performances, $A=B$) and $\sqrt{2}$ (worst performances, $NMI_{acc}=NMI_{stab}=0$, A is the point $[0, 0]$ in the xy plane).

Furthermore, as the algorithms genlouvain and FacetNet depend on the resolution parameters ω and λ , we made two preliminary analyses exploring the behavior of the algorithms with different values of these parameters. In practice, we performed two more ANOVA tests for repeated measures, one for genlouvain and one for FacetNet, considering different values of ω and λ . We built the first one in order to evaluate the effect of the factors ω (with values $[0.1, 0.2, 0.5, 1, 2, 5, 10]$), *clusters number*, *noise level*, *number of layers* on the performance of genLouvain. Similarly, we built the second one to evaluate the effect of λ (with values $[0.1, 0.2, 0.5, 0.7, 0.8, 0.9, 1]$), *clusters number*, *noise level*, *number of layers* on the performance of FacetNet. Hence, we evaluated such performance with the same indices shown above and we assessed which values of ω and λ are better to choose when we want to identify modules out of a multilayer network with stationary community structure. The results of these two analyses can be found in the Supplementary Material, paragraphs 1.6.3 and 1.6.4.

1.2.2.2. Evolving community structure

In this second paragraph, we present the simulation study we implanted to assess the clustering algorithms performance when used on multilayer networks with dynamic community structure. To generate benchmark networks, we exploited the toolbox in the version introduced in section 1.2.2.2. We simulated networks by setting the input parameters to the values reported above, but we also included the parameter **pn** (percentage of nodes changing allegiance to modules) with the following values, chosen to simulate progressive variations of the community composition:

- **pn = [10%, 30%, 50%, 70%, 100%]**

These networks present the variation only between the first and the second half of the layers, while within the two halves the community structure is stationary. Indeed, we want to simulate the case in which we long to track modules over two different tasks, or two classes of subjects (e.g. healthy vs. patients). So that we want a unique partition associated with the first half of the layers (task1/healthy people) and a second partition

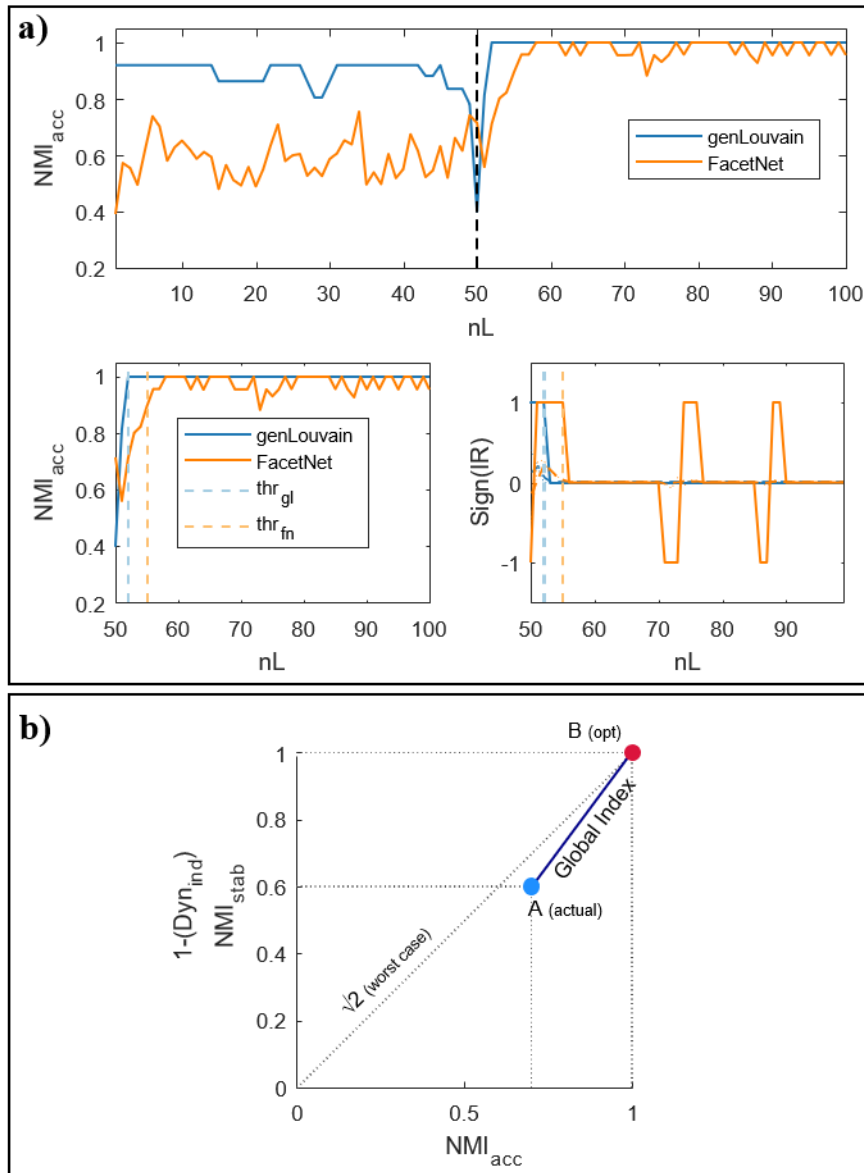


Figure 1.2. Example of dynamic and global indices computation. Panel a) Dynamic index. Top figure: Normalized Mutual Information computed between the output of the algorithms genLouvain and FacetNet and the actual community structure of a generated network with 100 layers. Lower left figure: Normalized Mutual Information from the snapshot in which community structure changes, and threshold samples (from which the algorithms go to regime) identified through the dynamic index. Lower right figure: sign of the first derivative smoothed and threshold samples. Panel b) The Global Index is indicated with the dark blue continuous line. A is the point corresponding to the actual values of NMI_{acc} and NMI_{stab}/Dyn_{ind} , while B is the point corresponding to the maximum values reachable by the indices.

associated with the second half (task2/patients). Again, we run the four algorithms and we performed an ANOVA for repeated measures using as dependent variables three different indices:

- I. *Accuracy*. To evaluate the algorithms' accuracy, we used the Normalized Mutual Information, NMI_{acc} , computed as in section 2.1.
- II. *Dynamics*. In networks with evolving community structure is also important to assess the rapidity with which the algorithms recognize the variation of the modules' composition. Thus, we defined and implemented an index that points out how much it takes to the algorithms, in terms of number of layers, to exactly detect the new structure. We started defining this index by observing the NMI_{acc} trend, which ideally should be V-shaped (Figure 1.2(a), upper): high and constant within the first and the second half of the layers, and lower in proximity of $nL/2$, where the community structure changes. The index mathematically identifies the layer (l_{thr}) from which the NMI_{acc} becomes stable and enters a sort of plateau (Figure 1.2(a), lower left). The idea is that computing the incremental ratio (IR) of the NMI_{acc} curve from $nL/2$ to nL , it will be positive until the algorithm goes to regime and null from that point on. Thus, we compute the IR, we smoothed it to avoid spurious peaks due to the noise, and we consider the sign, because we are only interested in when it becomes zero (Figure 1.2(a), lower right). We find the exact threshold layer through the formula:

$$l_{thr} \in \left[\frac{nL}{2} + 1, nL \right] := \arg \max_{l_{thr}} \left(\frac{\sum_{l=nL/2+1}^{l_{thr}} \text{sign}(IR_{smoothed})}{\sum_{l=l_{thr}+1}^{nL} \text{sign}(IR_{smoothed})} \right) \quad (\text{Eq. 3})$$

It scans all the layers from $nL/2 + 1$ to nL , and for each l it computes the ratio between the sum of this function $\text{sign}(IR_{smoothed})$ before and after l . Then it takes as threshold the l_{thr} to which the maximum of this ratio corresponds. Ideally at l_{thr} the numerator is positive (i.e. before l_{thr} the trend of NMI_{acc} is ascendant), and the denominator is equal to 0 (i.e. after l_{thr} the trend of NMI_{acc} is stable), so that the argument is infinite - the maximum possible. Once obtained l_{thr} , we normalized it for $nL/2$, to obtain an index that varies in the range $[0, 1]$, independently to the values of nL considered. We

will refer to this index as to Dyn_{ind} , and the lower it is the fastest are the algorithms in recovering the new structure.

- III. *Global performance.* In analogy to the previous analysis, we computed an index that summarizes the global performances of the algorithms, considering at the same time accuracy and dynamics. It is computed as explained before, but instead of NMI_{stab} , we consider the complement to the unity of Dyn_{ind} . We will refer to this index as GD_{ind} .

Also in this case of evolving communities, before executing the just described statistical analysis, we made a preliminary analysis to determine the optimal setting of the parameters ω and λ in the algorithms genLouvain and FacetNet respectively. Thus, we implanted an analogue statistical analysis in which instead of the factor algorithm we considered the factors ω and λ with the above-shown levels. The results of this test can be found in the Supplementary Material, paragraphs 1.6.3 and 1.6.4.

1.2.3. Multilayer community detection on EEG brain networks

For the purpose of validating the results of the simulation studies, we tested the algorithms in real EEG brain networks with features analogue to those investigated so far, relative to a simple and controlled condition.

EEG data has been recorded using 61 electrodes (according to the extended 10-20 International System) in a healthy subject (female, 33 years old) during rest at closed-eyes (CE) and open-eyes (OE). The subject gave informed consent prior to her participation and the experiment was approved by the local Ethics Committee before the data acquisition started. The session was composed of 26 trials of 200 seconds each. In the first 100 seconds, the subject was asked to keep her eyes closed (task1 – CE), while in the last 100 seconds she was asked to keep her eyes open (task2 – OE). We pre-processed the data through band-pass filtering (1-45 Hz), artifact rejection and segmentation in 2-seconds epochs. For each segment we estimated brain functional connectivity through Partial Directed Coherence (PDC) (Astolfi et al., 2006; Baccalá and Sameshima, 2001), a spectral

estimator based on Granger causality which provided us an estimation of the network for each frequency point. We then mediated the estimations in four EEG frequency bands, defined according to the Individual Alpha Frequency (IAF) (Klimesch, 1999) (IAF = 10 Hz): theta [IAF-6, IAF-3]; alpha [IAF-2, IAF+2]; beta [IAF+3, IAF+14]; gamma [IAF+15, IAF+30]. We assessed the significance of the connections through the asymptotic statistics (Takahashi et al., 2007; Toppi et al., 2016).

For each frequency band and for each of the two tasks we obtained 50 ($200s/[2s * 200Hz]$) binary networks of dimension 61x61. In this analysis, we focused on those relative to the alpha band, as of interest for resting state (Compston, 2010; Karbowski, 1990; Niedermeyer, 1997). Then we concatenated them so as to obtain 4 multilayer networks, sized 61ch*61ch*[2, 10, 50, 100] nL. For each value of nL the first half layers derive from task1 (CE) and the second half from task2 (OE), similarly to the simulation study. Finally, we run 100 times every algorithm under exam on the 4 multilayer networks. We run multiple times the algorithms because they are stochastic, which means they might provide more-or-less different partitions even if applied to the same network. In the simulation studies we address this issue as we perform an ANOVA test for repeated measures, which implies that for each combination of the parameters we compute several times the community detection.

1.3. Results

1.3.1. Simulation studies for algorithms comparison

In this section, we present the results of the simulation studies through which we analyze and compare the performances of the community detection algorithms.

1.3.1.1. Algorithms comparison on networks with stationary community structure

In *Table 1.1* we report the results of the comparative analysis made by exploiting simulated multilayer networks with stationary community structure and graph density equal to 0.3. Analogue results have been obtained setting the graph density to the lower level, $D=0.1$, and can be found in the Supplementary Material, paragraph 1.6.2. In general, the results of ANOVA together with Tuckey's post-hoc tests, show all the algorithms

	<i>dof</i> (b)	<i>dof</i> (w)	NMI _{acc}		NMI _{stab}		GS _{ind}	
			F	p	F	p	F	p
Alg	3	891	5393.2	<10 ⁻⁴	16108	<10 ⁻⁴	10549	<10 ⁻⁴
no	2	594	9110.4	<10 ⁻⁴	7518.9	<10 ⁻⁴	9392.2	<10 ⁻⁴
nL	3	891	1481	<10 ⁻⁴	110,35	<10 ⁻⁴	1427,1	<10 ⁻⁴
CN	2	297	473.31	<10 ⁻⁴	168.38	<10 ⁻⁴	420.19	<10 ⁻⁴
Alg*no	6	1782	844.84	<10 ⁻⁴	3360.3	<10 ⁻⁴	1752.3	<10 ⁻⁴
Alg*nL	9	2673	476.30	<10 ⁻⁴	71.038	<10 ⁻⁴	392.78	<10 ⁻⁴
Alg*CN	6	891	75.887	<10 ⁻⁴	422.88	<10 ⁻⁴	28.266	<10 ⁻⁴
Alg*no*nL	18	5346	163.80	<10 ⁻⁴	6.3538	<10 ⁻⁴	143.14	<10 ⁻⁴
Alg*no*CN	12	1782	115.89	<10 ⁻⁴	186.66	<10 ⁻⁴	170.10	<10 ⁻⁴
Alg*nL*CN	18	2673	56.644	<10 ⁻⁴	13.623	<10 ⁻⁴	51.239	<10 ⁻⁴
Alg*no*nL*CN	36	5346	36.189	<10 ⁻⁴	3.4496	<10 ⁻⁴	29.976	<10 ⁻⁴

Table 1.1. Results of the ANOVA test executed for the comparative analysis on networks with stationary community structure and graph density equal to 0.3. For each considered index (dependent variables of the test) we report the degrees of freedom (*dof*), *F* and *p*-values relative to single factors and the interactions among them.

having significantly higher performances in networks with low level of noise and high number of clusters. Overall, the figure shows genLouvain outperforming the other algorithms.

As for the accuracy (Figure 1.3) all the algorithms have performance inversely proportional to the level of noise simulated in the network. However, in noisy networks (*no*=50%) genLouvain and FacetNet show an improvement of the accuracy as the number of layers increases, above all if *CN*>2. In particular, genLouvain reaches almost the same level of accuracy in noisy and non-noisy networks, if *nL*≥10. On the contrary, as expected, the accuracy of ModStat is not affected by the number of layers, as it considers each slice of the network independently. Compared with the other algorithms, genLouvain displays higher level of accuracy in most combinations of Noise, Clusters Number and Number of Layers. The only exceptions are the case of low clusters number and low noise (*CN*=2, *no*=10%, *nL*= [2, 10, 50, 100]) in which modularity has better performances, for every value of *nL*.

Regarding the analysis of stability (Figure 1.4), namely the algorithms capability to recover a stable partition across the layers of the network, the algorithm with the highest performance is genLouvain for each combination of the ANOVA factors. In fact, it always

reaches the optimal value of NMI_{stab} , despite the level of noise, number of clusters and number of layers. On the contrary, the other algorithms are more sensitive to the ANOVA factors, especially to the level of noise and the clusters number. The algorithm ModStat

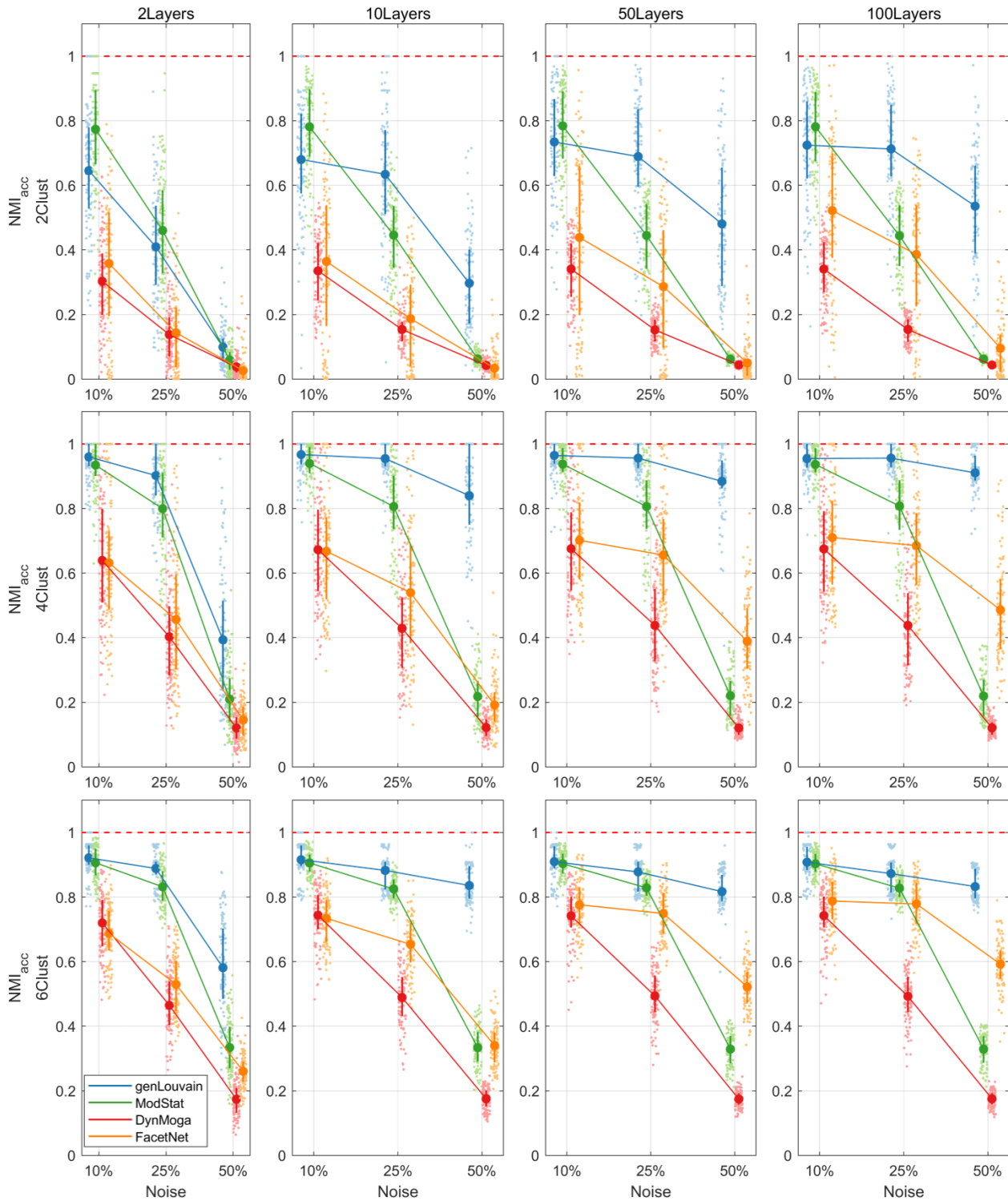


Figure 1.3. Plot of means and standard deviations of NMI_{acc} in the comparative analysis on networks with stationary community structure. In the rows and the columns of the pictures we report the results for different levels of clusters number (CN) and number of layers (nL) respectively. In each subplot the NMI_{acc} of each algorithm, identified with colors code, is shown for the different levels of percentage of noise (no).

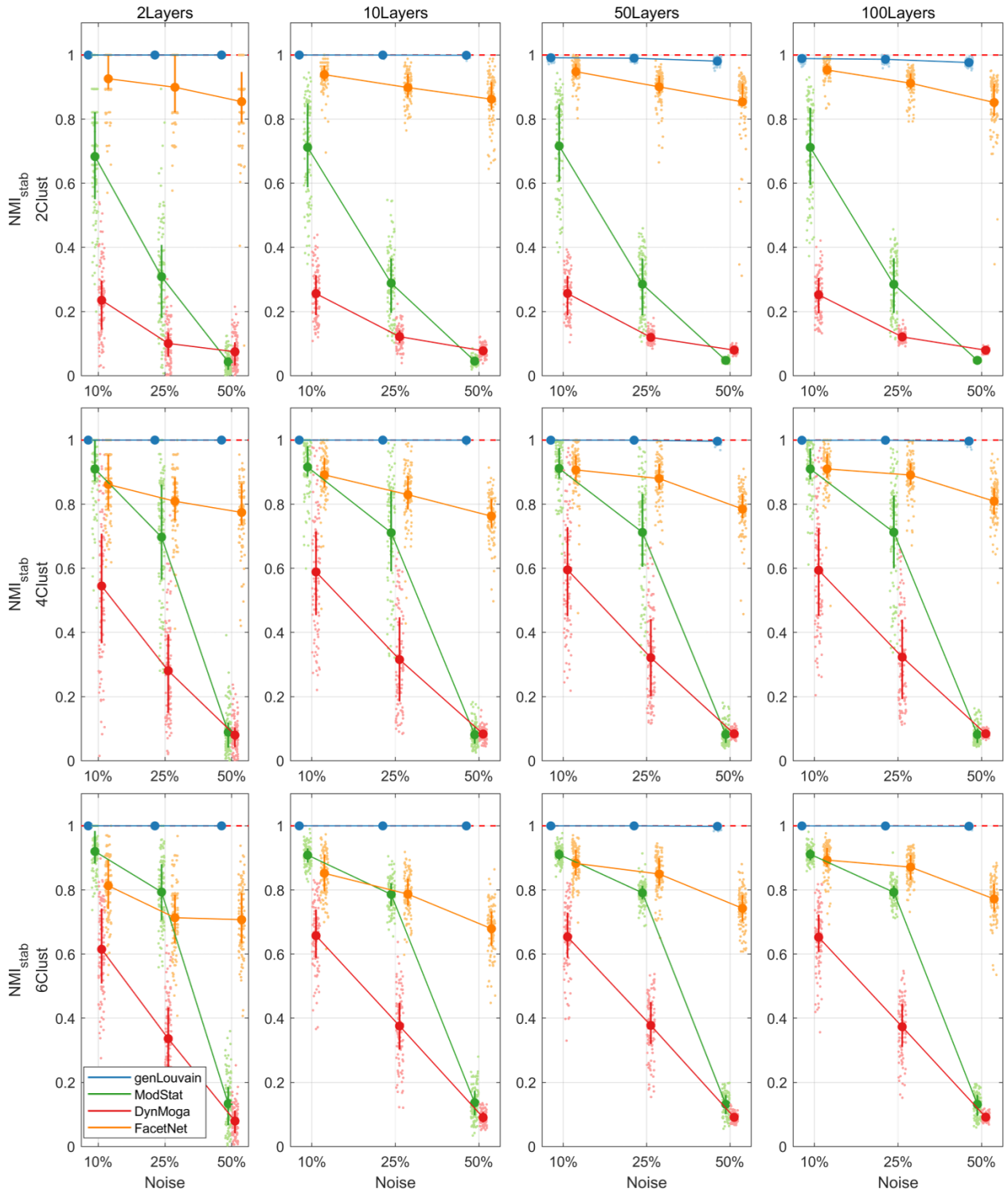


Figure 1.4. Plot of means and standard deviations of NMI_{stab} in the comparative analysis on networks with stationary community structure. In the rows and the columns of the pictures we report the results for different levels of clusters number (CN) and number of layers (nL) respectively. In each subplot the NMI_{stab} of each algorithm, identified with colors code, is shown for the different levels of percentage of noise (no).

has good performances, almost comparable with the genlouvain's ones, in networks with low noise (no=10%), while FacetNet is preferable to ModStat when $no \geq 25\%$.

The evaluation of the global performances summarizes what observed so far. Overall genlouvain has the best performances when the aim is the detection of stationary communities. A single layer modularity approach is also appropriate in case of few layers and low percentage of noise. FacetNet shows intermediate performances, as it seems to be able to mitigate the effect of a high level of noise when it has a high number of layers to work with.

1.3.1.2. Algorithms comparison on networks with evolving community structure

In Table 2 we report the results of the comparative analysis made to test the algorithms on multilayer networks with evolving community structure, density equal to 0.3 and clusters number unchanged. We observed analogue results in networks with lower density, $D=0.1$, and increasing/decreasing clusters number, and we report them on the Supplementary Material, sections 1.6.1. As in the previous analysis on stationary community structure, the results of ANOVA together with Tuckey's post-hoc tests, show all the algorithms having significantly higher performances in networks with low level of noise and high number of clusters. In reverse, the factor percentage of nodes moved (pn) does not

	NMI _{acc}				Dyn _{ind}				GD _{ind}			
	dof(b)	dof(w)	F	p	dof(b)	dof(w)	F	p	dof(b)	dof(w)	F	p
Alg	3	2241	122200	<10 ⁻⁴	2	1494	2932.5	<10 ⁻⁴	2	1494	36095	<10 ⁻⁴
no	2	1494	255900	<10 ⁻⁴	2	1494	255.81	<10 ⁻⁴	2	1494	23219	<10 ⁻⁴
nL	3	2241	36813	<10 ⁻⁴	2	1494	2577.4	<10 ⁻⁴	2	1494	6071.1	<10 ⁻⁴
p	4	2988	37.248	<10 ⁻⁴	4	2988	7.8124	<10 ⁻⁴	4	2988	16.168	<10 ⁻⁴
CN	2	747	14392	<10 ⁻⁴	2	747	477.02	<10 ⁻⁴	2	747	11828	<10 ⁻⁴
Alg*no	6	4482	18575	<10 ⁻⁴	4	2988	162.4	<10 ⁻⁴	4	2988	347.9	<10 ⁻⁴
Alg*nL	9	6723	12252	<10 ⁻⁴	4	2988	101.44	<10 ⁻⁴	4	2988	946.99	<10 ⁻⁴
Alg*p	12	8964	289.11	<10 ⁻⁴	8	5976	4.3169	<10 ⁻⁴	8	5976	6.8113	<10 ⁻⁴
Alg*CN	6	2241	425.4	<10 ⁻⁴	4	1494	341.71	<10 ⁻⁴	4	1494	475.52	<10 ⁻⁴
Alg*no*nL	18	13446	4514.8	<10 ⁻⁴	8	5976	7.1109	<10 ⁻⁴	8	5976	91.278	<10 ⁻⁴
Alg*no*p	24	17928	46.635	<10 ⁻⁴	16	11952	2.3138	0.0021	16	11952	5.4335	<10 ⁻⁴
Alg*no*CN	12	4482	3301.2	<10 ⁻⁴	8	2988	14.238	<10 ⁻⁴	8	2988	224.63	<10 ⁻⁴
Alg*nL*p	36	26892	33.267	<10 ⁻⁴	16	11952	3.2475	<10 ⁻⁴	16	11952	1.1954	0.2623
Alg*nL*CN	18	6723	856.5	<10 ⁻⁴	8	2988	17.014	<10 ⁻⁴	8	2988	5.5644	<10 ⁻⁴
Alg*p*CN	24	8964	308.26	<10 ⁻⁴	16	5976	6.5616	<10 ⁻⁴	16	5976	13.875	<10 ⁻⁴
Alg*no*nL*CN*p	144	53784	44.582	<10 ⁻⁴	64	23904	1.4109	0.017	64	23904	1.9990	<10 ⁻⁴

Table 1.2. Results of the ANOVA test executed for the comparative analysis on networks with evolving community structure and graph density equal to 0.3. For each considered index (dependent variables of the test) we report the degrees of freedom (dof), F and p-values relative to single factors and the interactions among them.

dramatically affect the global performances of the algorithms under analysis, meaning that the algorithms can detect small as well as big changes in community structure.

Specifically, we can unpack the results and observe the trend of each index separately. Regarding the accuracy, we show in the first row of Figure 1.5 the behavior of the algorithms with different levels of noise and number of layers. With low level of noise all the algorithms perform well, regardless of the number of layers, while as the noise increases there is a loss of accuracy. However, if $nL \geq 10$, both genLouvain and FacetNet have a significant improvement in the accuracy. In the second row is reported the effect of clusters number and number of layers on the accuracy, and it shows how the algorithms perform better when applied on networks with $CN \geq 2$, above all if $nL \geq 10$. In the third row we can observe the effect of the factors pn and no together. The percentage of nodes that change allegiance to modules does not substantially affect the accuracy of the algorithms. However, FacetNet and DynMoga show a little increase of performances when pn increases, meaning that they can easily detect big changes. Overall, genLouvain is the most accurate algorithm for each combination of the factors under analysis. The only exception is when $CN=2$ and $nL=2$, in which ModStat performs better. In general, genlouvain and ModStat have the same performances when the network has low level of noise or few layers ($nL=2$), while genlouvain is preferable in the other cases. FacetNet is more eligible with respect to ModStat only if the network presents a high level of noise and is composed of several layers ($nL \geq 10$).

As for the evaluation of the algorithm's dynamic (Figure 1.6) we only considered the performances of genLouvain DynMoga and FacetNet. Considering also ModStat would not be meaningful as it considers each layer independently. Moreover, we trivially considered only values of $nL \geq 2$. Also in this analysis genLouvain seem to be the most suitable algorithm as it is the fastest in identifying changes of the community structure for each combination of the factors no , nL , CN and pn . Only in the case in which $CN=4$ FacetNet is preferable. the factors noise and number of layers have an influence also on the rapidity of the algorithms.

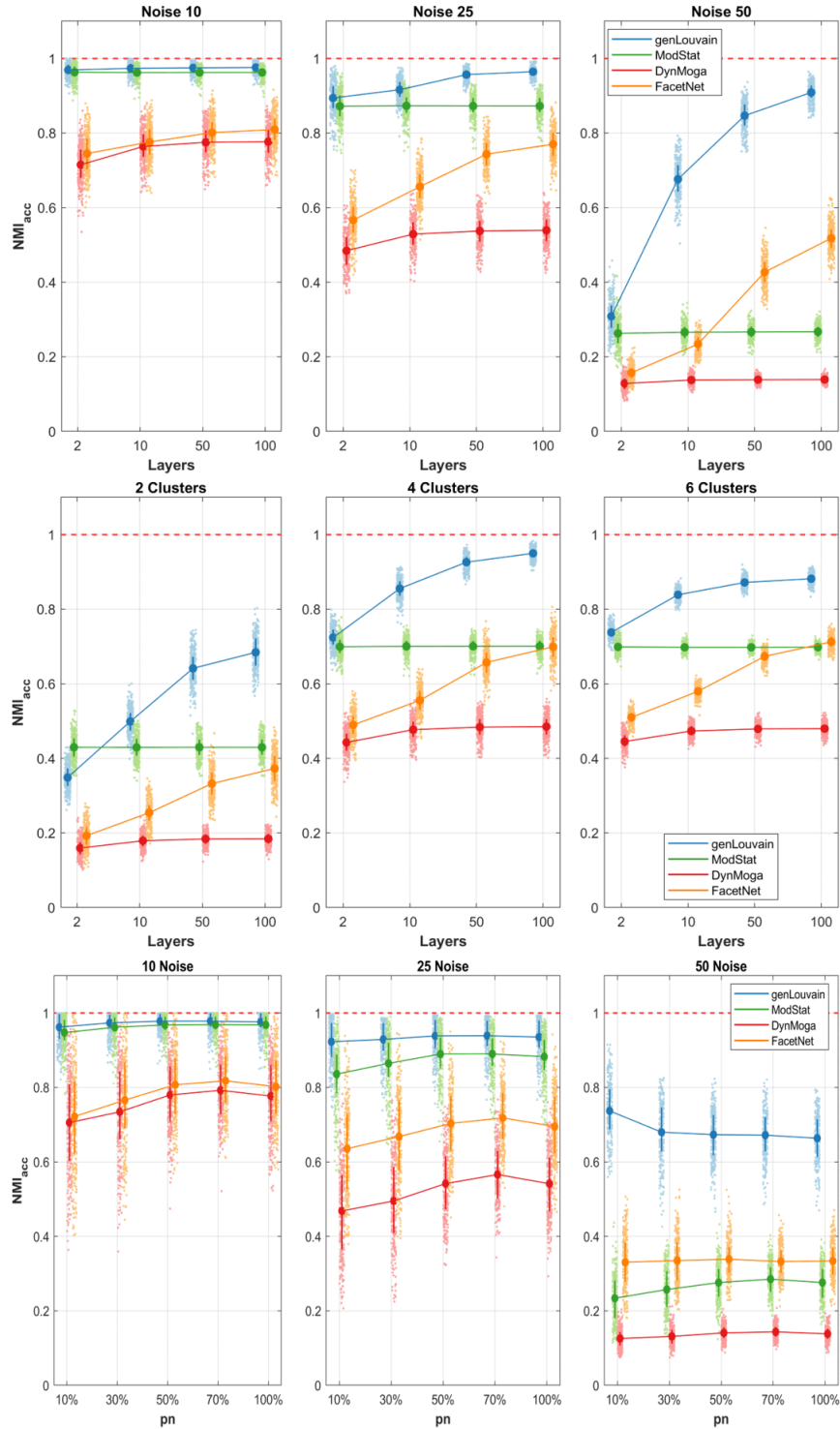


Figure 1.5. Plot of means and standard deviations of NMI_{acc} in the comparative analysis on networks with evolving community structure. In the first row we report the accuracy of the algorithms, identified with different colors, with respect to the different levels of number of layers, x-axis, and percentage of noise, columns. In the second row we show the trend of the algorithms' accuracies with respect to the number of layers, x-axis, and clusters number, columns. In the third row we represent the accuracies mean values for each algorithm to varying of the factor pn , x-axis, and level of noise, columns.

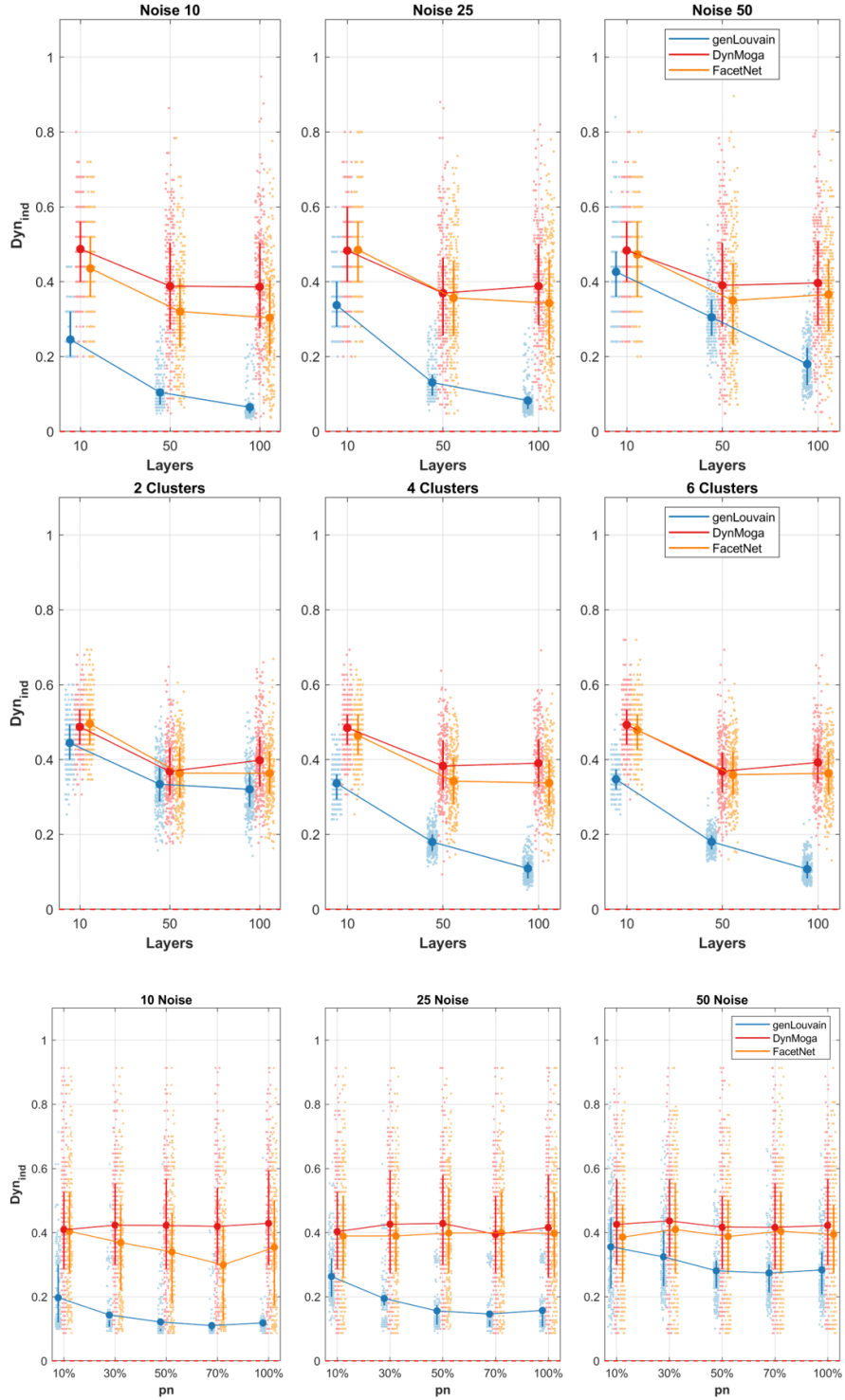


Figure 1.6. Plot of means and standard deviations of Dyn_{ind} in the comparative analysis on networks with evolving community structure. In the first row we report the dynamic of the algorithms, identified with different colors, with respect to the different levels of number of layers, x-axis, and percentage of noise, columns. In the second row we show the trend of the algorithms' speed with respect to the number of layers, x-axis, and clusters number, columns. In the third row we represent the Dyn_{ind} mean values for each algorithm to varying of the factor pn , x-axis, and level of noise, columns.

Finally, the global index confirms what shown with the previous indices. It suggests that the factors that have the greatest influence on the algorithms' performances are the level of noise and the number of layers: an increase of their value provokes respectively a breakdown and a boost of the performances. Also the number of clusters is proportional to the algorithms' performances, while the percentage of nodes that change community does not substantially affect their behavior. The most sensitive to the network's features is genLouvain, which in the comparative analysis is the outperforming one, while DynMoga is globally the less sensitive.

1.3.2. Multilayer community detection on EEG brain networks

In this section, we present the results of the application of the four algorithms under analysis to EEG networks subtending CE and OE resting state in alpha band. In Figure 1.7 we report the trend of the Normalized Mutual Information computed between the output of the algorithms across consecutive layers, for all the estimated networks with $nL=[2, 10, 50, 100]$. The black dashed line divides the CE state from the OE. Ideally one would expect high and stable values of NMI in the two halves and a collapse of the index near to the dashed line. That would mean that the algorithm is able to extract two steady partitions in the two conditions which are different one from each other. In the case of $nL=2$ of course the NMI would assume a value inferior to 1, hopefully low. In line with the simulation study, genlouvain is the algorithm that better approximate this behavior. Moreover, as proven in the previous sections genlouvain and FacetNet show higher stability and maximum discriminability between the two conditions when the number of layers increases. DynMoga shows a mild increment of performance with a higher number of layers, even if it is not as good as the others. Conversely, ModStat behaves independently from the number of layers, as it works on a single layer level.

We finally show in Figure 1.8(a) how these multilayer networks are parsed in clusters by genlouvain, which is the most advisable algorithm after our simulations. The figure reports as representative one of the 100 repetitions computed which, as indicated by the

narrow confidence interval in Figure 1.7, are very much similar among them. The partitions are consistent across all the levels of nL and in Figure 1.8(b-c) we show the partitioning of the network for each condition, CE and OE in the case in which $nL=50$. During the CE phase there is a cluster that involves the occipital electrodes and two clusters composed of electrodes from the left and the right hemisphere, respectively. During the OE phase the first cluster is dismembered between the left and the right hemispheres, and one can observe modules becoming more hemispheric-specific. Such results are observed both in the EEG network made of $nL=2$ and in the ones with $nL>2$, with different ω -values properly chosen according to the preliminary analysis (Supplementary Material, section C), suggesting that this preliminary study is correct.

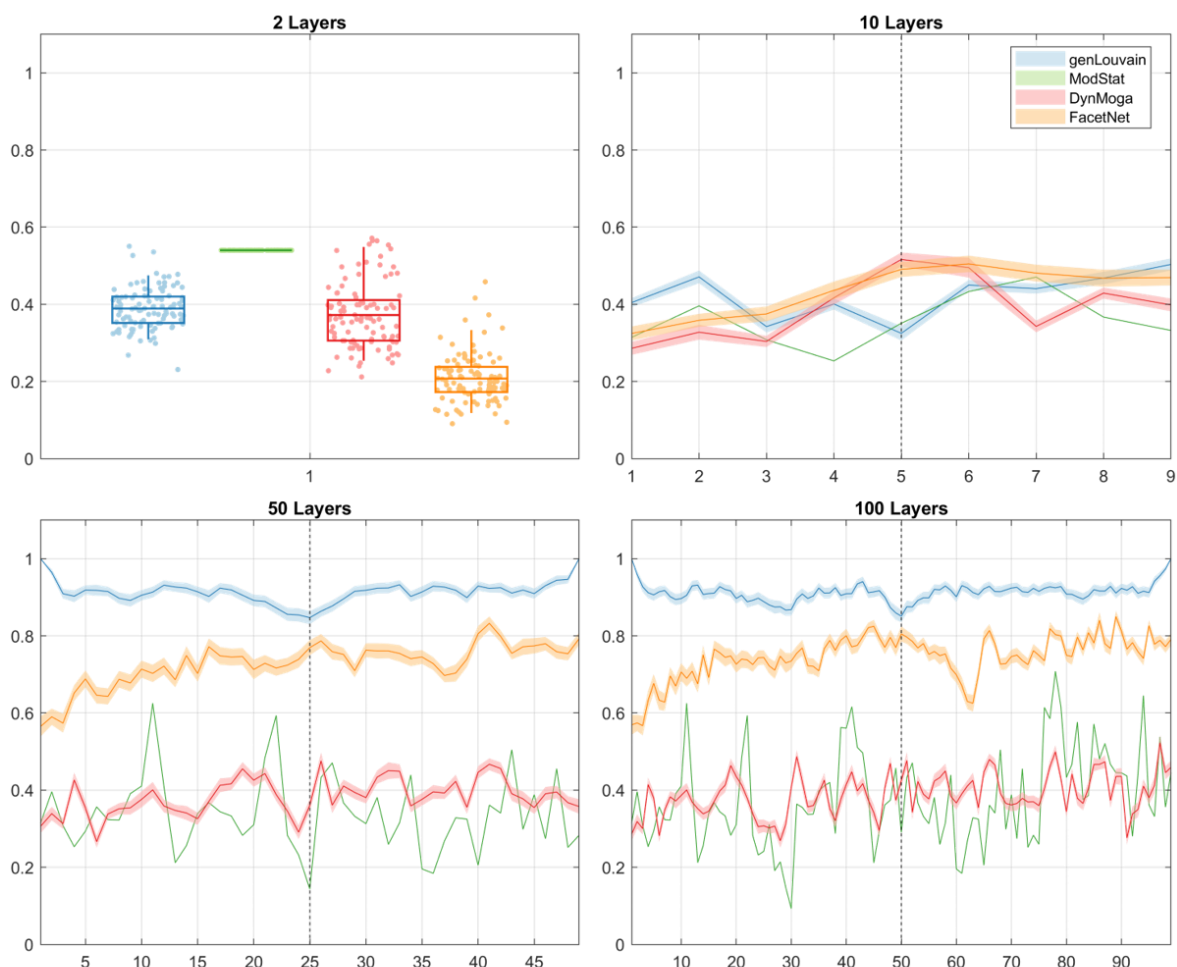


Figure 1.7. Normalized Mutual Information computed between the output of the algorithms, identified with color-code, at consecutive layers of the multilayers network. As we run the algorithms 100 times we report the means of the NMI at each snapshot, bounded by the confidence interval, represented with a lighter color. Each graph corresponds to one of the 4 networks extracted with different number of layers.

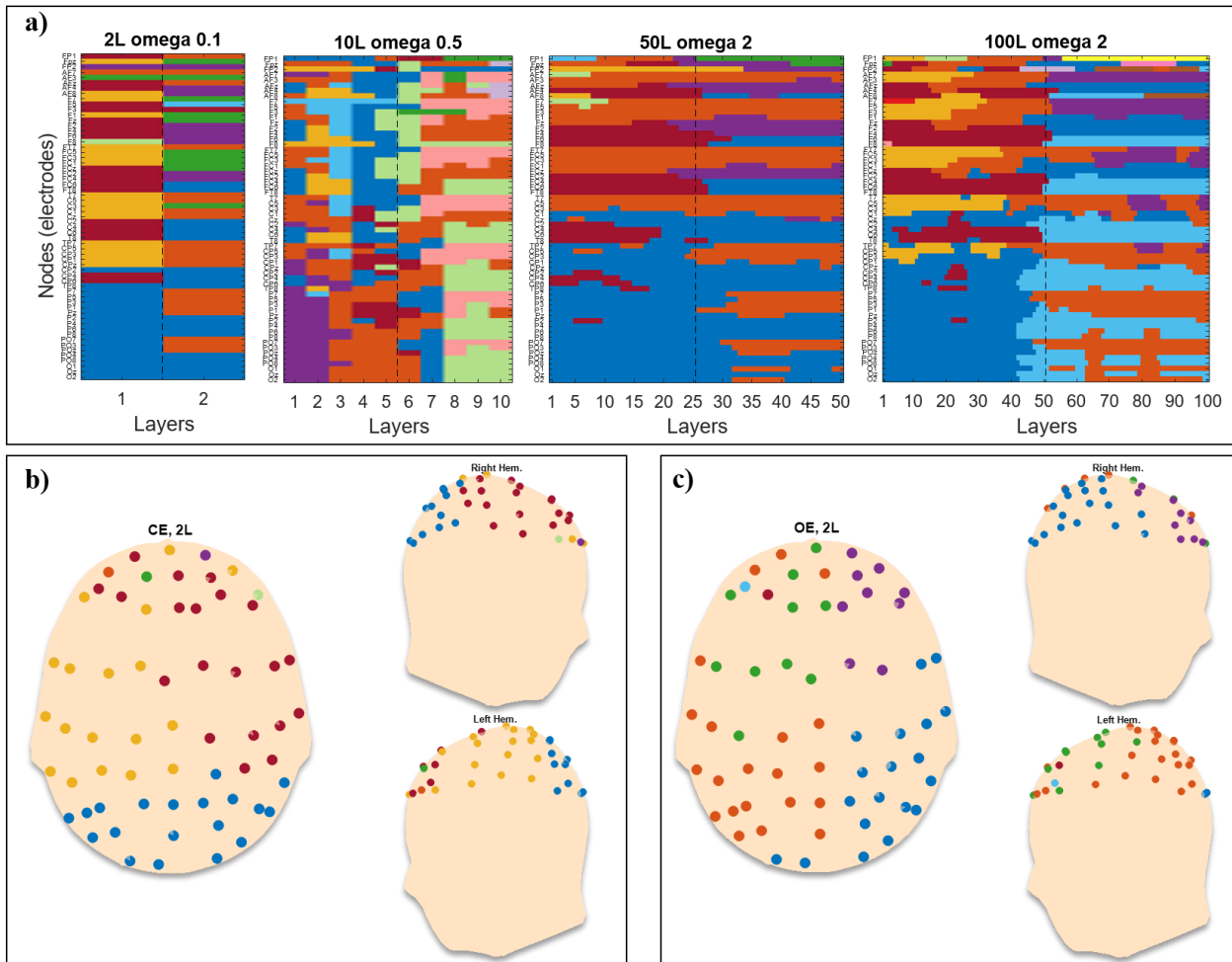


Figure 1.8. Example of partitions obtained by running *genLouvain* on the EEG brain networks. In panel a, the four images stand for the four networks with different number of layers. Each image has on the y-axis the nodes (channels), on the x-axis the layers, and cluster's membership is represented through colors. In panel b and c are reported projections of the detected communities on a 3D model of scalp for the two conditions CE and OE respectively. In each panel the 3D model is seen from above, with the nose pointing to the upper side of the page, and laterally. The dots are the 61 electrodes, grouped into clusters displayed with different colors.

1.4. Discussion

This work aims to provide guidelines for the use of multilayer algorithms of community detection on brain networks. For this purpose, we tested and compared them on an artificial dataset that spans a wide range of network's features.

We obtained our dataset by defining and implementing a tool able to generate pseudo-random multilayer networks with community structure. Among all the definitions of communities, we are considering the assortative one, namely communities made of groups of nodes densely connected with each other, and poorly connected with the other

nodes of the network. In fact, previous findings have shown that this is a very plausible way with which nodes organize themselves in brain networks (Bertolero et al., 2015; Sporns and Betzel, 2016). With respect to previously introduced tools (Granell et al., 2015; Kim and Han, 2009; Lin et al., 2008), we conceived this generator in a way that it can have as input as many settable parameters as possible, so that we could be able to simulate a variety of conditions with which testing the algorithms. In particular a potential user can set as input the number of nodes, graph density, number of communities, ratio between intra-clusters and inter-clusters density, level of noise of the network, percentage of nodes shifting community across layers, and if the number of clusters diminishes, increases or remain unchanged across layers. Thus, the main advantage of this generator is its flexibility in creating networks with different properties. Hence, we simulated multilayer networks with features that are observable to brain functional networks estimated from EEG signals. We then considered two cases in which the community structure is stationary, or it presents an evolution across the layers. While previous studies essentially focused on the second case, both cases are of great interest in the neuroscience field, as they both are possible cases of study. In the first case we aim to extract homogeneous community partitions among a certain number of networks, and this could be useful when analyzing groups of subjects with same features, or tasks in which the brain connectivity pattern is supposed to be stationary with the only variations due to the noise. In this case we seek algorithms able to be as much stable as possible avoiding the noise, that in EEG based network could arise because of acquisition's inaccuracy or connectivity estimation error. In the second case of evolving community structure we want our algorithm to track small and big variations as fast as possible. This could be reported to the case in which we want to identify the modular organization underpinning cognitive functions relative to dynamic tasks, or the differences between heterogeneous groups of people (e.g. healthy subjects and clinical cohorts).

The results of the simulation studies show that all the algorithms are sensitive to the network's features that we simulated. As one can imagine, their performances decrease as the level of noise simulated increases, because the community structure gets less and

less clear. Moreover, their ability to exactly recover the imposed community structure diminishes when such structure is made of few clusters. In the second case, of time-varying communities, our analysis suggests that the proportion with which the clusters reconfigure does not affect consistently the algorithms' performances, except in few cases in which, intuitively, the more it changes the easier the algorithms detect the variation. Genlouvain, the algorithm based on the optimization of the multilayer formulation of modularity, outperforms compared to the others.

Our work is not the first one attempting to address the issue of multilayer clustering algorithms performances. In (Silva et al., 2016) and in (Schmidt et al., 2018) authors propose a similar analysis. However, in the former, the focus is only on algorithms based on evolutionary clustering, which have been tested in a simple synthetic network and in three real networks not neuroscience related. In the latter authors tested two approaches based on consensus clustering on a synthetic network. Still, such testing has not statistical validity, as the two approaches have only been tested in one network, even if more realistic and closer to those experimentally estimated from EEG signals. Moreover, that work differs from ours as their main purpose was to exploit multilayer clustering approaches to threshold fully connected networks. For this reason, they introduced two new community detection algorithms, rather than considering the well-established multilayer optimization of modularity, which has already been proven to provide interesting insights into the brain functioning and organization, as in (Bassett et al., 2011b). Another testing of the clustering algorithms has been done in (Bazzi et al., 2019) on benchmark networks similar to those here proposed. However, the main focus of that work was introducing a generative model for multilayer networks, so that the algorithms performances have been evaluated only varying the coupling across layers. Here we performed a more comprehensive analysis, comparing the algorithms' behaviour systematically varying a set of network's features, like cluster number, level of noise, coupling across layers, number of layers and network's density.

After having tested the algorithms on artificial networks we also looked for a proof of concept in a real EEG dataset with controlled conditions. The dataset consisted of signals

collected during sessions of open and closed eyes resting state, from which we estimated multilayer networks in which the first half of the layer was relative to one condition and the second half to the other condition. We considered different values of number of layers in accordance with the analysis made on artificial networks. The results agree with what previously found. In fact, genlouvain seems the best algorithm also in this case. It is the one that, more than the others, detect quite stable communities within the two conditions and differences in the partitioning between the two conditions. The topological representation of the community organization underlying the two conditions tells us that the closed eyes condition gives rise to a cluster made of occipital electrodes - brain areas. On the other side, during the open eyes condition, this cluster splits into two clusters, one for each hemisphere, and in general, all the clusters become more hemispheric specific. This result is physiologically plausible. In fact, during the resting state at closed eyes there is an increase of alpha rhythm associated with circuits originated in the occipital region, which disappears if the subject opens his eye.

The purpose of this application to an EEG dataset was threefold. First of all, it confirms the results obtained with the simulation studies. Moreover, as an indirect consequence, it validates the goodness of our model and our generator with which we tested the algorithms. Finally, it supports the applicability of community detection to EEG based brain networks. In fact, while several studies already shown the potentiality of employing graph theory instruments in EEG derived networks to investigate brain functioning (Fallani et al., 2010; Micheloyannis et al., 2006; Petti et al., 2016; Pichiorri et al., 2018), community detection has been poorly investigated in the electrophysiological context. Rather, most of the studies, (Bassett et al., 2011b; Betzel et al., 2014, 2017; Wig, 2017) just to cite a few of them, focused on the analysis of the communities in neuroscience are carried on brain networks obtained from Magnetic Resonance Images. MRI data have the privilege of having a good spatial resolution, however, EEG signals have a great temporal resolution, which is what is needed to study time-varying phenomena through a multilayer analysis. For this reason, future focus will be on studying how community structure evolves during tasks that elicit a dynamic configuration of the brain network,

because this might provide interesting insights into brain functional organizational principles underlying cognitive functions.

Future investigations might also include the use of the toolbox that we furnished to extend our analysis to other cases. For example, a similar analysis could be made generating networks with a higher number of nodes and consequently also a higher number of clusters. Ultimately, this work could be useful in a cross-disciplinary way, regardless of our specific attention to EEG based brain networks. In fact, the guidelines we provide can be applied to every network with these (multiple) simulated features, where community structure is supposed to be assortative.

1.5. Conclusion

In conclusion, this work operated a comparative analysis among multilayer community detection algorithms. We selected three different clustering approaches based on single layer modularity, multilayer modularity, and evolutionary clustering. We tested them on artificial networks with modules generated through a toolbox defined for this purpose, which allows to set as input most of the parameters characterizing the graphs, that we systematically varied, in a range typical of EEG based brain networks, in order to provide a comprehensive analysis of the algorithms. Specifically, we tested the algorithms' ability to recover stable and dynamic partitions out of multilayer networks with stationary and evolving community structure, respectively. Our results suggest that the performance of the algorithms depends on the network's features, such as number of clusters, number of layers and level of noise in the network. After the simulations studies, the community detection algorithm based on the optimization of the multilayer formulation of modularity turned out to be the most suitable within the simulated conditions. The application of the algorithms to real networks estimated from EEG signals confirms these results and prove the applicability of such algorithms to electrophysiological data.

1.6. Supplementary material

1.6.1. Comparative analysis on networks with evolving community structure and increasing or decreasing clusters number

Here, we report the results of the simulation studies implanted as in section 1.2.2.2. but in which we evaluated the algorithms' performances in recovering a dynamic community structure with increasing or decreasing clusters number. We present results in figures S1-S2 (increasing) and S3-S4 (decreasing), where we show the algorithms' performance under the accuracy and dynamicity point of view.

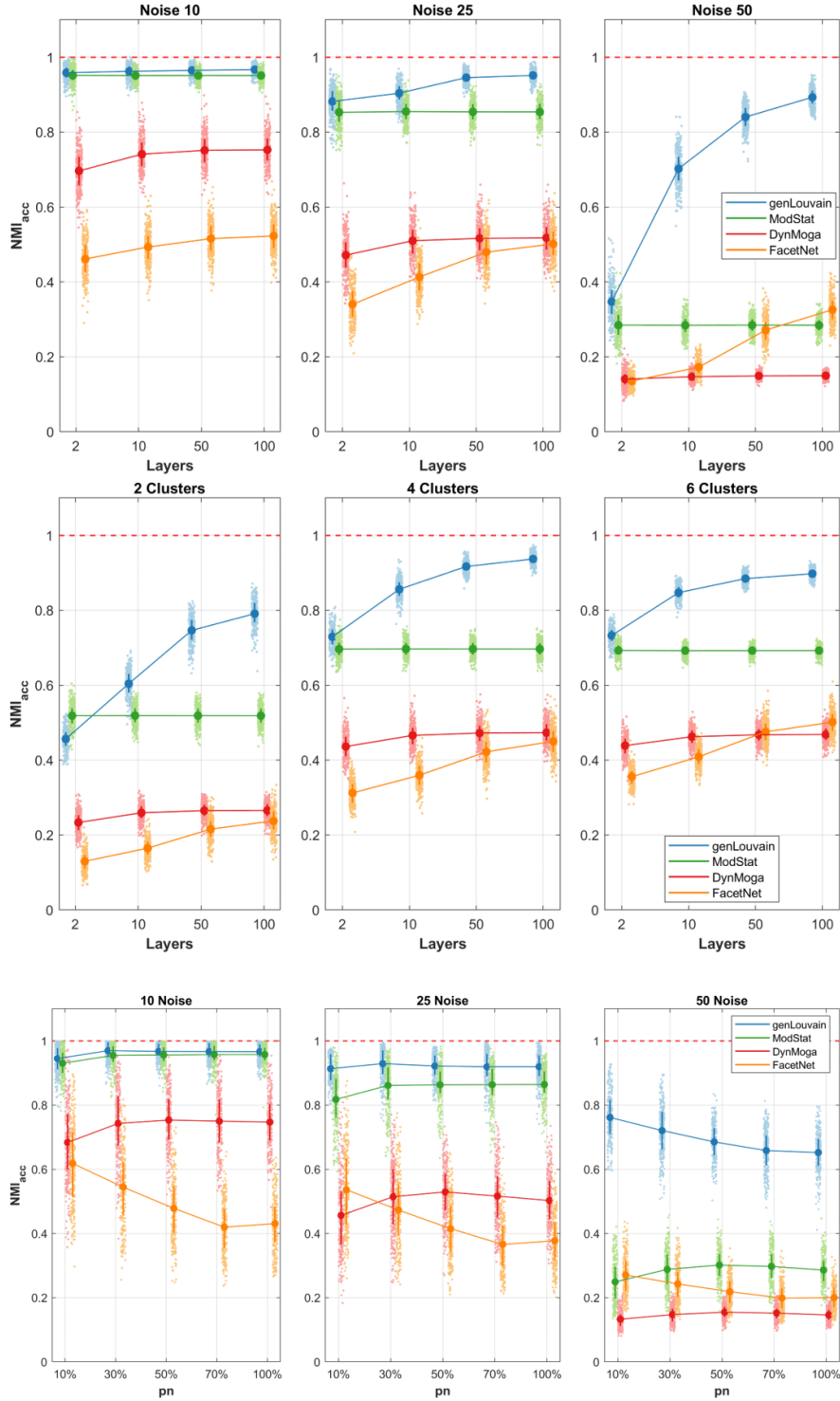


Figure S1. Plot of means and standard deviations of NMI_{acc} in the comparative analysis on networks with evolving community structure with increasing clusters number. In the first row we report the accuracy of the algorithms, identified with different colors, with respect to the different levels of number of layers, x-axis, and percentage of noise, columns. In the second row we show the trend of the algorithms' accuracies with respect to the number of layers, x-axis, and clusters number, columns. In the third row we represent the accuracies mean values for each algorithm to varying of the factor pn , x-axis, and level of noise, columns

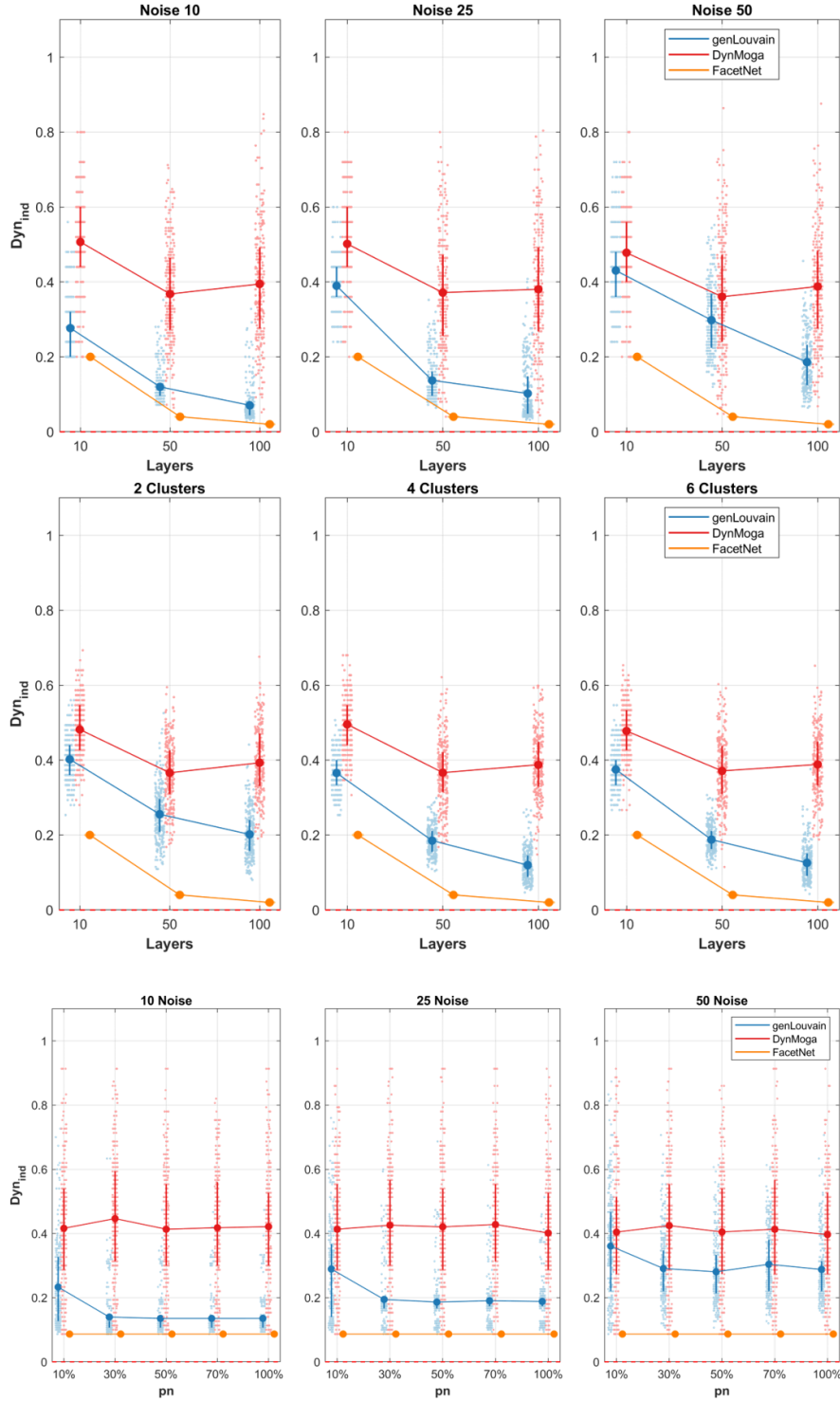


Figure S2. Plot of means and standard deviations of Dyn_{ind} in the comparative analysis on networks with evolving community structure with increasing clusters number. In the first row we report the dynamic of the algorithms, identified with different colors, with respect to the different levels of number of layers, x-axis, and percentage of noise, columns. In the second row we show the trend of the algorithms' speed with respect to the number of layers, x-axis, and clusters number, columns. In the third row we represent the Dyn_{ind} mean values for each algorithm to varying of the factor pn , x-axis, and level of noise, columns

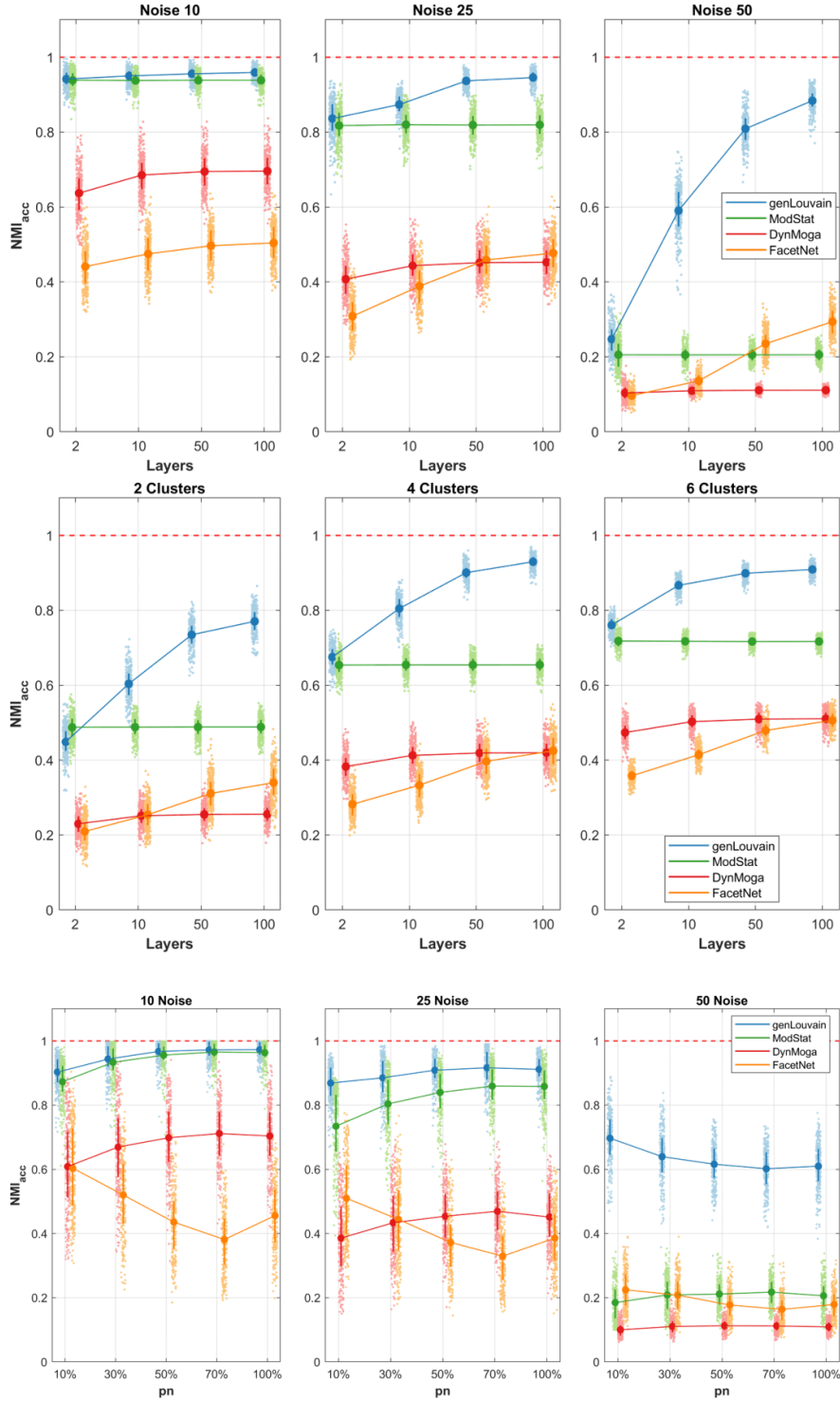


Figure S3. Plot of means and standard deviations of NMI_{acc} in the comparative analysis on networks with evolving community structure with decreasing clusters number. In the first row we report the accuracy of the algorithms, identified with different colors, with respect to the different levels of number of layers, x-axis, and percentage of noise, columns. In the second row we show the trend of the algorithms' accuracies with respect to the number of layers, x-axis, and clusters number, columns. In the third row we represent the accuracies mean values for each algorithm to varying of the factor pn , x-axis, and level of noise, columns

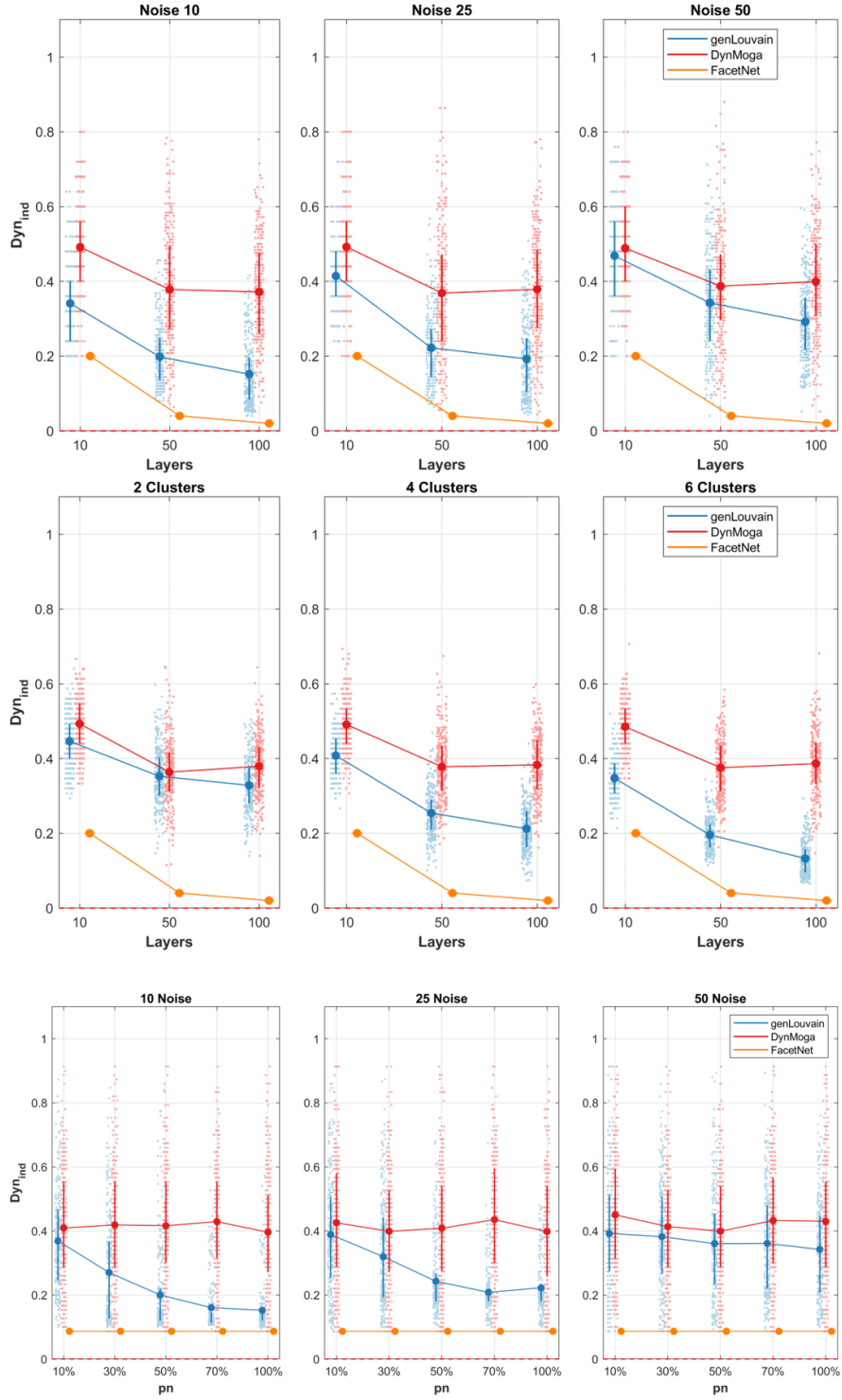


Figure S4. Plot of means and standard deviations of Dyn_{ind} in the comparative analysis on networks with evolving community structure with decreasing clusters number. In the first row we report the dynamic of the algorithms, identified with different colors, with respect to the different levels of number of layers, x-axis, and percentage of noise, columns. In the second row we show the trend of the algorithms' speed with respect to the number of layers, x-axis, and clusters number, columns. In the third row we represent the Dyn_{ind} mean values for each algorithm to varying of the factor pn , x-axis, and level of noise, columns

The accuracy trends remain similar to those shown in the main analysis, with all the algorithms displaying a higher accuracy in non-noisy networks and with more than two clusters. In these two cases too, the algorithms genLouvain and FacetNet are the only ones whose performance depends on the number of layers in a proportional way. One difference instead is that when the clusters of the network augment or diminish the algorithm DynMOGA show better performance than FacetNet. GenLouvain and ModStat are still the best algorithms, with the first outperforming the second in networks with increasing noise and layers. This time, the factor p influences a bit more the algorithms' behavior. In network with noise $n < 50\%$ all the algorithms are more accurate when the number of nodes changing cluster is high, meaning that they are more suitable to detect big changes, except for FacetNet who presents an opposite trend. This is true above all in the case in which the number of clusters in the networks diminishes. The evaluation through the dynamic index provided similar results described in the main analysis.

1.6.2. Comparative analysis on networks with lower graph density

In this section, we present the results of the simulation studies through which we analyzed and compared the performances of the community detection algorithms on graphs with a lower density value, set to 0.1. In figures S5 and S6 we report the results of the study made on networks with stationary community structure, while in figures S7 and S8 those of the study made on networks with evolving community structure (as designed in sections 1.2.2.1 and 1.2.2.2, respectively).

In both cases (stationary and evolving community structure) the trends of the algorithms' accuracy and stability/dynamicity over the different combinations of the factors do not change substantially with respect to the analysis shown with $D = 0.3$. The main difference is that with lower density all the algorithms globally perform worst, especially when the networks are made of few clusters (i.e. two clusters).

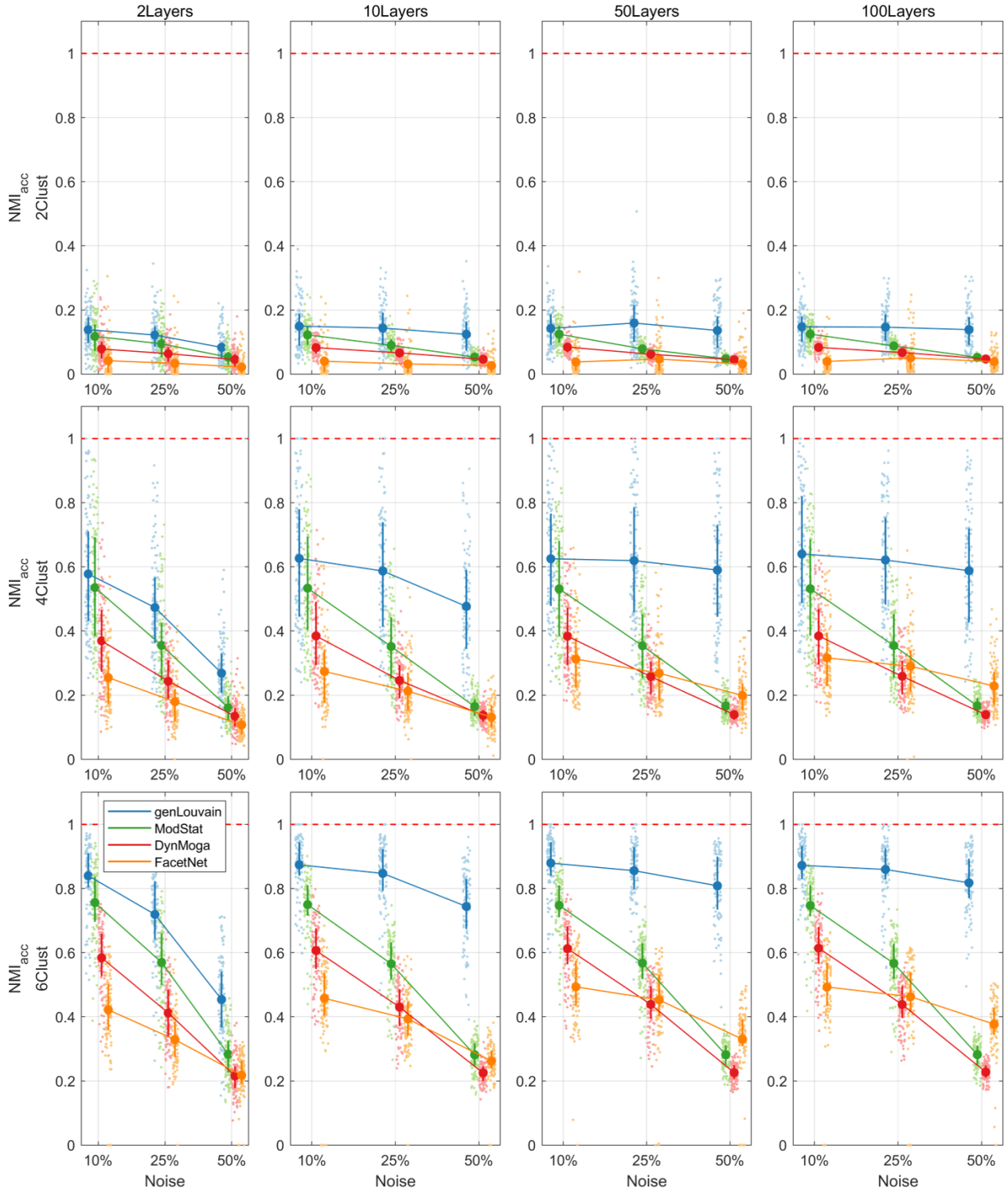


Figure S5. Plot of means and standard deviations of NMI_{acc} in the comparative analysis on networks with $D=0.1$ and stationary community structure. In the rows and the columns of the pictures we report the results for different levels of clusters number (CN) and number of layers (nL) respectively. In each subplot the NMI_{acc} of each algorithm, identified with colors code, is shown for the different levels of percentage of noise (no).

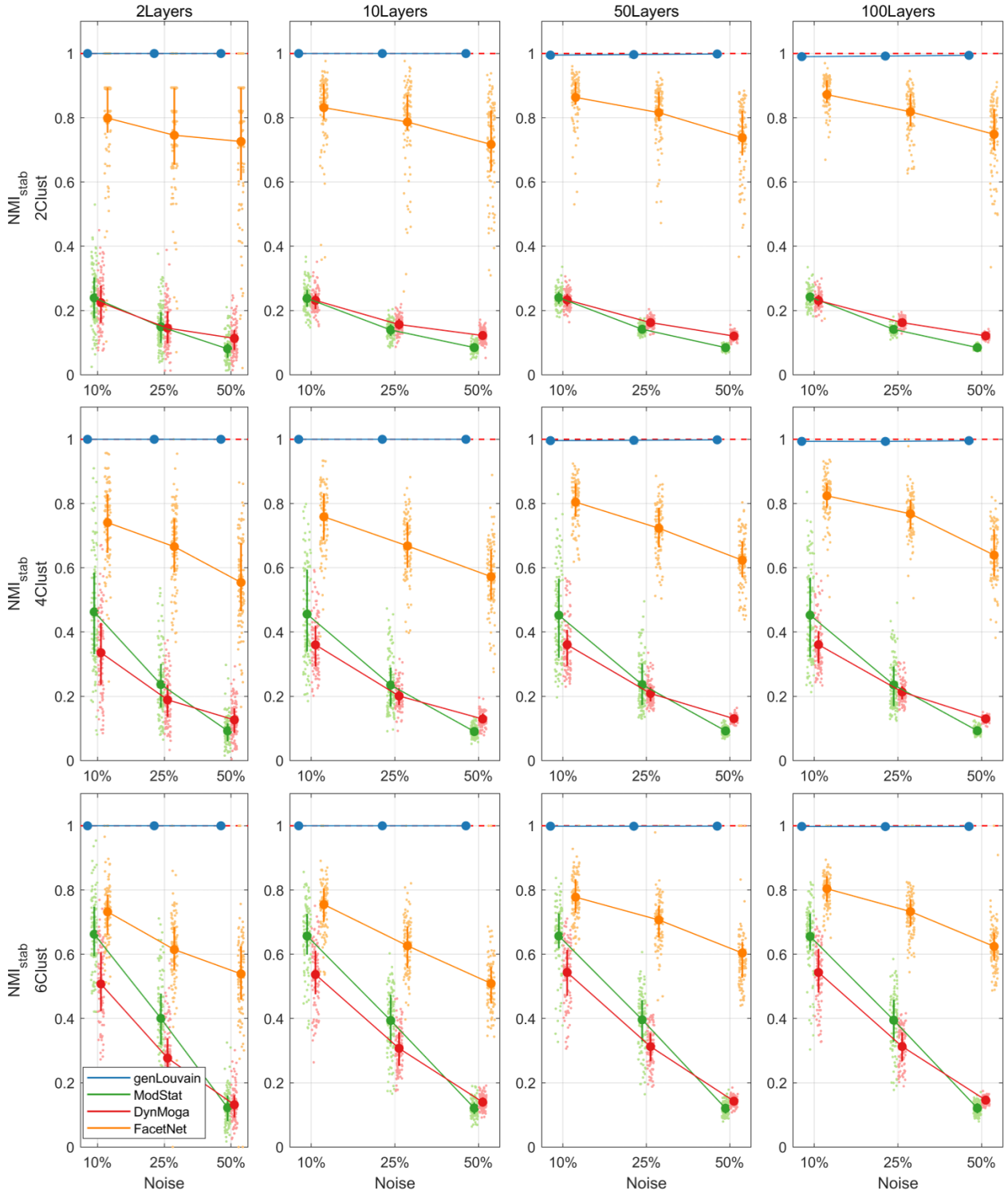


Figure S6. Plot of means and standard deviations of NMI_{stab} in the comparative analysis on networks with $D=0.1$ and stationary community structure. In the rows and the columns of the pictures we report the results for different levels of clusters number (CN) and number of layers (nL) respectively. In each subplot the NMI_{stab} of each algorithm, identified with colors code, is shown for the different levels of percentage of noise (no).

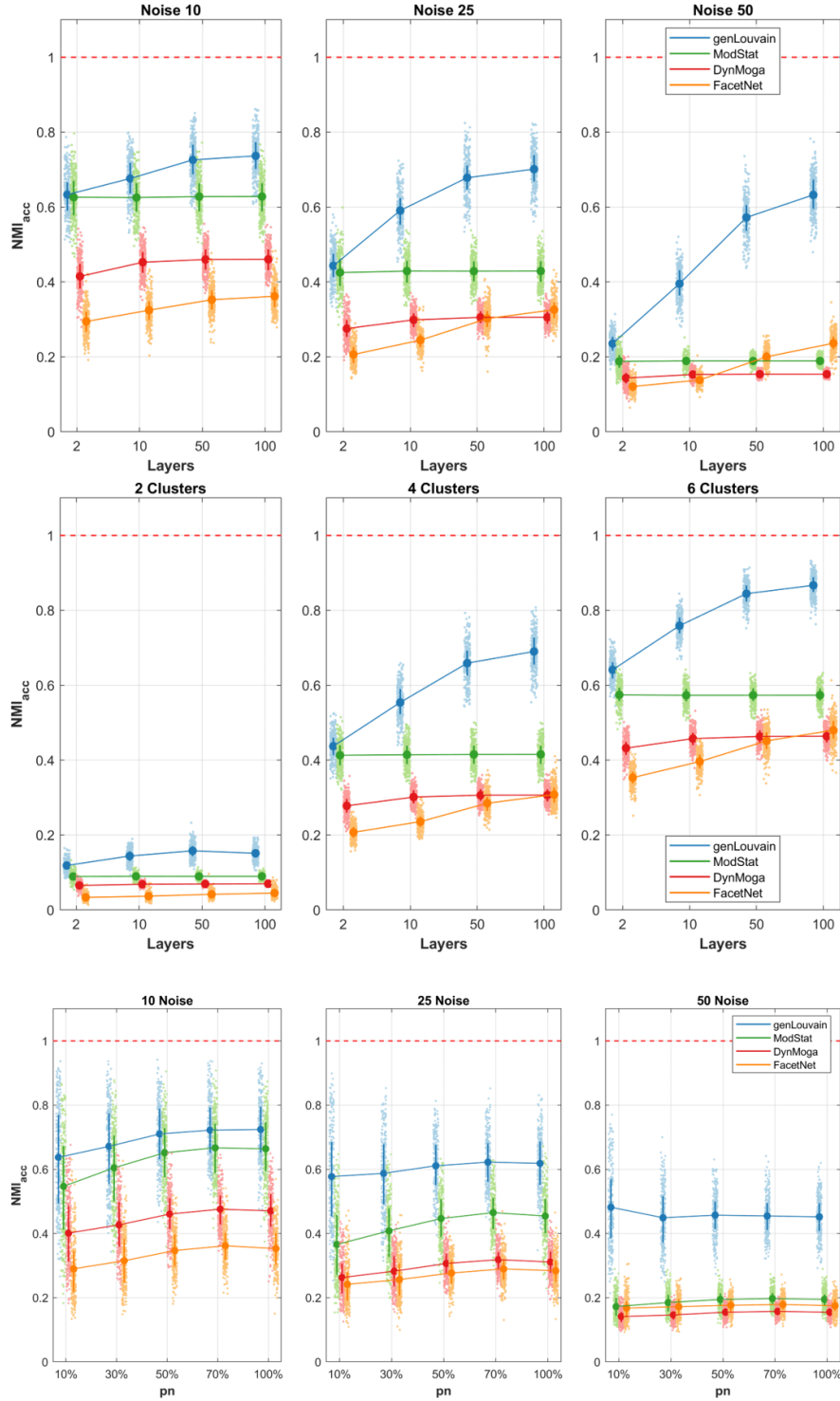


Figure S7. Plot of means and standard deviations of NMI_{acc} in the comparative analysis on networks with $D=0.1$ evolving community structure. In the first row we report the accuracy of the algorithms, identified with different colors, with respect to the different levels of number of layers, x-axis, and percentage of noise, columns. In the second row we show the trend of the algorithms' accuracies with respect to the number of layers, x-axis, and clusters number, columns. In the third row we represent the accuracies mean values for each algorithm to varying of the factor pn , x-axis, and level of noise, columns.

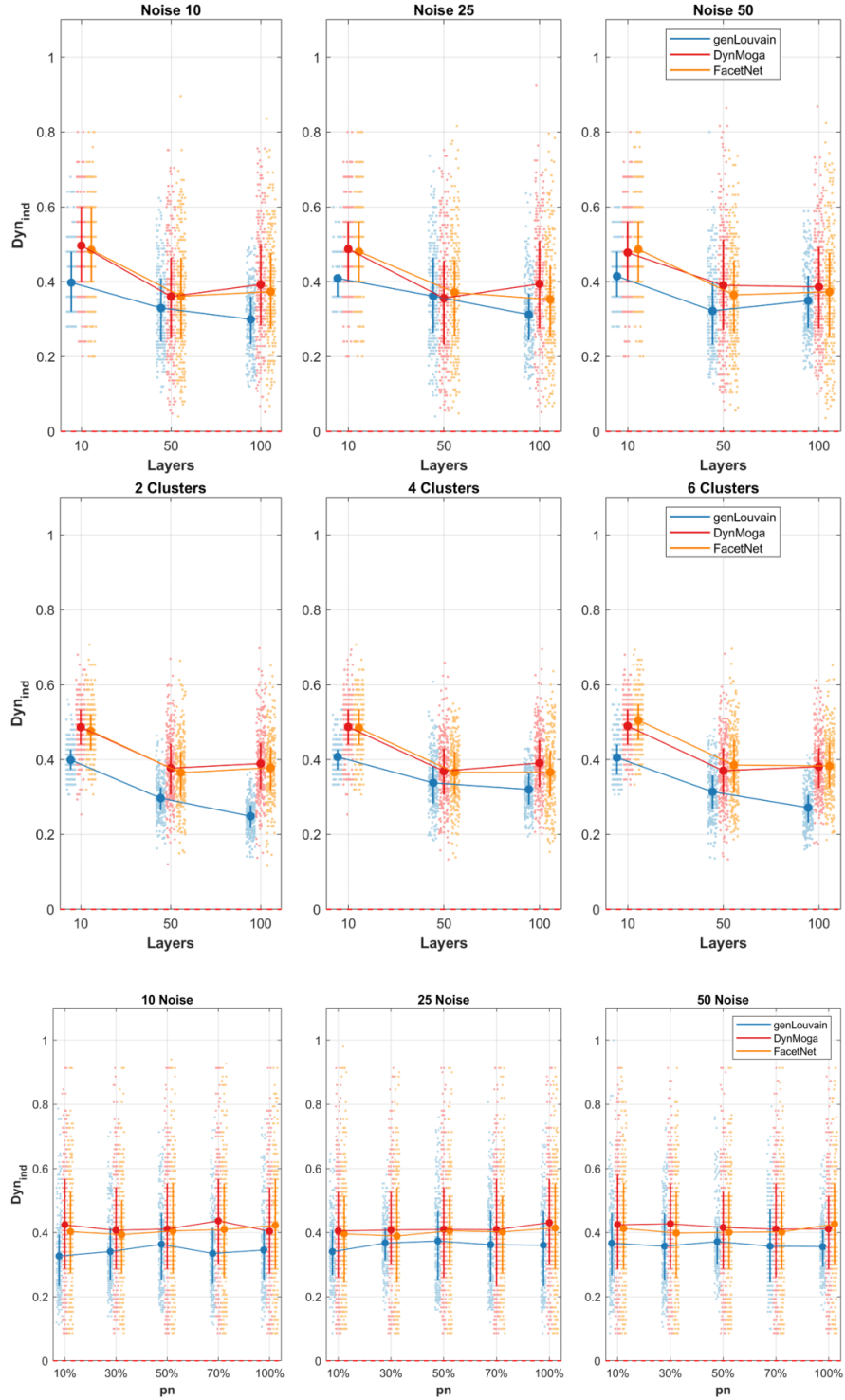


Figure S8. Plot of means and standard deviations of Dyn_{ind} in the comparative analysis on networks with $D=0.1$ evolving community structure. In the first row we report the dynamic of the algorithms, identified with different colors, with respect to the different levels of number of layers, x-axis, and percentage of noise, columns. In the second row we show the trend of the algorithms' speed with respect to the number of layers, x-axis, and clusters number, columns. In the third row we represent the Dyn_{ind} mean values for each algorithm to varying of the factor pn , x-axis, and level of noise, columns.

1.6.3. Preliminary investigation on the temporal resolution parameter in the multilayer modularity optimization algorithm, genlouvain

The genLouvain algorithm depends on two resolution parameters, γ and ω , which impact the dimension of the recovered clusters and their coupling across the layers, respectively. Several studies have already pointed out how modularity-based algorithms perform changing γ , and several strategies have been developed to select proper values. This work focuses on the multilayer aspect of the modules' detection, so that our focus was on the evaluation of the behavior of genLouvain with different ω -values. Thus, while setting $\gamma = 1$ (its default value), we explored the range $\omega = \{0.1, 0.2, 0.5, 1, 2, 5, 10\}$, in both cases where community structure is stationary over the layers or it changes. We implanted two simulation studies as in 1.2.2.1 and 1.2.2.2 replacing the factor *algorithm* with the new factor ω . Part of these results have been shown in (Puxeddu et al., 2019).

In figures S9 and S10 we reported the results obtained in the first case (stationary community structure), under the accuracy and stability point of view, respectively. The algorithm shows high values of accuracy in networks with low noise level, number of clusters ≥ 4 , no matter with which ω -value. However, higher values ($\omega > 0.5$) are more suitable when the noise increases, above all in networks made of several layers. Exploiting genLouvain with high $\omega > 0.5$ guarantees an optimum level of accuracy even with $n=50\%$. The analysis of the algorithm's stability led to analogous insights.

In figure S11 and S12 we reported the results obtained in the second case (evolving community structure), under the accuracy and dynamicity point of view, respectively. In this case, the number of layers plays a key role in the choice of ω . Indeed, overall our results suggest that when the change of the community structure happens rapidly, in few layers (e.g. when we are observing time-varying phenomena), low ω -values are more suitable ($\omega < 1$) and provide higher accuracy of the output partition. On the contrary, when the change separates two community structures that are stable over several layers (e.g. when we are observing networks underlying two different tasks) higher ω -values are more advisable. This is even truer in noisy networks. Intuitively, the lower the ω , the more genLouvain acts as a single-layer modularity algorithm. Therefore, the accuracy of

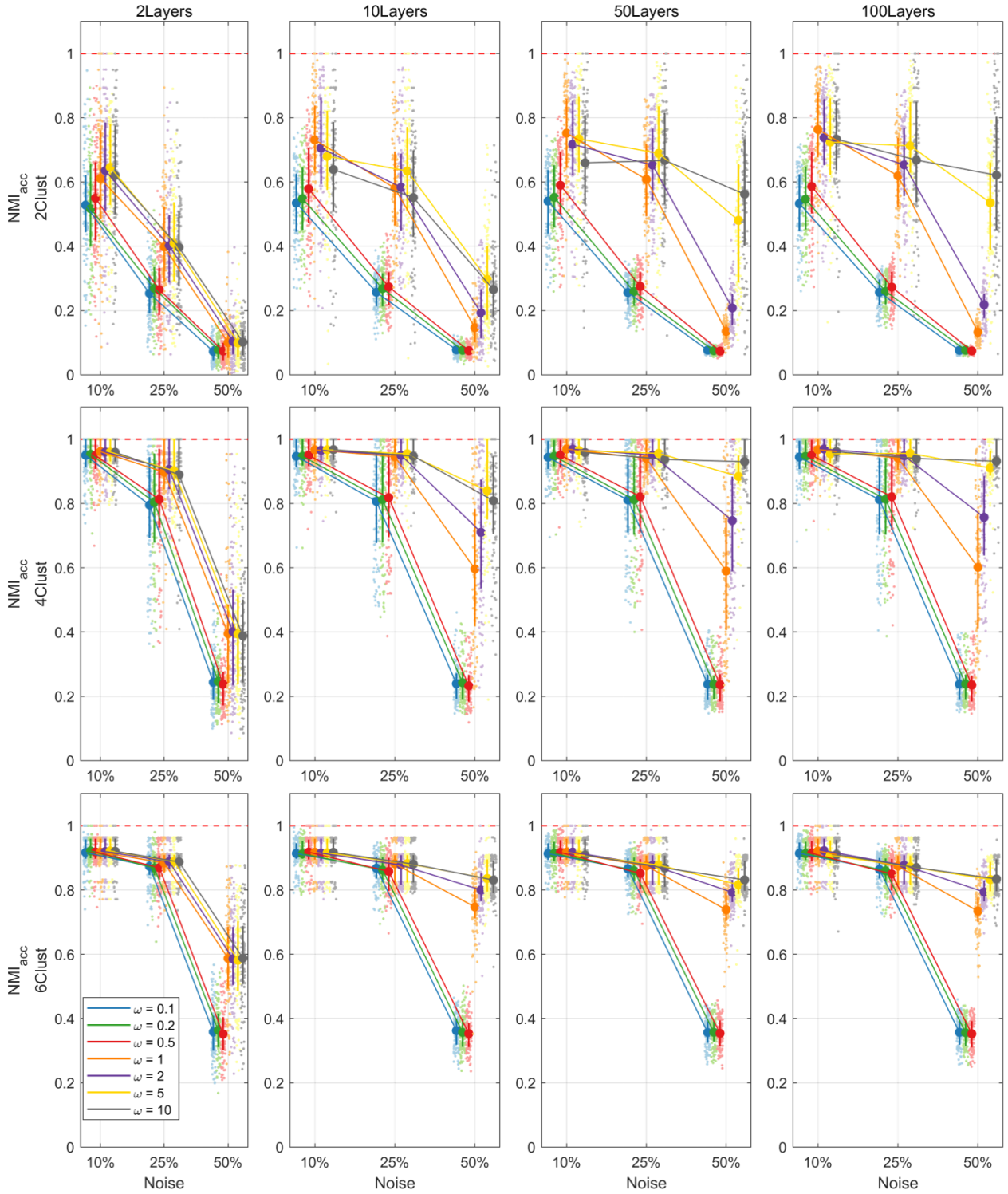


Figure S9. Plot of means and standard deviations of NMI_{acc} in the preliminary analysis regarding genlouvain on networks with stationary community structure. In the rows and the columns of the pictures we report the results for different levels of clusters number (CN) and number of layers (nL) respectively. In each subplot the NMI_{acc} of each algorithm, identified with colors code, is shown for the different levels of percentage of noise (no).

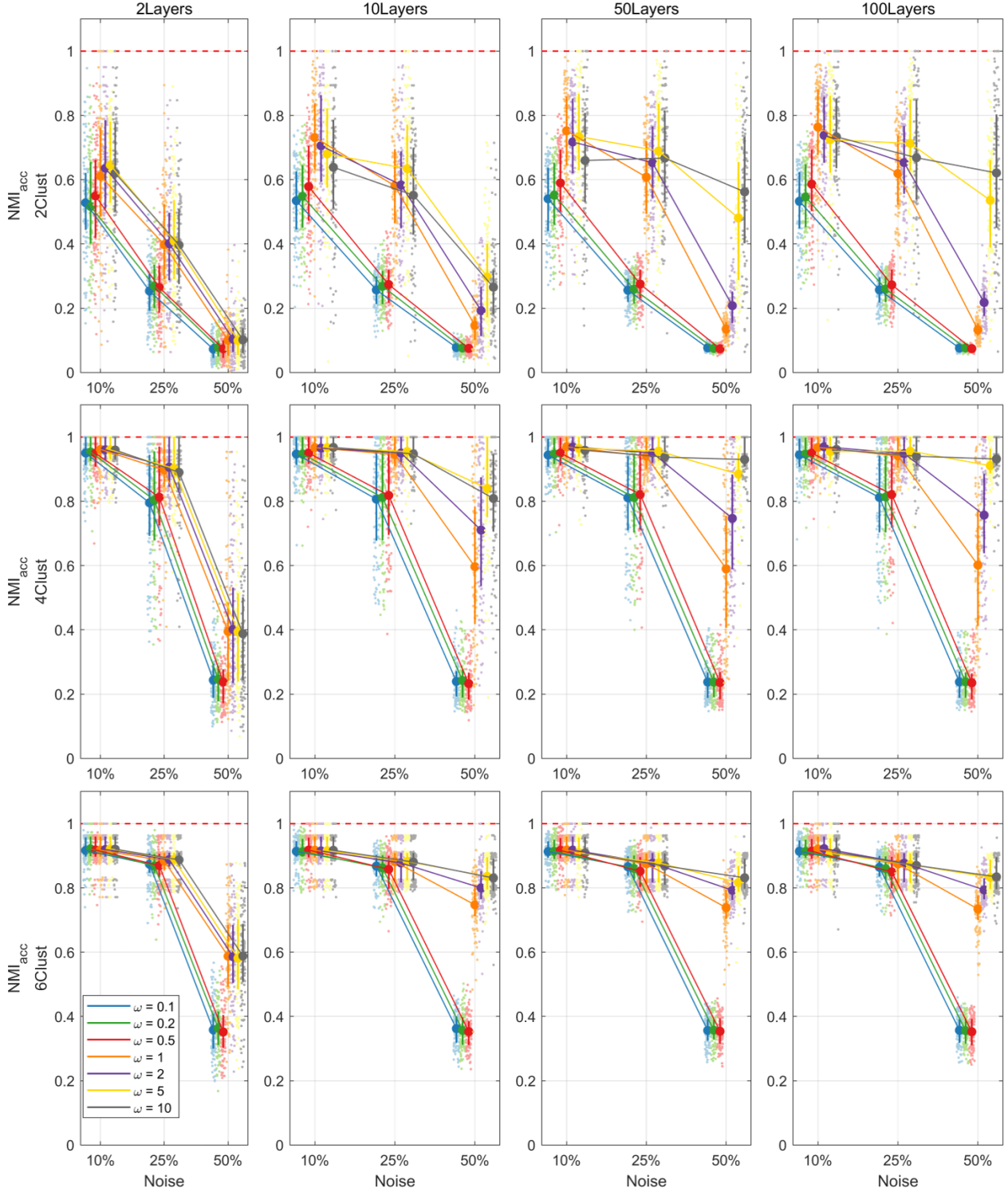


Figure S10. Plot of means and standard deviations of NMI_{stab} in the preliminary analysis regarding genlouvain on networks with stationary community structure. In the rows and the columns of the pictures we report the results for different levels of clusters number (CN) and number of layers (nL) respectively. In each subplot the NMI_{stab} of each algorithm, identified with colors code, is shown for the different levels of percentage of noise (no).

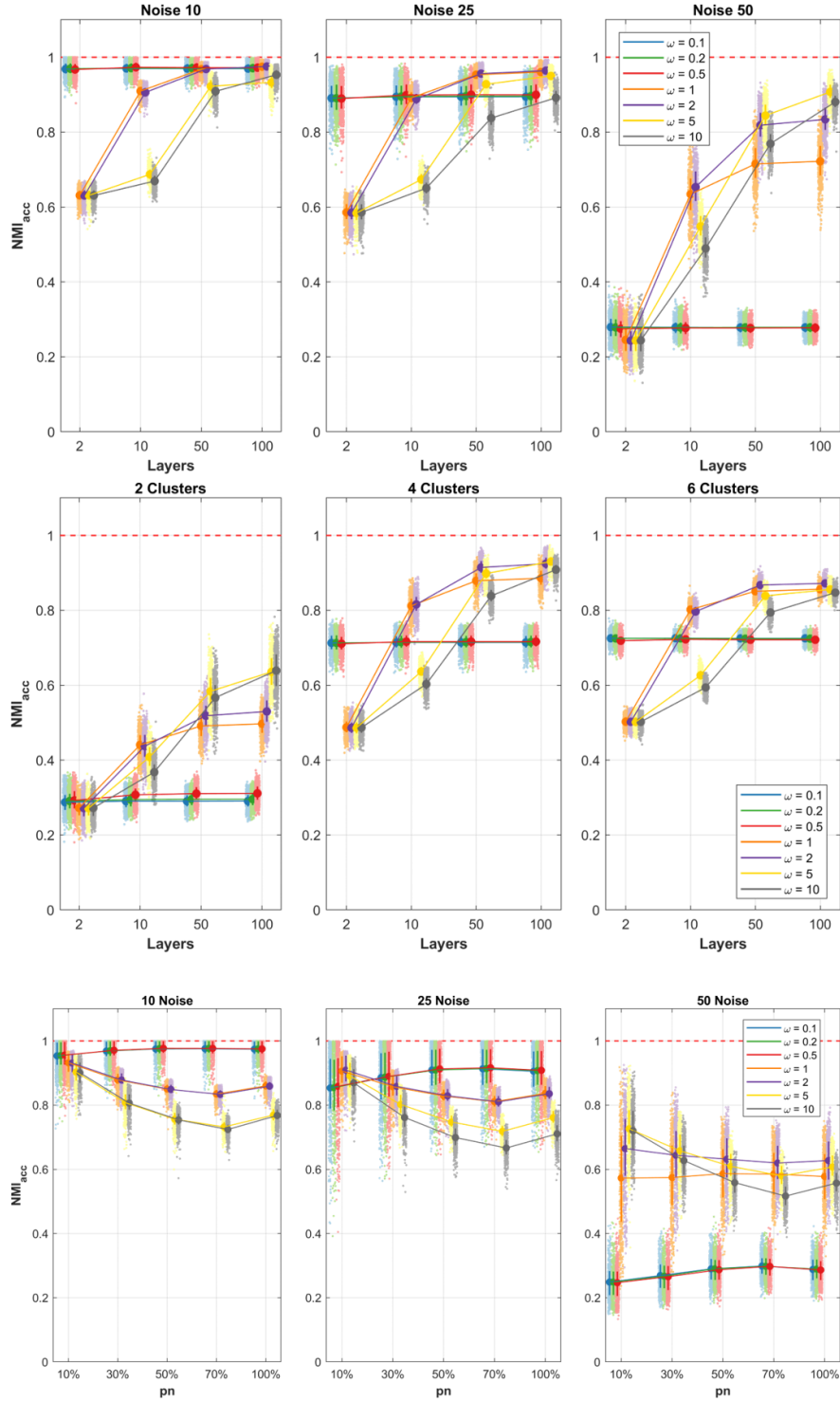


Figure S11. Plot of means and standard deviations of NMI_{acc} in the preliminary analysis regarding genlouvain on networks with evolving community structure. In the first row we report the accuracy of the algorithms, identified with different colors, with respect to the different levels of number of layers, x-axis, and percentage of noise, columns. In the second row we show the trend of the algorithms' accuracies with respect to the number of layers, x-axis, and clusters number, columns. In the third row we represent the accuracies mean values for each algorithm to varying of the factor pn , x-axis, and level of noise, columns.

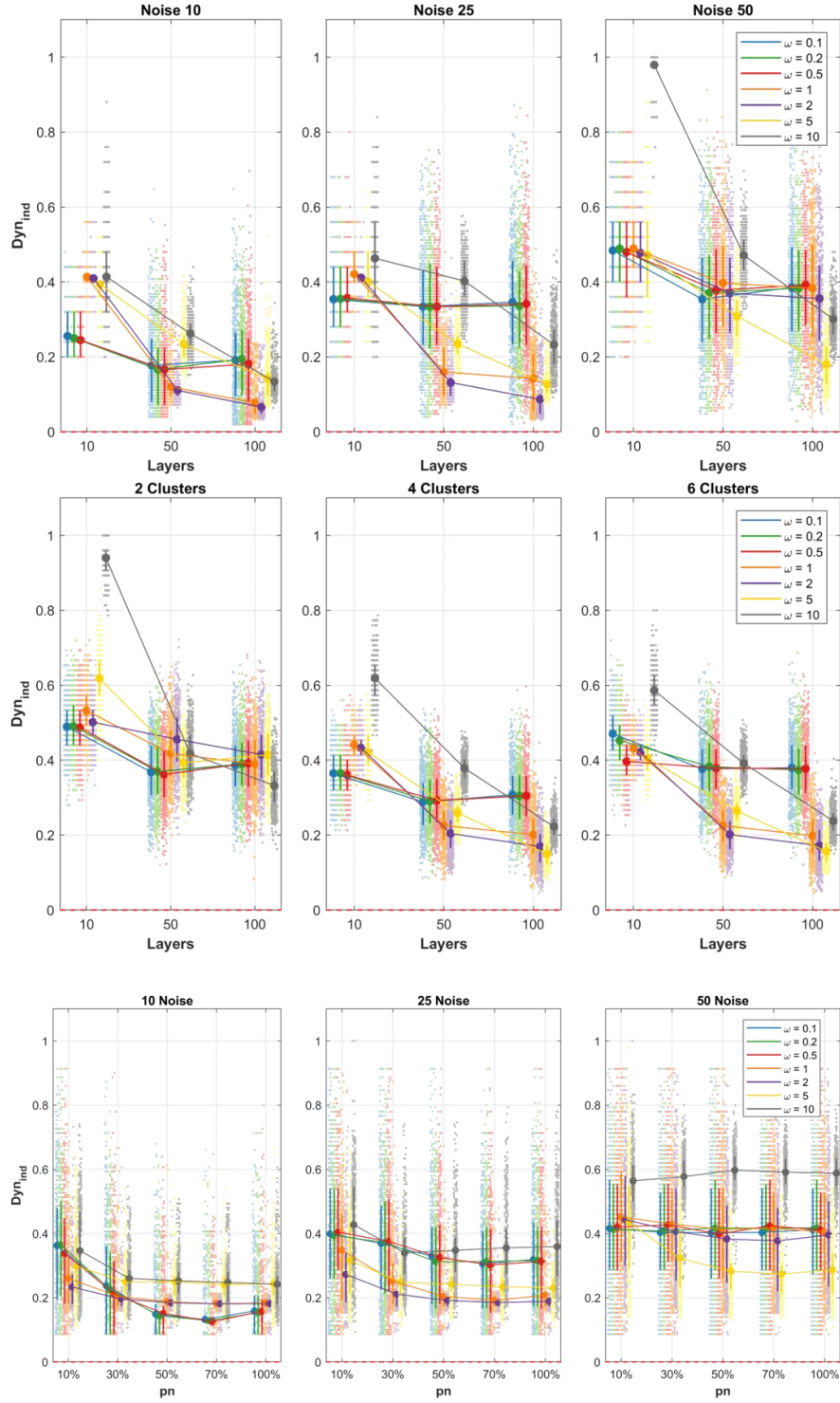


Figure S12. Plot of means and standard deviations of Dyn_{ind} in the preliminary analysis regarding genlouvain on networks with evolving community structure. In the first row we report the dynamic of the algorithms, identified with different colors, with respect to the different levels of number of layers, x-axis, and percentage of noise, columns. In the second row we show the trend of the algorithms' speed with respect to the number of layers, x-axis, and clusters number, columns. In the third row we represent the Dyn_{ind} mean values for each algorithm to varying of the factor pn , x-axis, and level of noise, columns.

genLouvain used with $\omega < 0.5$ neither depends on the number of layers, nor on the factor p , and is extremely sensitive to the noise. Similar reasoning can be done with the dynamic index. In fact, lower ω -values are preferable in networks made of few layers, meaning they tend to rapidly recover rapid changes. Higher ω -values instead are better when the change separates two stationary conditions.

1.6.4. Preliminary investigation on the trade-off parameter in the multi-objective function optimization algorithm, FacetNet

The FacetNet algorithm depends on a trade-off parameter, λ , that balance the accuracy of the partitions at each layer and their coupling over the layers. It can vary between 0 (no coupling among layers) and 1 (coupling across layers prevails over single-layer accuracy). We explored the behavior of FacetNet for $\lambda = \{0.1, 0.2, 0.5, 0.7, 0.8, 0.9, 1\}$, in both cases of stationary and evolving community structure. As in the previous paragraph, we implanted two simulation studies as in 1.2.2.1 and 1.2.2.2 replacing the factor *algorithm* with the new factor λ .

We report the results in the case of stationary community structure in Figures S13 and S14, where we show the algorithm's accuracy and stability, respectively. In this case, higher λ -values are always preferable. However, choosing $\lambda=1$, despite provides excellent stability of the algorithm's output, results in lower accuracy. Thus, the most suitable values are $\{0.8, 0.9\}$.

The results obtained on networks with evolving community structure are reported in Figure S15 and S16. From the dynamicity point of view, lower λ -values are always preferable. However, from the accuracy point of view, choosing higher λ -values provides better outputs in noisy networks made of many layers. On the contrary, if the network is not noisy or it has few layers (e.g. from 2 to 10) lower values are more suitable.

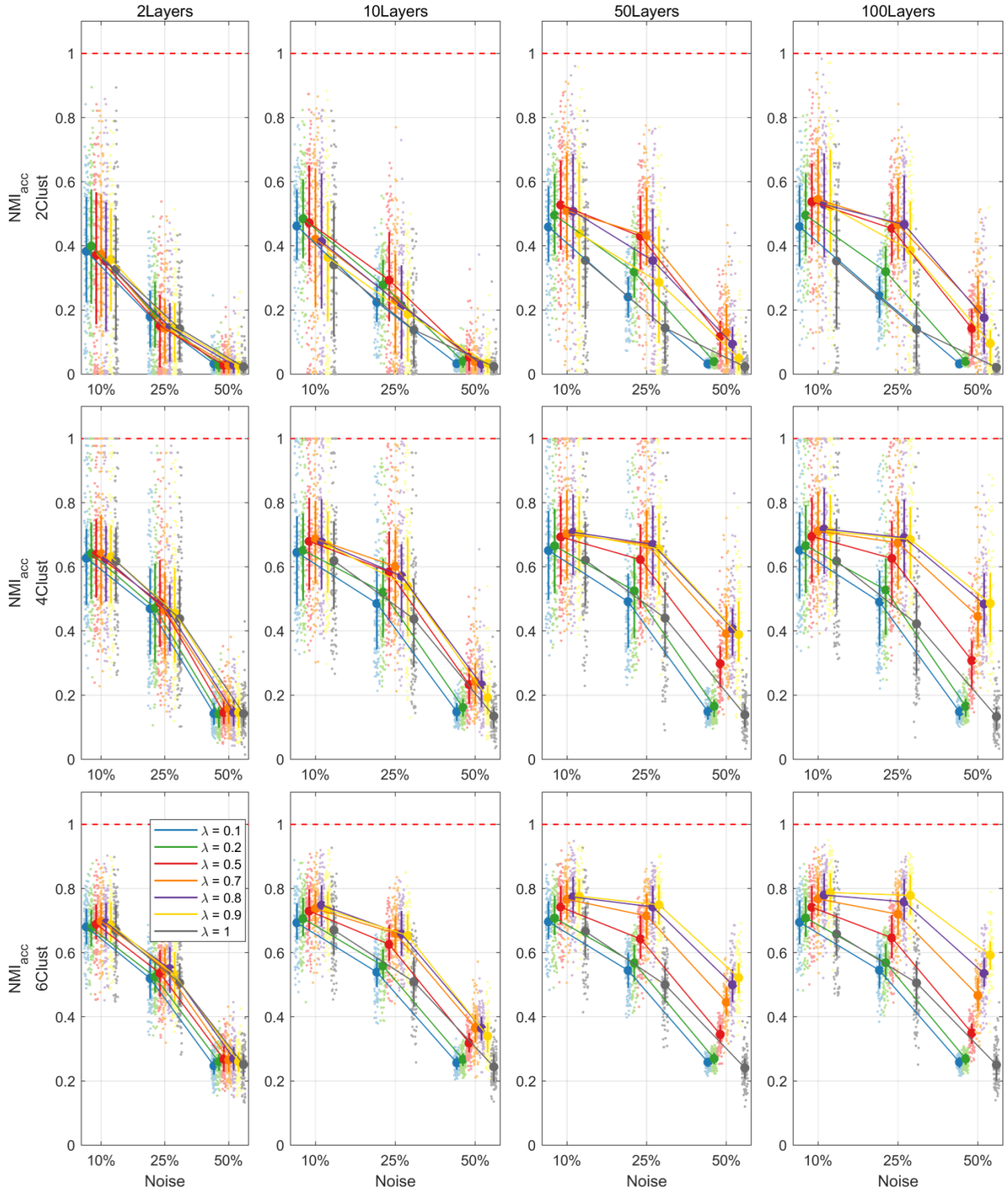


Figure S13. Plot of means and standard deviations of NMI_{acc} in the preliminary analysis regarding facetnet on networks with stationary community structure. In the rows and the columns of the pictures we report the results for different levels of clusters number (CN) and number of layers (nL) respectively. In each subplot the NMI_{acc} of each algorithm, identified with colors code, is shown for the different levels of percentage of noise (no).

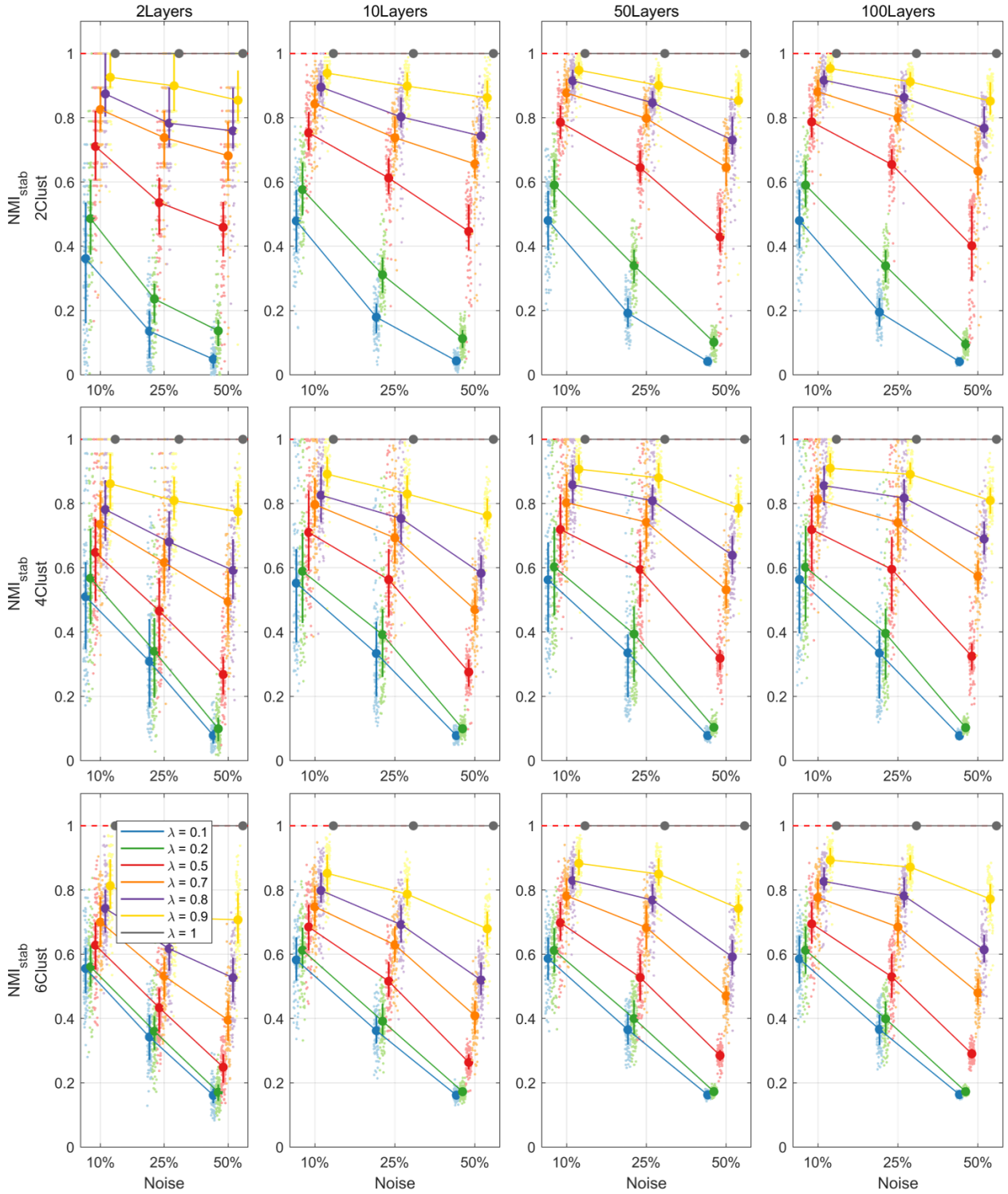


Figure S14. Plot of means and standard deviations of NMI_{stab} in the preliminary analysis regarding facetnet on networks with stationary community structure. In the rows and the columns of the pictures we report the results for different levels of clusters number (CN) and number of layers (nL) respectively. In each subplot the NMI_{stab} of each algorithm, identified with colors code, is shown for the different levels of percentage of noise (no).

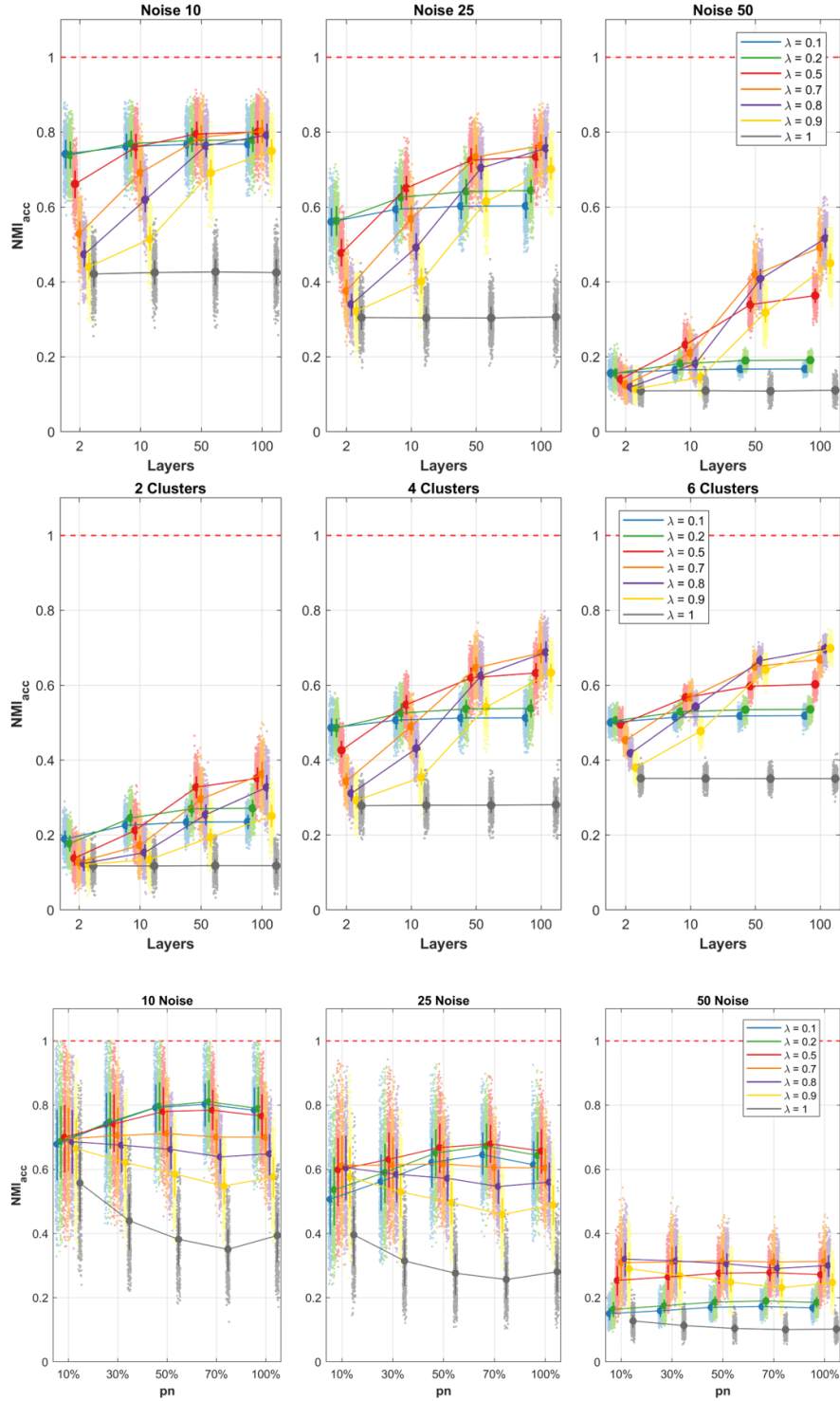


Figure S15. Plot of means and standard deviations of NMI_{acc} in the preliminary analysis regarding facetnet on networks with evolving community structure. In the first row we report the accuracy of the algorithms, identified with different colors, with respect to the different levels of number of layers, x-axis, and percentage of noise, columns. In the second row we show the trend of the algorithms' accuracies with respect to the number of layers, x-axis, and clusters number, columns. In the third row we represent the accuracies mean values for each algorithm to varying of the factor pn , x-axis, and level of noise, columns.

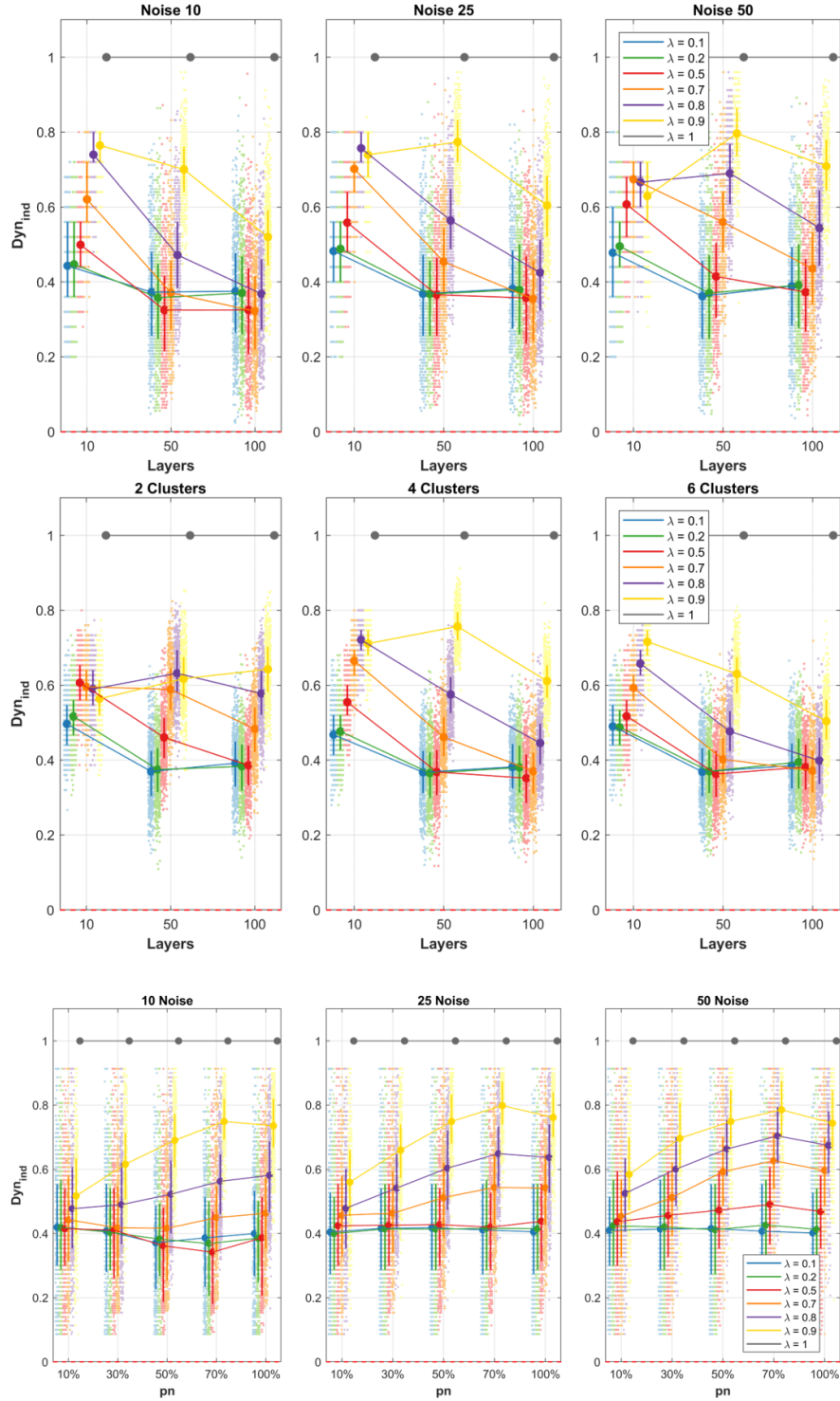


Figure S16. Plot of means and standard deviations of Dyn_{ind} in the preliminary analysis regarding facetnet on networks with evolving community structure. In the first row we report the dynamic of the algorithms, identified with different colors, with respect to the different levels of number of layers, x-axis, and percentage of noise, columns. In the second row we show the trend of the algorithms' speed with respect to the number of layers, x-axis, and clusters number, columns. In the third row we represent the Dyn_{ind} mean values for each algorithm to varying of the factor pn , x-axis, and level of noise, columns.

SECTION II

The modular organization of the human brain networks across the lifespan

- 2.1. Introduction
 - 2.2. Methods
 - 2.2.1. Experimental dataset and data processing
 - 2.2.2. Multilayer network construction
 - 2.2.3. Multilayer and multiscale community detection
 - 2.2.4. Analysis of the communities
 - 2.2.4.1. Statistics of the multilayer modularity maximization
 - 2.2.4.2. Age-related changes of the modular structure
 - 2.3. Results
 - 2.3.1. Statistics of the multilayer multiscale modularity maximization
 - 2.3.2. Age-related changes of the modular structure
 - 2.4. Discussion
 - 2.4.1. Age-related description of the connectome's modular structure
 - 2.4.2. Methodological innovations of the multilayer framework
 - 2.4.3. Limitation and future advancements
 - 2.5. Conclusion
-

2.1. Introduction

The human brain is a complex system that can be modeled as a network of anatomically interconnected brain regions, referred to as the *connectome* (Bullmore and Sporns, 2009; Sporns, 2011). Modeling the brain as a network allows the use of graph theory tools to explore properties of brain connectivity (Bassett and Sporns, 2017), through which we can enhance our understanding of the neurocognitive function and better characterize neurobiological variation across subjects or clinical populations (Kelly et al., 2012; Sporns, 2014). Network neuroscience approaches also allow for the tracking of networks across time, across different developmental stages, and in aging. Previous studies have shown that the brain and white matter connectivity exhibits characteristic changes across the human lifespan (Imperati et al., 2011; Lebel et al., 2012; Westlye et al., 2010; Yeatman et al., 2014), as well as specific changes in connectivity during adolescent development (Byrge et al., 2014; Di Martino et al., 2014), adulthood (Duffau, 2014), and senescence (Andrews-Hanna et al., 2007; Buckner et al., 2009; Filippi et al., 2013; Zhou et al., 2012).

New efforts, made possible by large multi-modal neuroimaging datasets, have focused on charting brain networks across the entire human lifespan. This approach is key for better understanding developmental processes and the age-related decline of executive and cognitive function.

Recent cross-sectional studies (for review see (Zuo et al., 2017)) have already applied complex network tools to evaluate local and global changes in the connectome during the lifespan. For example in (Betzel et al., 2014; Lim et al., 2015) an age-related decrease in the number of recovered connections between brain areas has been recorded. However, few attempts have been made to characterize how the connectome's community structure (Fortunato, 2010; Newman, 2012a; Porter et al., 2009), a hallmark of complex networks, evolves across the lifespan. Community structure is expressed at a mesoscale level (Betzel and Bassett, 2017) (between local and global) allowing observations on how the network's units organize themselves into clusters (communities) to form coherent and distributed systems that balance integration and segregation between brain regions. While different definitions of communities exist (Betzel et al., 2018b; Schaub et al., 2017), it is well established that anatomical brain networks exhibit assortative communities (Bassett et al., 2011a; Sporns and Betzel, 2016), called modules. Modular structure implies the presence of different internally dense and externally sparse subnetworks, usually related to specific domains of brain function. Studies on functional connectivity have found an age-related increase in between-module connectivity and a decrease in within-module connectivity (Betzel et al., 2014; Chan et al., 2014), plus an overall decrease in the assortativity of modules (Cao et al., 2014). Furthermore, studies using structural networks reported an increase in between-module connectivity when comparing two groups of younger and older adults (Chen et al., 2011). In (Baum et al., 2017) brain networks were analyzed in a restricted age range of 8 to 22 years, and a reinforcement of the hub edges between and within modules was demonstrated, associated with network maturation.

To date, two main strategies have been employed to track variations in the network architecture across stages of life: (i) comparison among representative networks or (ii) among averages formed over large groups. However, these strategies could be

confounded by differences in network properties (Fornito et al., 2013; Wijk et al., 2010) that are not of interest to the current analysis. In fact, topological measures, such as communities, depend on the network's density and edge distribution (Rubinov and Sporns, 2010), which vary not only across the lifespan (Betz et al., 2014; Lim et al., 2015; Zuo et al., 2017), but also exhibit non-age related individual differences, making a comparison based on representative subjects difficult. At the same time, averaging networks across larger populations likely leads to significant loss of information.

In this work, we aim to investigate how the connectome's modular structure evolves during a large part of the lifespan, while addressing these methodological issues. We leverage an extensive neuroimaging dataset (620 subjects ranging from 7 to 85 years old), and we propose a novel framework, based on multilayer networks (De Domenico, 2017; Kivela et al., 2014; Muldoon and Bassett, 2016; Vaiana and Muldoon, 2018) where layers represent narrow age ranges. The multi-layer model synthesizes connectivity information from multiple subjects, representing these data in a single network model without discarding data from any of the participants. Using this methodology, the variability of connection patterns across layers will be explicitly associated with age and, as a consequence, so will modular structure. Constructing ensembles of multi-layer networks, we systematically track the evolution of modular structure across the life span. Consistent with previous studies, we find an age-related loss of connectivity within modules. Our study adds to our current understanding of age-related changes in the organization of the connectome, specifically its modular organization. Moreover, our ensemble multi-layer network approach may be useful for future statistically robust investigations of network topology across large imaging or biomedical datasets.

2.2. Methods

2.2.1. Experimental dataset and data processing

The main objective of this work is to study how the modular organization of the brain connectome evolves during the lifespan. For this purpose, we leveraged the openly available Nathan Kline Institute – Rockland Sample dataset (NKI-RS,

http://fcon_1000.projects.nitrc.org/indi/enhanced/); an ongoing project which aims to collect a large scale (N>1000) community sample of participants across the lifespan (Nooner et al., 2012). Institutional Review Board approval was obtained for this project at the Nathan Kline Institute (#226781 and #239708) and at Montclair State University (#000983 A and #000983B) in accordance with relevant guidelines. All participants gave written informed consent or assent. The anonymized dataset is freely available through an Amazon S3 Bucket at http://fcon_1000.projects.nitrc.org/indi/enhanced/neurodata.html. Both T1-weighted (T1w) and diffusion (dMRI) images are provided, collected with a 3T Siemens Magnetom Tim Trio scanner, using a 12-channel head coil. T1w images were pre-processed with the *FreeSurfer* (<http://surfer.nmr.mgh.harvard.edu/>) *recon-all* pipeline to reconstruct the *Yeo17* network parcellation, which renders 114 cortical nodes (<https://github.com/ThomasYeoLab>). dMRI images were denoised, corrected for motion and susceptibility distortion, and then aligned to the corresponding T1w. Deterministic streamline tractography was run using *Dipy* (Garyfallidis et al., 2014). Finally, we extracted the structural connectivity matrices normalizing the number of streamlines that connect each region of interest (ROI) of the network parcellation, by the geometric mean volume of the connected ROIs (regions of interest) (Betz et al., 2018; Faskowitz et al., 2018). In this way, we obtained weighted anatomical connectivity matrices where weights represent the connection density between brain regions. We performed rigorous quality control on these matrices excluding subjects based on T1w viability, presence of artifacts on dMRI, quality of tractography reconstruction and excessive sparseness of the adjacency matrix. More details about data processing can be found in (Faskowitz et al., 2018).

2.2.2. Multilayer network construction

Following data processing, we obtained an ensemble of 620 anatomical weighted networks covering participants non-uniformly distributed between 7 and 85 years old. The networks were summarized as adjacency matrices $\mathbf{W} = [w_{ij}]$, made of N=114 nodes

representing cortical ROIs of the Yeo parcellation (Thomas Yeo et al., 2011), $ij \in [1, 114]$, whose entries denote the structural connection weights between each pair of nodes.

From these data, we constructed a multilayer network in which layers represent sequential and heterogeneous age groups of people. We implemented a statistical method based on bootstrap theory (Efron and Tibshirani, 1993) which is summarized in Figure 2.1. This procedure included:

- a) dividing the entire dataset into 2-year temporal bins, i.e. $NG = 39$ groups of subjects equally spaced in time, each one spanning 2 years;
- b) assigning a subject-level network to every single bin.

Since in (a) the number of the participants was not uniformly distributed across the groups, we obtain the networks in (b) through a reiterated probabilistic procedure based on two phases:

- b.i) bootstrapping with replacement: we randomly picked 10 networks within each temporal bin;
- b.ii) averaging of these networks to obtain one for each bin.

In order to avoid an artificial increase in network density, we employed an averaging process that maintains the mean number of connections over the 10 networks, by removing extra edges. In doing so, we take into account that anatomical brain networks usually have strong short-distance and weak long-distance weights (Betzel et al., 2018a; Betzel and Bassett, 2018). Thus, simply removing the weakest edges after averaging would lead to networks with only short-distance connections, which is not realistic. Rather, we evaluate the frequency with which connections occur, and we remove edges starting from the least frequent, until we obtain a network whose density is equal to the mean density computed over the 10 networks. In a way similar to (Betzel et al., 2018a), we preserve the edge length distribution. Finally, we repeat steps (b.i) and (b.ii) many times ($nIT = 1000$) to obtain an ensemble of equivalent multilayer networks made of NG layers representative of the lifespan human connectome at NG consecutive age stages.

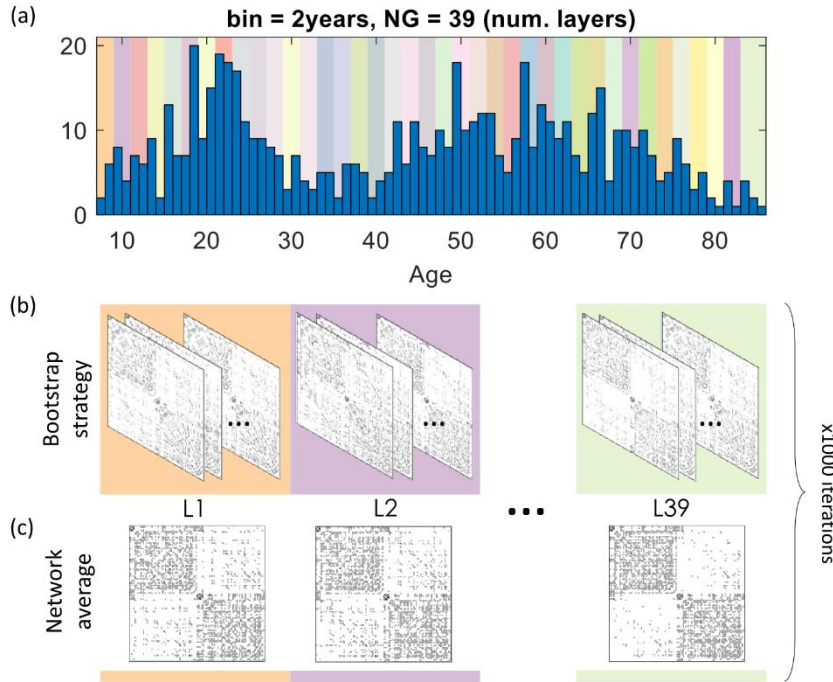


Figure 2.1. Schematic representation of the steps undertaken to obtain the multilayer network. Panel (a): division of the dataset into 39 temporal bins, identified by color code, each spanning 2 years and comprised of a different number of subjects. Panel (b): random selection of 10 networks within each temporal bin. Panel (c): averaging of each subset of networks. The procedure in panels b and c is iterated 1000 times to obtain 1000 multilayer networks made of 39 layers.

2.2.3. Multilayer and multiscale community detection

The primary focus of this work is on brain network organization from the modular structure point of view. To recover the modular organization of the inferred networks we adopted a multilayer community detection algorithm. Numerous previous studies have used modularity maximization (achieved through optimizing a modularity quality metric, Q) for uncovering the modular structure of brain networks (Sporns and Betzel, 2016). Modularity (Q) (Girvan and Newman, 2002; Newman and Girvan, 2004) assesses the goodness of a given partition with respect to a null model so that the maximization of Q returns a plausible partition of the network into non-overlapping modules. Here, we employed a multilayer version of the modularity quality function (Mucha et al., 2010) already reported in Eq. 2, in the introductory chapter, and already proved to be effective in the previous section. The term P_{ij} in the equation refers to a null model. Though there exist many possible definitions of it, the most common (and the one used here), is the

configuration model $P_{ij} = \frac{k_i k_j}{2m}$, in which each node's connection strength is preserved but edges are placed in a random fashion.

The optimization of the multilayer modularity can be used to identify assortative communities at different scales by varying its spatial and temporal resolution parameters, γ and ω . The value assigned to the spatial resolution parameter γ influences the number and size of the detected modules. When γ is small many elements A_{ijr} will probably exceed the null model, and consequently, maximizing Q_{ml} would produce few large communities. Vice versa, high γ -values are likely to produce many small communities. In this study, we set these parameters in a data-driven way. The temporal resolution parameter, ω , corresponds to the strength of the edges linking a node to itself across layers. Since in our case the layers represent temporally adjacent age bins, we track temporal variations by employing a null-model in which ω is expressed only between adjacent layers, rather than an all-to-all configuration. The value of ω impacts the homogeneity of the community assignments across the layers. Intuitively, when $\omega=0$ nodes are uncoupled across layers and maximizing Q_{ml} would be akin to maximizing Q separately in each layer. More generally, small and large ω -values lead to variable and stable partitions, respectively. Because the connectome's modular structure spans multiple scales, all potentially plausible (Betz et al., 2017), we considered partitions obtained with different combinations of resolution parameters, $\gamma = [0.5, 1, 2]$ and $\omega = [0.1, 0.5, 1, 5]$, in order to obtain modules diversely resolved in the cortex and across ages. As in section I, we optimized multilayer modularity using the free *genlouvain* package implemented in MATLAB (Jutla et al., n.d.), which consists of a generalized version of the Louvain algorithm (Blondel et al., 2008).

2.2.4. Analysis of the communities

Through the multilayer modularity maximization, we obtain an ensemble of multilayer partitions – 1000 per each combination of γ and ω – that we characterized by computing several measurements.

2.2.4.1. Statistics of the multilayer modularity maximization

First, we derived the Variation of Information (VI) matrix. This is a measure of distance between two partitions (Meilă, 2007), closely related to the mutual information and entropy of the communities. Each entry rs of the VI matrix corresponds to the VI value computed between the partitions at layers r and s . We compute the VI matrix for each combination of the resolution parameters in order to identify interesting community structures and exclude non-interesting ones for the aim of our study. In fact, even if multiple partitions of the connectome at different temporal scales are plausible, we focus on those that show a reasonable variation over the lifespan. Therefore, we omit partitions relative to ω values producing communities that do not consistently vary across the layers, or whose variation rate is excessively high even over networks representing close ages. By calculating the distance between each pair of partitions we can evaluate the magnitude of variations across the layers.

We also restrict our investigation to a specific spatial scale. We wanted to analyze partitions with a number of clusters consistent with the number of large-scale anatomical or functional subnetworks derived in previous work (around ten) (Eickhoff et al., 2007; Thomas Yeo et al., 2011). Thus, we computed the number of clusters and their dimension and we excluded those γ -values that returned partitions with too few clusters. Among the parameter values we considered for γ and ω we identified a combination that returns a multilayer community structure C_{opt} with a biologically plausible number of modules that exhibit a reasonable rate of reconfiguration on a physiological time scale. The following metrics focus on this subset of communities.

2.2.4.2. Age-related changes of the modular structure

For every partition of C_{opt} , we computed the single layer modularity, whose expression is reported in Eq. 1., in order to evaluate how much the brain subsystems are segregated across years.

We then evaluated the node and layer flexibility (Bassett et al., 2011b). We built a flexibility matrix F of dimension $[N * (NG - 1)]$ and filled its columns either with ones or zeros depending on whether node i has changed cluster assignment going from layer r to

layer $r+s$ or not. The average over the rows and columns will return the node and the layer flexibility, respectively. The node flexibility, f_i , represents the percentage of partitions in which node i changes its community allegiance. It allows us to quantify the strength with which brain regions reconfigure across the lifespan. The layer flexibility, f_l , is measured between all the pairs of consecutive partitions and captures the average node flexibility between such partitions: $f_{l(rs)} = \frac{1}{N} \sum_i f_{irs}$. It enables us to investigate the possible existence of age stages in which brain modular organization strongly rearranges.

Then, we examined how the distribution of the modules on the cortex varies with age, tracking their disposition within and between the hemispheres.

Finally, for each node and for each layer we calculated the participation coefficient (Guimerà and Amaral, 2005), (Eq. 4):

$$p_i = 1 - \sum_c \left(\frac{k_{ic}}{k_c} \right)^2 \quad (\text{Eq.4})$$

With k_{ic} representing the total weights involving node i within module c , and k_c the total weights inside cluster c . This measure captures how the connections of node i are distributed across all the modules. By computing p_i across the lifespan, we aim to reveal if the brain's sub-systems become more segregated or integrated during specific time periods.

The above-listed measures were computed on each one of the 1000 resulting multilayer partitions. Their mean and standard deviation were compared to a null model obtained with the same multilayer framework, but with randomly permuted age-bins, within each of the 1000 repetitions. The use of a null model allowed to test whether results obtained from the ensemble of lifespan multi-layer networks were robust against permutations of the age structure of the data. Each measure in the actual model was statistically compared with those of the null model through a permutation test (100,000 permutations; statistical significance set to $p < 0.05$).

2.3. Results

The principal aim of this study was to investigate age-related changes in the human connectome modular organization. For this purpose, we processed diffusion MRI data of the NKI dataset and implemented a probabilistic procedure to obtain an ensemble of multilayer networks representative of the anatomical connectome at different ages. Each layer represents a mean model of structural connectivity in an age range covering 2 years. Since the participants ranged from 7 to 85 years old, we obtained multilayer networks constituted by 39 age-dependent layers (Figure 2.1). We generated an ensemble of 1000 such multilayer networks, and we identified their modular structure through a multilayer modularity optimization algorithm, obtaining for each layer the brain regions' community assignment. The output of this algorithm depends on two parameters defining spatial and temporal resolution, γ and ω . We tuned both parameters in order to examine partitions at different spatial and temporal scales, which affect the number of clusters, their size, and their reconfiguration rate across the lifespan.

2.3.1. Statistics of the multilayer multiscale modularity maximization

First, we quantified the extent to which brain regions reconfigure across age as a function of the temporal resolution parameter, which plays a key role in this regard. We report in Figure 2.2 the VI matrices obtained for each tested parameter combination. VI matrices are square matrices of dimensions equal to the number of layers (i.e. 39), in which each entry represents the distance between layer r and layer s . They allow us to visually evaluate the similarity of partitions across layers. As expected, running the multilayer modularity optimization with low ω -values produces communities that rarely cover multiple layers, and the dissimilarity score between two general partitions r and s is high. In contrast, increasing ω -values yields stable communities that span several layers, and the VI between two partitions r and s is low. All the temporal scales defined by the different ω -values could be of interest. For example, stable partitions across the layers, produced with high ω , could highlight possible structures that do not change over the lifespan. On the other extreme, highly age-specific partitions, produced through low ω , could represent community structure expressed in specific age ranges. Here, we are

interested in an intermediate regime, in which modules reconfigure across longer time periods, while also remaining robust across shorter time periods. Hence, we adopted $\omega = 0.5$. Here, communities tend to be similar along the main diagonal of the matrix ($VI \approx 0$), namely along consecutive years of the lifespan, but they diverge more and more farther away from the main diagonal. In contrast, with lower ($\omega = 0.1$) and higher ($\omega = [1, 5]$) values of inter-layer coupling, partitions respectively appear highly variable, even between consecutive layers, or barely variable, even at the extremes of the lifespan.

Second, we examined how cluster numbers and their sizes vary among different γ -values, in order to identify a spatial scale in which the number of modules is congruent with the number of subnetworks encountered in previous studies (Eickhoff et al., 2007; Thomas Yeo et al., 2011). Going from low to high γ -values we pass from a coarser to a

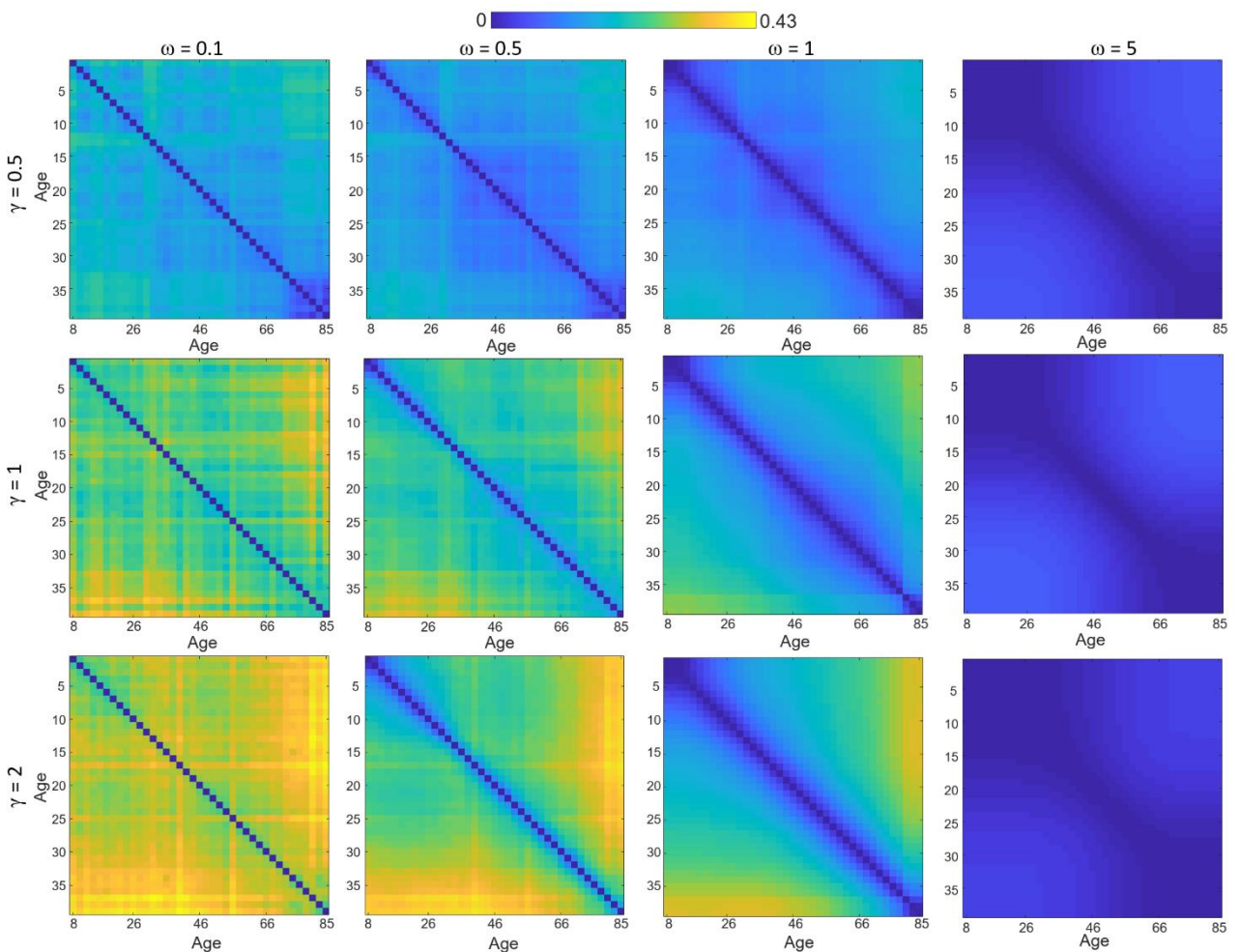


Figure 2.2. Variation of Information (VI) matrices computed for each combination of γ and ω (reported in rows and columns). In each matrix, entries represent the VI computed between two layers r and s . Values span the range $[0, 0.43]$.

finer scale (Figure 2.3). On average, setting $\gamma = 0.5$ yielded only 2-3 modules comprising about 40-60 nodes each, which mainly correspond to the hemispheres. By increasing γ to 1 we obtained partitions made of 4-6 modules composed of 20-30 nodes. Finally, with $\gamma = 2$ we found on average 9-12 clusters made of 8-12 nodes each, for a partitioning scheme that most closely resembles the number of large-scale anatomical and functional systems derived in previous studies (Eickhoff et al., 2007; Thomas Yeo et al., 2011). Different γ -values also affect how clusters rearrange across the lifespan (Figure 2.3c). We found that for $\gamma \leq 1$ the number of communities decreases with age, going from 3 to 2 ($\gamma = 0.5$ green subspace) and from 6 to 4 ($\gamma = 1$, yellow subspace), while for $\gamma = 2$ this number increases from 9, in the early lifespan, to 12, in the late lifespan (violet subspace). Among the three values of γ , only $\gamma = 2$ produces continuous variations in cluster sizes. Thus, this setting not only seems to be more physiologically interesting, but also better matches our model,

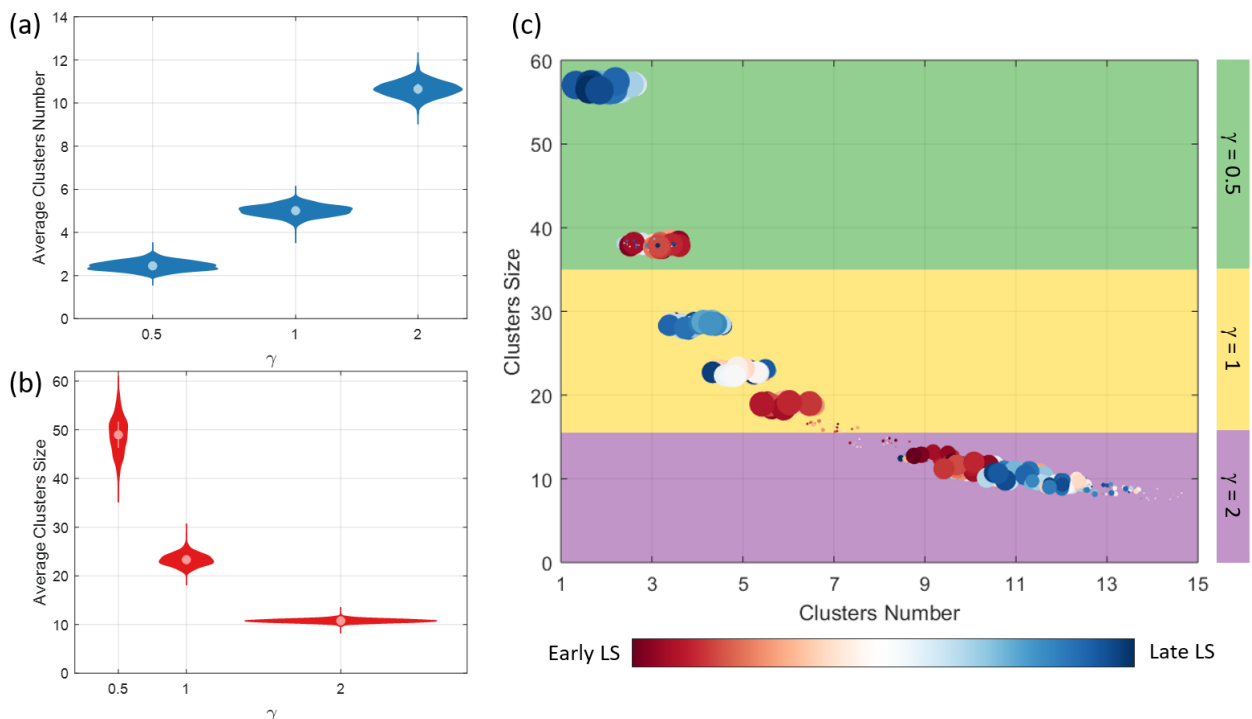


Figure 2.3. Clusters number and clusters size of the partitions detected with $\omega = 0.5$. Violins in panels (a-b) report their average distribution over the 39 layers and 1000 iterations, for each γ value. Panel (c) shows how clusters number (x-axis) and clusters size (y-axis) vary as a function of age and γ . Age is indicated with colors, from red (early lifespan) to blue (late lifespan). The dimension of the dots in the scatterplot is proportional to the frequency with which that value is observed across the 1000 multilayer networks. We render a scatterplot for each γ value [0.5, 1, 2], which occupy the xy plan in three different zones (green, yellow and violet).

which is designed to track modules' evolution over multiple narrow adjacent temporal bins, and not over big age ranges. Given these considerations, we restrict the following investigations on the multilayer modular structure identified by optimizing the multilayer modularity in the subset of parameters [$\gamma = 2$, $\omega = 0.5$].

2.3.2. Age-related changes of the modular structure

First, we aimed to find any relationship between age and segregation of the brain subnetworks. For this purpose, we computed on each layer separately the single layer modularity Q (Eq.2). Modularity returns an estimation of the extent to which communities are internally connected, or segregated one from another. We computed Q both for our actual model (Q_{obs}) and for the null model (Q_{null}). We found (Figure 2.4) that Q_{obs} varies systematically with age, following a U-shape, while Q_{null} , does not show any age-related trend. In the early (7-20 years) and in the late (72-85 years) lifespan, Q_{obs} is statistically higher than Q_{null} . In contrast, in the middle lifespan (20-72 years) Q_{obs} shows lower values than Q_{null} .

In order to explain this trend, we calculated the number of intra-cluster edges (example in Figure 2.4c) and their weights across the layers of the network. Indeed, given a network and a partition of its nodes into modules, Q is proportional to the difference between the within-module weights of the network and those in the configuration null model multiplied by γ , within each cluster (Eq.2). The results (Figure 2.4b) suggest that there are two factors contributing to increased modularity observed at the extremes of lifespan. As for the early lifespan, the number of intra-clusters edges is considerably higher than in the following middle lifespan. This number and age are negatively correlated (p -value < 0.0001, $r = -0.58$), suggesting that aging is associated with a loss of intra-clusters edges, probably causing higher modularity values in this first part of the considered timeline. In the late lifespan, instead, the weights of the intra-clusters' edges are significantly higher. This variable positively correlates with age (p -value < 0.0001, $r = 0.72$), resulting in higher modularity at the end of the age range. To further demonstrate these two factors driving modularity, we plot the Q_{obs} -values with respect to the intra-clusters' weights and edges (Figure 2.4d-g), exhibiting a positive and negative tendency, respectively. Thus, weather

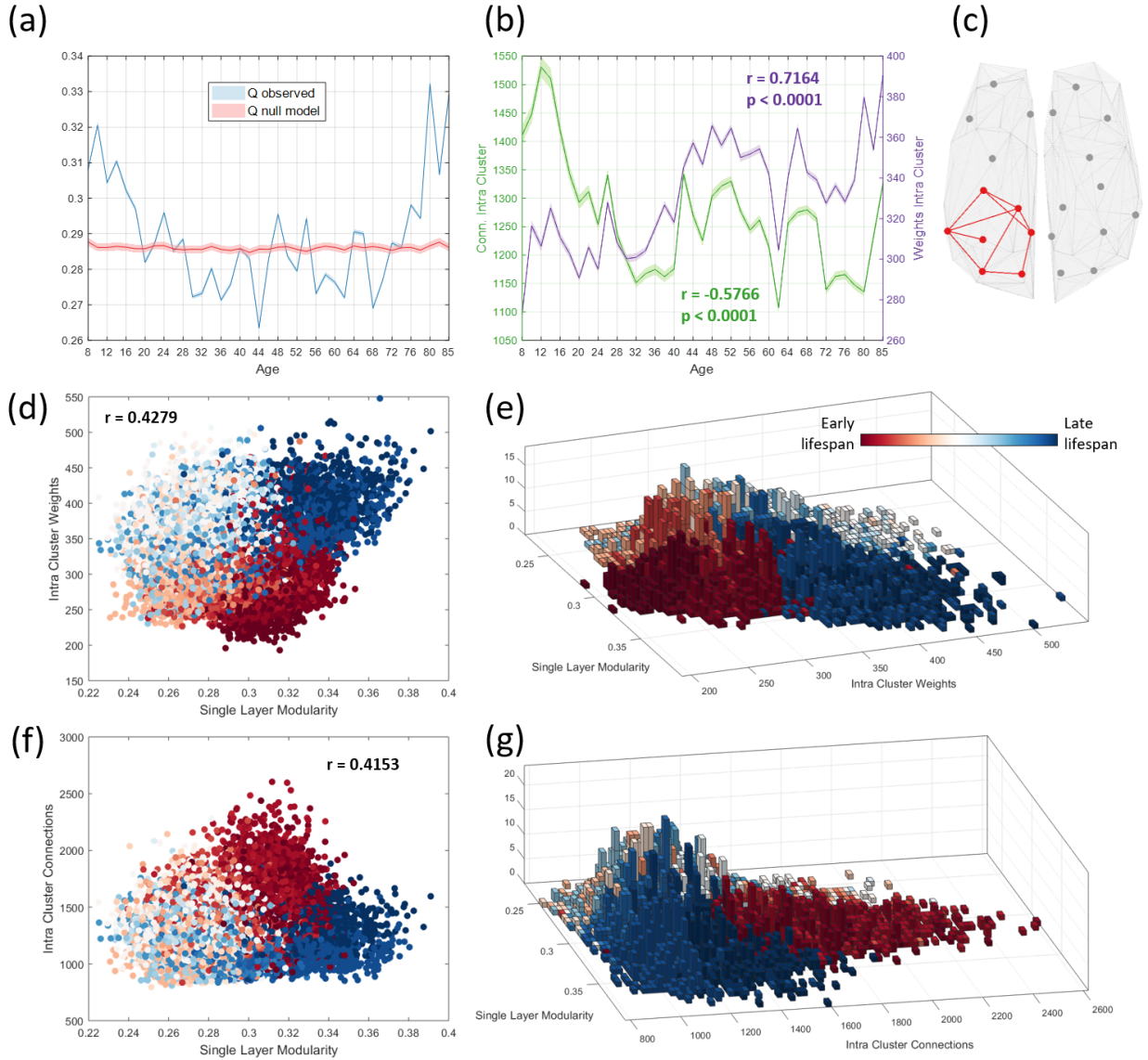


Figure 2.4. Single-layer modularity. Panel (a): trend of the modularity across the layers for the actual model (blue) and the null model (red). Panel (b): trend of the number (green) and weights (violet) of intra-clusters connections. In both panels bounded lines represent the mean and confidence interval over the 1000 iterations. Panel (c): example of a cluster with its intra-cluster links. Panels (d-e): scatter plot and 2D histogram of the weights of intra-clusters edges against single layer modularity (for all the 1000 multilayer networks). Dots are colored according to age, from dark red (early lifespan) to dark blue (late lifespan). We also report the mean Pearson correlation coefficient computed between the two variables (calculated considered only the significant outputs ($p < 0.05$)). Panels (f-g): scatter plot and 2D histogram of the intra-clusters' connections.

Q_{obs} increases or decreases with age is an effect of the edges' distribution within clusters, their weights, and their relationship with the configuration null model.

Next, we quantified the extent to which modular structure changes with age, and which brain regions are more likely to change community membership, by analyzing the layer and node flexibility, F_l and F_i (Figure 2.5), comparing observed and null models. The layer flexibility of our model, F_{l-obs} , resulted in values in the range [0.02, 0.2] (Figure 2.5, panel *a*). It shows high dependency with age as it monotonically increases across the temporal bins (computing the Spearman correlation between F_{l-obs} and age was significant ($r = 0.76$, p -value < 0.0001)). This suggests that among older participants, modules reconfigure more compared to younger participants. Conversely, no age-related trends were found in the null model, F_{l-null} , whose values remain around an intermediate level, ~ 0.14 , across the entire lifespan. In the first part of the lifespan, until 36 years old, F_{l-obs} is lower than F_{l-null} , while in the late lifespan, from 72 years old, it becomes significantly higher. In the middle part of the lifespan, F_{l-obs} and F_{l-null} assume similar values.

Looking into node flexibilities, we determined which brain regions are more prone to change modular allegiance (Figure 2.5*b*). Overall, the medial part of the cortex surface is less flexible with respect to the lateral one. The less flexible brain nodes belong to the visual cortex and the auditory area. On the contrary, the temporal lobe, Wernicke's area, and the pre-frontal lateral cortex have higher F_i values. These regions are functionally involved in the posterior dorsal attention subnetwork, the temporo-parietal default mode network (DMN), and the limbic area (Figure 2.5*c*). We also examined F_i within specific age ranges, 7-38 and 38-85 years old (Figure 2.5*d-f*), as in these periods the F_i exhibits different trends in the actual and the null model. Generally, brain areas more flexible in the early lifespan remain more flexible in the late lifespan. The only exception is represented by nodes located in the inferior temporal cortex, which change from lower to higher flexibility across age.

We then examined how structural modules are topographically distributed on the cortical surface across the lifespan. In Figure 2.6*a*, we display for each temporal bin the number of clusters that span both hemispheres. While in the null model this number does not change across layers, with the intact model it is first higher and then diminishes. Until the middle lifespan there are 6 clusters involving brain areas of both hemispheres. Given

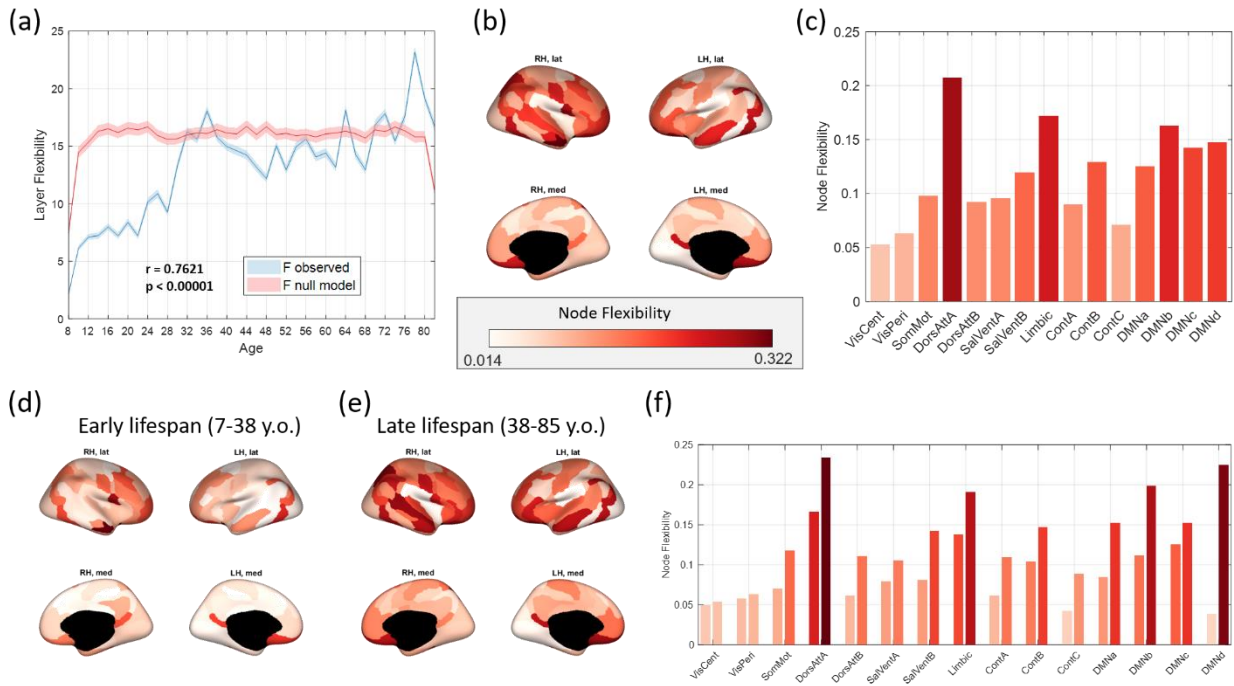


Figure 2.5. Flexibility. Panel (a): trend of the layer flexibility across the lifespan for the actual model (blue) and the null model (red). The bounded lines represent mean and confidence interval computed on the partitions of the 1000 equivalent multilayer networks. Panel (b): mean nodes flexibility across the lifespan (averaged over the 1000 iterations). Brain regions are colored from white to dark red proportionally to their flexibility value. Panel (c): Nodes flexibility averaged within the functional subsystems of the current parcellation. Panels (d-f): nodes flexibility and their average within the functional subsystems in the age ranges [7, 38] and [38, 85] years old. Left (right) bars in panel (f) are referred to younger (older) participants.

that in this portion of the lifespan we counted 9 to 10 clusters, this means that most of them involve both the right and left hemispheres. After the middle lifespan the number of modules spanning the two hemispheres linearly decreases with age until, in the last temporal bin, only one cluster exhibits this feature, essentially comprising brain areas located on the anteromedial cortex, and partially in the medial sensory association area (Figure 2.6f).

To understand a plausible cause for this drop of inter-hemispheric modules, we examined how the number of edges and their weights are dispersed within and between the hemispheres during the lifespan (Figure 2.6b-c). While the amount of intra-hemispheric connections is constant, inter-hemispheric connections decrease. Interestingly, this decrease starts at the same period in the lifespan where the number of inter-hemispheric clusters begins diminishing, ~ 48 years old. Observing the weights of the connections, this consideration is even more accentuated, as the inter-hemispheric

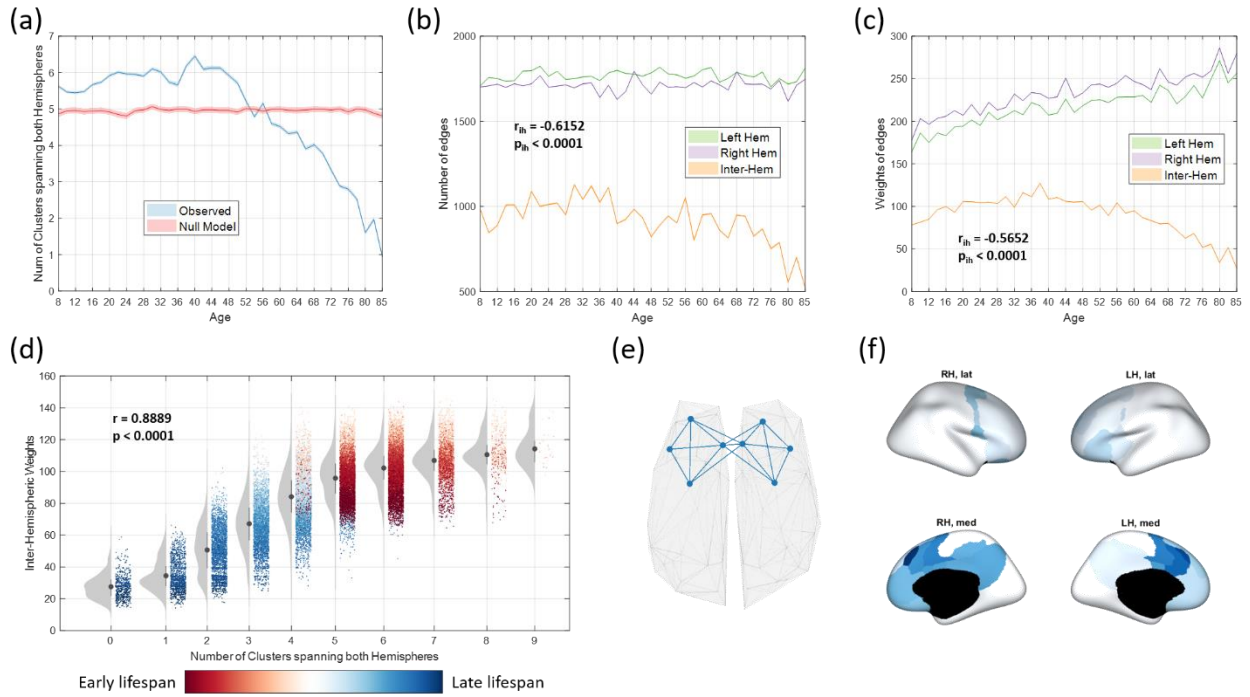


Figure 2.6. Topographical clusters analysis. Panel (a): number of clusters that over the lifespan involve brain regions from both hemispheres, observed in our model (blue) and in the null model (red). Panel (b) and (c): trend across the lifespan of the number and weights of the connections located in the left hemisphere (green), right hemisphere (violet), and inter-hemispheres (orange). We report correlation coefficients and p -values of the Spearman correlation computed between the average of inter-hemispheric edges/weights and age. In all the three panels bounded lines indicate the mean and confidence interval of the distribution of such variables across the 1000 equivalent multilayer networks. Panel (d): rain-cloud plot of the inter-hemispheric edge weights against the number of clusters spanning both hemispheres. Dots are colored with an age-based criterion, from dark red (early lifespan) to dark blue (late lifespan). We also display the correlation coefficient and p -value of the Spearman correlation computed between the means of variables on the cartesian axis. Panel (e): Example of a cluster spanning the two hemispheres. Panel (f): heatmap on the cortex representing the brain regions that more frequently belong to the cluster that in the last temporal bin spans the two hemispheres. The blue intensity is proportional to this frequency.

weights drop, and the intra-hemispheric ones increase. Thus, the age-dependent loss of inter-hemispheric connections appears associated with a reconfiguration of structural modules to become hemispheric-specific. Indeed, inter-hemispheric weights and number of hemispheric specific modules were found to be highly correlated ($r = 0.89$, p -value < 0.0001) (Figure 2.6d).

Finally, we wanted to characterize the integration of the different brain areas with respect to the whole network and the modules to which they belong. We did so computing for each node the participation coefficient p_i , as it quantifies how uniformly distributed its connections are across modules. The smaller it is the more the node interacts exclusively

with other nodes of the cluster to which it belongs. We report the participation coefficient values of each layer, $p_l = \frac{\sum_i p_i}{N}$, across the ages, for the actual (p_{l-obs}) and the null (p_{l-null}) models (Figure 2.7). The p_{l-null} values do not show any age-related trend, remaining around 0.61, while p_{l-obs} exhibits an inverted U-shape trend. Its values increase in the first part of the lifespan, until ~ 32 years old, going from 0.56 to 0.62. Then, it remains in the range [0.6, 0.63] until ~ 72 years old, to finally decrease until the last layer, reaching a value of 0.57. This trend confirms that early and late lifespan are characterized by well-segregated sub-systems, while in the middle lifespan brain regions interact more closely despite their membership in system-specific modules. To explain this trend in p_{l-obs} , we looked at the number of the inter-cluster edges over the years (Figure 2.7b), discovering that they also follow an inverted U-shaped curve.

We identified brain nodes that mostly contribute to this non-linear trend, by finding those whose integration in the network is significantly influenced by age. For each node, we computed the Spearman correlation between p_i and age in three different ranges: 7-38 years old, 38-85 years old, 7-85 years old. Within the first age range, almost all the brain regions' p_i are positively correlated with age; nodes belonging to the somatosensory and sensory association areas both in the medial and lateral parts of the cortex are those mostly contributing to this trend. Such regions subtend the control, limbic and DMN networks. During the second interval, most of the nodes' p_i are negatively correlated with age. Specifically, somatosensory association areas and dorsal attention areas, as well as the medial visual cortex and the pre-frontal cortex associated with the medial DMN, become strongly anti-correlated with age. In contrast, the temporal cortex (the areas subtending the control network and the temporal DMN) instead, remains positively age-correlated. Looking at the entire lifespan, we identified two sets of nodes whose p_i significantly correlates with age in a positive and negative direction respectively. The temporal cortex and sensory areas fall in the first case, while the prefrontal cortex and somatosensory association brain regions in the second one. Overall, the visual cortex and the medial DMN are systems whose integration with the network is less affected by age.

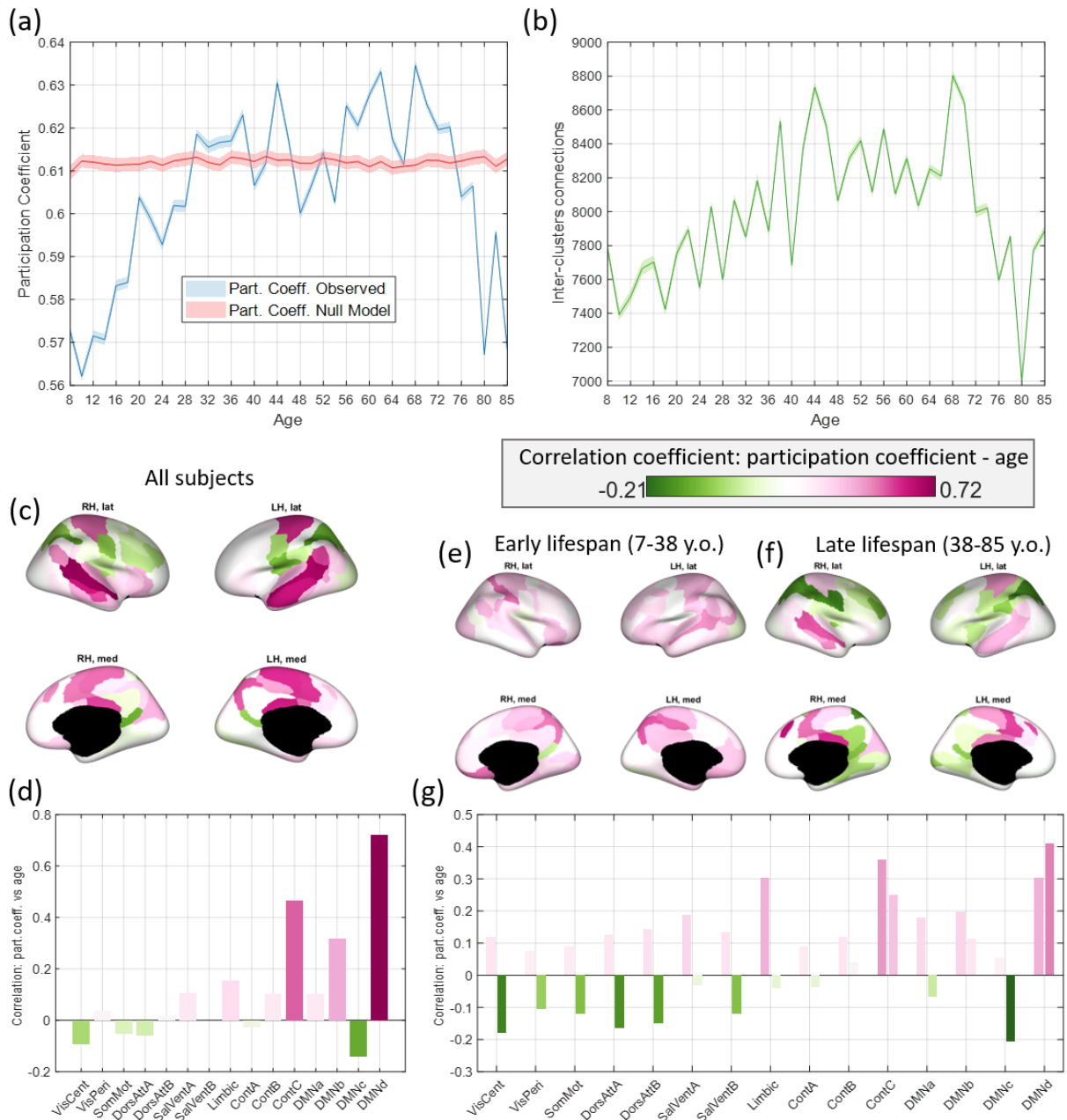


Figure 2.7. Participation Coefficient. Panel (a): course across the lifespan of the participation coefficient (average among all the nodes) computed on the partitions of our model (blue lines) and the null model (red lines). Panel (b): trend of the number of inter-clusters connections. The bounded lines in panels a-b indicate the mean and confidence interval of the distributions of such variables over the 1000 iterations. Panel (c): representation on the cortex surface of the correlation coefficients of the Spearman correlation computed between ages and participation coefficient values of each node. Brain regions for which the outcome was not significant are white. Brain regions whose participation coefficient is significantly positively/negatively correlated with age are illustrated in pink/green. Panel (d): Average of the correlation coefficients within the functional subsystem identified by the current parcellation. Panels (e-g): representation on the cortex surface and average within the Yeo functional subnetworks of the correlation coefficients of the Pearson correlation computed between participation coefficient values and age in the range [7, 38] and [38, 85] years old. Left (right) bars in panel (g) are referred to younger (older) participants.

2.4. Discussion

In this work, we address a number of open questions regarding the network structure of connectome across the lifespan by developing and applying a novel ensemble multi-layer approach. In doing so, we provide a plausible description of the evolution of the connectome's modular structure during a large portion of the lifespan.

2.4.1. Age-related description of the connectome's modular structure

The results obtained in this study confirm that the human connectome's modular structure is age-dependent. Our first finding saw the number of clusters increasing with age, from 9 in the early lifespan to 12 in the late lifespan, while, as a consequence, their size decreases. The metric of modularity exhibits an age-related U-shaped trend (Figure 2.4), with higher values at the beginning and at the end of the age range. Nonlinear U-shaped trends, with opposite trends over the early and the late lifespan, are often encountered in lifespan studies, prompting a fundamental question about the relationship between patterns of brain connectivity during development and aging: is the aging process a simple reversal of the developmental one? Or does the U-shape arise as a result of distinct processes? We tried to answer these questions by looking at the number and weight of intra-modules edges, which showed a decreasing and increasing trend, respectively. We found that high values of modularity may be due to two different processes: in the early lifespan, modules are internally densely connected, while in the late lifespan they are internally strongly connected. These results agree with previous findings, where an overall decrease of cortical connectivity with age has been observed (Betz et al., 2014; Dennis et al., 2013; Gong et al., 2009; Hagmann et al., 2010), linked in (Lim et al., 2015) to loss of within-module connectivity through preferential detachment. The same mechanisms, plus the inverted U-shaped trend observed for the number of inter-clusters connections, may contribute to form the non-linear (inverted U-shaped) curve followed by the participation coefficient (Figure 2.7).

While modularity and participation coefficient exhibit non-linear age-dependent behavior, we found that the flexibility of brain regions linearly increases with age (Figure 2.5), indicating that modular organization tends to reconfigure more and more as age

advances. This result aligns with those in (Wu et al., 2012), where connectome's properties have been analyzed over three age stages (young, middle, and old), and differences in the modules' composition have been observed only between the last and the first two groups, but not between the first two. Another variable that varies linearly with age, decreasing from the maturation to senescence, is the number of modules that span both hemispheres (Figure 2.6). We demonstrated that this is due to a drop in inter-hemispheric connections, possibly caused by a physiological age-related shrinkage of the corpus callosum (Raz et al., 2010).

Some brain regions appeared to be less prone to age-related changes, such as the medial cortex, the anterior cingulate, the orbito-frontal and superior-frontal cortex. They display low flexibility values, and their participation coefficient is not significantly correlated with age. Moreover, these regions constitute the cluster which continues spanning the two hemispheres into senescence. Interestingly, previous observations (Buckner, 2004) pointed out that changes in frontal-striatal circuits may be associated with a decline of memory and executive function. A previous study (Persson et al., 2006) suggested that older adults with declining memory performance show different DTI measures of the anterior white matter compared to older adults with intact memory functions. Also, the lateral occipital cortex shows low flexibility and non-age-related values of the participation coefficient.

The brain areas which reconfigure most across the lifespan are located mainly on the lateral part of the cortex, specifically in temporal regions, motor and sensory areas, the parietal lobe, and the posterior cingulate. Here we found high nodal flexibility, and a significant relationship between participation coefficient and age. However, these regions reconfigure in different ways. The participation coefficient of the temporal lobe and the superior central cortex subtending the sensory-motor area is positively correlated to age, so that these nodes become more integrated in the network with age. The opposite happens for the parietal cortex, whose participation coefficient is negatively correlated to age, becoming more segregated with age. These alterations we found on structural organization might underpin functional age-related alterations observed in the same

areas in (Sambataro et al., 2010), where modifications of the DMN due to age have been associated to connectivity changes in the posterior cingulate cortex and the bilateral parietal regions, impacting the working memory functions, while no significant differences have been found in the anterior cingulate cortex.

We schematically summarize our findings reporting representative partitions (with lowest within-layer VI) at three age stages (Figure 2.8). The network becomes more segregated with years, with the appearance of hemispherically-specific modules. The number of intra-cluster edges decreases with age, while their weight increases, causing non-linear trends of modularity and participation coefficient. Overall, the modules' reconfiguration rate increases with age.

2.4.2. Methodological innovations of the multilayer framework

Our study attempts to track multiple variables in a large, multi-modal dataset. Every approach used to detect changes in some variables must distinguish between meaningful trends and statistical noise. We tackled this challenge by implementing a probabilistic scheme, based on bootstrapping, that extracts an ensemble of multilayer networks, where

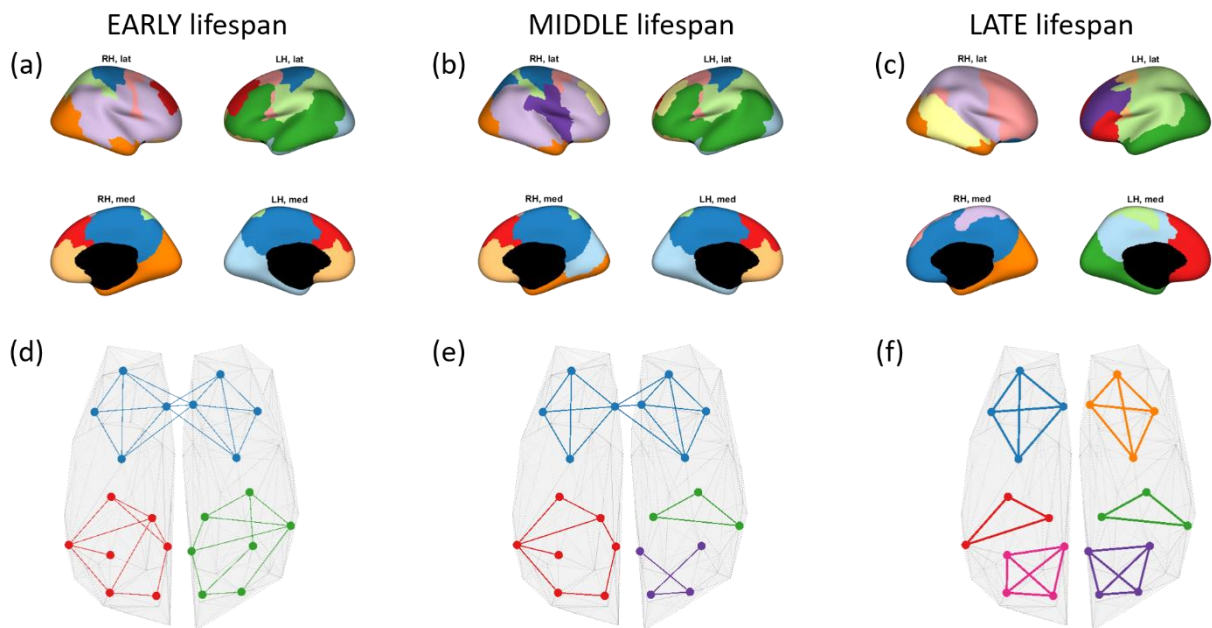


Figure 2.8. Representative partitions (first row, panels a to c) and toy model (second row, panels d to f) of the modular structure of the brain connectome in three phases: early, middle and late lifespan. Different colors indicate different clusters. In the toy model the thickness of the edges is proportional to their weights.

layers represent homogeneous and contiguous age intervals. It also addresses a relevant issue in the context of comparison among subjects, or categories of subjects, based on the analysis of their MRI networks. In fact, MRI networks exhibit unique, subject-specific, patterns of connections, so that even within the same population, different individuals can show different network properties, such as degree distribution, which in turn can drive differences in modular structure (Fornito et al., 2013; Rubinov and Sporns, 2010; Wijk et al., 2010). Our ensemble-based strategy, in which a network average is computed many times on a small subset of subjects, offers a solution to link changes of structural connectivity specifically to development, maturation, and aging processes, while minimizing the impact of individual differences not due to age. Therefore, it also overcomes the problem of heterogeneity in the age distribution of the sample. Moreover, thanks to the large data sample, we could build a multilayer network where layers represent narrow age intervals (2 years), so that we also avoided comparing modular structure across large age groups (usually children, adults, and elderly participants) that are internally highly heterogeneous. Instead, we could monitor modules' properties over an extended period of the lifespan.

To track the evolution of modules across the lifespan, we adopted a multilayer community detection algorithm (Mucha et al., 2010) that, according to the study in section I, has good performance in identifying assortative communities. While this is only one possible way of representing network organization, previous studies did suggest that modular architecture represents a neurobiologically meaningful aspect of brain connectivity (Sporns and Betzel, 2016), and it has been useful to describe learning processes (Bassett et al., 2011b), inter- and intra-subject variability (Betzel et al., 2019), differences among clinical cohorts (He et al., 2018), or model the brain network's dynamics (Khambhati et al., 2018). Our multilayer approach has the advantage of partitioning all the network's slices simultaneously, providing consistent partitioning of nodes across the layers and facilitating comparison of modules. Indeed, these are matched so that one can determine which brain regions change modular allegiance and in which

period in the lifespan. Hence, rather than working independently on snapshots, this unified framework is more suitable to monitor age-related modules variations.

Community detection algorithms, including the Louvain algorithm adopted here, have stochastic properties that result in outputs with increasing heterogeneity as the size of the network increases (Good et al., 2010). Proposed solutions to this issue include consensus clustering (Lancichinetti and Fortunato, 2012), which produces an agreement among a set of partitions, or selecting a near-optimal representative partition. Here, we pursued an ensemble-based resampling approach. Instead of applying the algorithm multiple times on a given network and then selecting a partition, we applied it once for each member of a set of equivalent multilayer networks, and we statistically described the ensemble of output partitions, focusing on statistical consistency. This approach aims to highlight meaningful trends and mitigate variations due to chance, which can be encountered relying on a single representation of community structure. Robustness and statistical consistency are also promoted by the large sample size of participants. Previous work characterizing connectome during development showed discordant results, such as increasing (Chen et al., 2013) decreasing (Huang et al., 2015) or no change of modularity (Hagmann et al., 2010), possibly due to small sample sizes. Overall, we aimed for robust results through a large sample, a stringent resampling scheme and a multilayer approach that reinforces the analysis.

By optimizing multilayer modularity, we explored the connectome's architecture at multiple spatial and temporal scales, as evidence suggests that the human brain network can be parsed in several – physiologically equally meaningful – ways (Betz et al., 2013; Betz and Bassett, 2017). However, after having obtained modules with different sizes and degrees of variability across layers, we focused on a specific subset. We were interested in modules that reconfigure in an intermediate time scale, neither too fast nor too slow. To identify a proper scale, we considered the VI matrix (Figure 2.2), which we hypothesized should have high similarity between partitions on the main diagonal and lower values outside. We also focused on a single spatial scale. While there is no exact number of modules with which brain networks must be divided, current practice has

converged onto a set of functional modules that are reliably observed (Damoiseaux et al., 2006; Power et al., 2011; Thomas Yeo et al., 2011). They usually include the visual, somatomotor, dorsal attention, limbic, default mode, control and salience systems. Previous works demonstrated that structural and functional connectivity matrices are significantly related (Fukushima et al., 2018; Goñi et al., 2014a), supporting the notion that structural connectivity underpins and drives functional organization. For this reason, we focused on a spatial scale that returned a number of modules consistent with canonical functional systems, which have also been identified in a previous analysis of structural connectivity (Faskowitz et al., 2018).

2.4.3. Limitation and future advancements

There are several limitations inherent in MRI data. Diffusion imaging and tractography provide an estimation of the anatomical connectivity, but not a direct measurement of it (Sotiropoulos and Zalesky, 2019). Through our approach to network construction and the multi-layer resampling methodology, we tried to ameliorate some biases such as the paucity of long-range connections detected with tractography data.

Another issue regards the node definition, as this choice might impact the properties of the derived network (Fornito et al., 2010). In order to be consistent with previous studies (Betz et al., 2015, 2014; Cao et al., 2014; Faskowitz et al., 2018), we used a parcellation of the cortex based on a canonical partition of the surface into functional subsystems (Thomas Yeo et al., 2011). To add robustness to our findings, future works could replicate the same analysis with a finer parcellation, or by defining nodes according to anatomical constraints (Destrieux et al., 2010).

While our study included much of the human lifespan, it did not cover early postnatal stages of development (ages 0-5 years). This period is characterized by rapid anatomical growth and behavioral/cognitive changes that we expect to be reflected in the topology of brain connectivity. As more data covering this early lifespan period becomes available, our ensemble multi-layer approach could be extended to cover the human lifespan more fully and comprehensively.

Finally, now that we provided a description of the evolution of the community structure during the lifespan, these patterns could also be assessed for cohorts of clinical subjects. The goal would be assessing the impact of specific pathologies on developmental or aging processes and helping to identify targeted interventions. Further studies might also attempt to correlate connectional features with behavioral features and normalize interindividual variations in cognition relative to the actual developmental status.

2.5. Conclusion

In conclusion, we develop an ensemble multi-layer approach and provide evidence that the human brain exhibits an age-dependent modular organization. The number of modules increases with age while their size decreases. The modularity of the partitions reaches the highest values in the early and in the late lifespan, whereas the opposite happens for the participation coefficient. We also found that the rate of the modules' reconfiguration increases with age, resulting in modules that are more restricted to single cortical hemispheres. Our findings broaden a body of literature aimed at understanding connectome evolution across lifespan, while the methods developed can be used to monitor variables of interest in structural and functional brain networks across other large datasets.

SECTION III

The modular organization of the human brain networks across functional and structural connectivity and across subjects

3.1. Introduction

3.2. Methods

3.2.1. Experimental dataset and data processing

3.2.2. Multi-modal multi-subject community detection

3.2.3. Analysis of the communities

3.2.3.1. Preliminary analysis

3.2.3.2. Principal component analysis

3.2.3.3. Variations of the community structure across modality and across subjects

3.2.4. Correlation with behavioral assessments

3.3. Results

3.3.1. Preliminary analysis of the communities

3.3.2. Modes of variability between and within modality

3.3.2.1. Principal component analysis – patterns of inter-modality variations

3.3.2.2. Principal component analysis – patterns of inter-subject variations

3.3.3. Variability between and within modalities at specific scales

3.3.3.1. Inter-modality variations across η

3.3.3.2. Inter-subject variations across ω

3.3.4. Correlation with behavioral assessments

3.4. Discussion

3.4.1. Relationship between structural and functional modular structure

3.4.2. Methodological innovations of the multilayer framework

3.4.3. Limitation and future advancements

3.5. Conclusion

3.1. Introduction

The recent endeavor of network neuroscience (Bassett and Sporns, 2017) of modeling brain structure with network science instruments resulted in the achievement of accurate mapping of white matter connections among neural populations, the connectome (Hagmann et al., 2008; Sporns, 2011). Shaped by this wiring diagram emerges a coherent neural activity that can be recapitulated by statistical dependences under the term of functional connectivity (Fox et al., 2005; Friston, 2011, 1994). In this sense, human cognition and behavior are thought to be driven by complicated patterns of connections among different brain areas (McIntosh, 2000; Mišić and Sporns, 2016).

Linking brain function to its architecture is a long-standing question. Despite evidence suggesting that brain anatomy and structure underpin brain activity through functional interactions, the way these two faces of the coins are linked is still an open question (Honey et al., 2010; Park and Friston, 2013). An increasing body of literature addressed this issue usually trying to predict functional connectivity features from the structural ones (Messé et al., 2015). This has been done for example implementing new statistical (Mišić et al., 2016; Vázquez-Rodríguez et al., 2019) or communication (Crofts and Higham, 2009; Goñi et al., 2014b; Mišić et al., 2015) frameworks, or considering the coupling with biophysical dynamic systems (Adachi et al., 2012; Breakspear, 2017; Deco et al., 2009; Honey et al., 2007; Stam et al., 2016).

In this work, we aim to explore the relationship between structural and functional connectivity under the network organization's point of view, knowing that it is underpinned by its modular structure (Meunier et al., 2010, 2009; Sporns and Betzel, 2016). Modular structure implies the presence of groups of nodes subtending specific function of the system. A first contextual study (Betzel et al., 2013) mapped structural communities (defined in terms of random walks) to patterns of functional connectivity, suggesting that such communities model brain function. More recently, in (Fukushima et al., 2018) the states of integration and segregation, given by the partition of brain networks into modules, have been reconducted to the similarity between patterns of structural and functional connectivity.

Here, we want to directly investigate the relationship between anatomical and functional modules, knowing that brain networks are subject-specific and intrinsically multi-scale (Betzel and Bassett, 2017). This feature implies that brain networks can be parsed in different physiological ways, with either small clusters, made of functionally-specialized areas (Rosenthal et al., 2017), or large clusters, supporting higher-order cognitive functions. In (Betzel et al., 2019) the community structure has been investigated across subjects at different scales. Here, we designed a new framework that, given the structural and functional connectivity matrices of a certain number of subjects, can simultaneously map communities across subjects and type of connectivity. Our

framework has been conceived as an extension of the well-known, and already employed, multilayer modularity maximization model (Mucha et al., 2010). Given a multilayer network, it returns, for each a layer, a partition of the network into assortative communities whose dimensions and consistency across layers depend on two parameters of spatial and a temporal resolution. We reformulated this model by adding a third resolution parameter that regulates the coupling between structural and functional connectivity modules. By applying this model to a sample of subjects we show that the modular structure of the brain networks varies across subjects and across connectivity modality in different ways, depending on the resolutions at which we observe communities. Finally, we demonstrate that also behavioral measures associated with executive cognition are correlated to the brain network organization in a scale-dependent way.

3.2. Methods

3.2.1. Experimental dataset and data processing

As in the previous section, we exploited the data coming from the Nathan Kline Institute – Rockland Sample project (Nooner et al., 2012) (NKI-RS, http://fcon_1000.projects.nitrc.org/indi/enhanced/). Institutional Review Board approval was obtained for this project at the Nathan Kline Institute (#226781 and #239708) and at Montclair State University (#000983 A and #000983B) in accordance with relevant guidelines.

Here we preprocessed the dataset in order to obtain both structural and functional connectivity matrix. To obtain anatomical weighted networks we followed the steps listed in paragraph 2.2.1, with the only difference that a probabilistic streamline tractography (and not deterministic) was run using *Dipy* (Garyfallidis et al., 2014). We empirically found that a probabilistic tractography results in a better correlation between structural and functional networks.

Functional images were preprocessed using the fMRIPrep 1.2.5 (Esteban et al., 2019), a Nipype (Gorgolewski et al., 2011) based tool. The fMRIPrep is based on a boilerplate

distributed with the software covered by a “no rights reserved” (CCO) license. It mainly uses the packages Nilearn 0.5.0, ANTs 2.2.0, FreeSurfer 6.0.1, FSL 5.0.9, and AFNI v16.2.07.

Each T1w (T1-weighted) volume was corrected for INU (intensity non-uniformity) using *N4BiasFieldCorrection* (Avants et al., 2008; Tustison et al., 2010) and skull-stripped using the *antsBrainExtraction.sh* workflow. Brain surfaces were reconstructed using recon-all from *FreeSurfer* (Dale et al., 1999) and the brain mask estimated previously was refined with a custom variation of [the method to reconcile ANTs-derived and FreeSurfer-derived segmentations of the cortical gray-matter](#) of Mindboggle (Klein et al., 2017). Spatial normalization to the *ICBM 152 Nonlinear Asymmetrical template version 2009c* (Fonov et al., 2009) was performed through nonlinear registration with the *antsRegistration* tool, using brain-extracted versions of both T1w volume and template. Brain tissue segmentation of cerebrospinal fluid (CSF), white-matter (WM) and gray-matter (GM) was performed on the brain-extracted T1w using FSL’s *fast* (Zhang et al., 2001). Functional data was slice time corrected using *3dTshift* from AFNI and motion corrected using *mcflirt* (Jenkinson et al., 2002). This was followed by co-registration to the corresponding T1w using boundary-based registration (Greve and Fischl, 2009) with 9 degrees of freedom, using *bbregister* (FreeSurfer v6.0.1). Motion correcting transformations, BOLD-to-T1w transformation and T1w-to-template (MNI) warp were concatenated and applied in a single step using *antsApplyTransforms* using Lanczos interpolation.

At the end of this workflow we obtain NIFTI files for each participant. These have been subjected to a image quality control made with fMRIPrep’s visual reports and MRIQC 0.15.1 (Esteban et al., 2017). Functional data were excluded if greater than 25% of the frames exceeded 0.2 mm framewise displacement (Parkes et al., 2018), or marked as outliers.

A functional parcellation was used to define 100 brain regions (*Schaefer 100* (Schaefer et al., 2018)) on the cerebral cortex in the same space of the BOLD nifty. This parcellation is designed to optimize both local gradient and global similarity measures of the fMRI

signal. The nodes are also mapped in the Yeo canonical functional networks (Thomas Yeo et al., 2011).

At this point, we removed some of the nuisance variables from the BOLD signal of each cortical node (like motion throughout the scan). To do that we band-pass filtered (0.008-0.08 Hz) the data, applied a confound regression and standardized using Nilearn's *signal.clean*, that removes confounds orthogonally to the temporal filters (Lindquist et al., 2019). The regression was made as in (Satterthwaite et al., 2013), because this strategy has been proven to be effective for reducing motion artifacts (Parkes et al., 2018). Downstream, we can obtain residual mean BOLD time series for each parcel, from which we can compute the Pearson correlation to obtain the correlation coefficient that will fill the functional connectivity matrix.

Out of the structural and functional connectivity matrices obtained (SC and FC), we further executed an accurate quality control removing subjects with average values of functional connections too high, or entropy values of the same edges too low. We also excluded subjects whose correlation's values between functional and structural connectivity weights were too low with respect to the others. Finally, because the focus of the work is to study structure-function relationship, to make the networks' properties comparable between the two modalities, we got a correlation matrix out of the structural connectivity one. Moreover, we only kept adult subjects (between 20 and 40 years old), avoiding differences in connectivity patterns due to age.

3.2.2. Multi-modal multi-subject community detection

The main objective of this work is to study the relationship between functional and structural connectivity from their modular structure point of view. For this sake, we recovered communities in the estimated networks through community detection (Fortunato, 2010). Even if many community detection algorithms exist, based on different definitions of community, we are interested in finding assortative (i.e. modular) structures (Sporns and Betzel, 2016), as they well represent brain networks organization. Thus, we employed an algorithm based on modularity optimization. In the previous

sections of this dissertation, we already introduced the modularity maximization algorithm, in both its single layer (Eq. 1) and multilayer (Eq. 2) formulations.

In this work, we propose a further extension of the multilayer modularity quality function, that we formulated in order to encode also the information about acquisition modality (Figure 3.1). Its expression is given by:

$$Q(\gamma, \omega, \eta) = \sum_{ijrtfs} \{[(W_{ijrf} - \gamma P_{ijrf})\delta_{rt} + \omega\delta_{ij}]\delta_{fs} + \eta\delta_{ij}\}\delta(\sigma_{irf}\sigma_{jts}) \quad (\text{Eq. 5})$$

In this formulation, $\delta(x, y)$ is equal to 1 if $x = y$ and 0 otherwise, and besides the spatial resolution parameter γ , we simultaneously consider two temporal resolution parameters, η and ω , that couples each node i with itself across subjects (indicated with r and t) and modalities (indicated with f and s) respectively. In this way, ω controls the homogeneity of the communities across all the participants, and we call it subject resolution parameter, while η regulates the coupling of the partitions between FC and SC networks within each participant, and we call it modality resolution parameter.

When using multilayer modularity, the parameter ω can be considered in two configurations: (i) all-to-all, meaning that nodes are linked to themselves through ω across all the layers (used if layers represent categorical variables); (ii) temporal, connecting nodes only between consecutive layers (used in time-varying networks). In this case, layers connected through ω represent different subjects, so that we used the first configuration. Regarding the null-model P_{ijrf} , there exist many possible definitions,

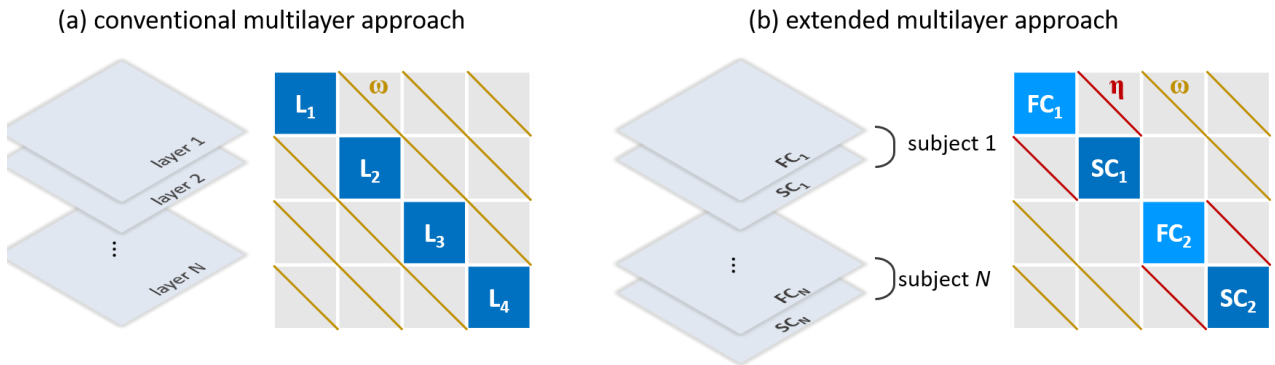


Figure 3.1. Schematic representation of the classical multilayer maximization framework (panel a), and our multilayer maximization framework (panel b), in which we added a resolution parameter η that couples the nodes across modalities.

however we set $P_{ijrf} = 1$ for all i, j, s, f . This choice has been proven optimal to deal with modularity maximization in correlation matrices, providing communities with well-known topographic features.

Thus, in order to detect the communities in our networks, we aligned them in blocks on the main diagonal of a square matrix of dimension $NS \times N \times \text{Modalities}$ (number of subjects * number of nodes * connection modality: $123 \times 100 \times 2$), following the order $\{FC_{\text{sbj}1}, SC_{\text{sbj}1}, FC_{\text{sbj}2}, SC_{\text{sbj}2}, \dots, FC_{\text{sbj}NS}, SC_{\text{sbj}NS}\}$. Then, we run the optimization of the introduced extended multilayer modularity with 50 values of each resolution parameter, taken linearly spaced in the range $[w_{\min}, 1]$, with the lower boundary indicating the minimum weight of the 123 SC matrices ($w_{\min} = 2.12 \times 10^{-6}$). We finally obtain an ensemble of 125000 partitions ($50 \times 50 \times 50$ combinations) for each subject and each modality. To run the optimization, we exploited the free *genlouvain* package, implemented in MATLAB (Jutla et al., n.d.), based on a generalization of the single-layer *louvain* algorithm.

3.2.3. Analysis of the communities

3.2.3.1. Preliminary analysis

Through the multilayer modularity maximization, we obtained a partition of the anatomical and functional brain networks into groups of nodes for each subject and for each combination of the resolution parameters (a total sample of 250.000 partitions per subject). Even if focusing on specific values of resolution parameters is a widespread practice and might result in easier analysis, in this study we preferred to explore a full range of them, as brain networks can be organized in different ways across different scales (Betzl and Bassett, 2017). However, to deal with this large amount of results, first of all, we restricted any further investigation to a subgroup of them, relative to combinations of resolution parameters that provided interesting, non-trivial, partitions. Criteria to operate this restriction included:

- a) Number of clusters. We avoid considering partitions with too many (few) clusters made by too few (many) nodes. We choose a range of interest partitions made by 5-20 clusters, with an average of 20-5 nodes respectively (being the network made of

100 nodes). Hence, we only kept those in which at least one subject presents more than 5 and less than 20 clusters.

b) Variability among subjects. We discarded partitions in which the community structure was identical across all the subjects, as many studies demonstrate that the patterns of brain connectivity are highly subject-specific. We quantified the variability of each node's assignment through the normalized entropy:

$$h_i = -\frac{1}{\log_2(K)} \sum_{k=1}^K p_i(k) \log_2(p_i(k)) \quad (\text{Eq. 6})$$

Where k indicates the communities, and $p_i(k)$ is the fraction of subjects in which node i belong to community k . By dividing for $\log_2(K)$ we normalized this measure in the range $[0, 1]$, with 0 indicating identical assignments and 1 maximal variability. Then we can average this vector to obtain $H = \frac{1}{N} \sum_{i=1}^N h_i$, a measure of the variability of the entire partition across subjects. We ignored resolution parameters providing $H=0$ across subjects simultaneously.

A deeper investigation of the relationship between the organization of anatomical and functional brain networks has been carried out, limited to the subspace of resolution parameters identified in this paragraph.

3.2.3.2. Principal component analysis

In order to analyze the variation of the brain network's organization across modalities and subjects, we computed the entropy between and within modality, respectively, as this measure captures the variability of each node assignment across the considered partitions. Its values, however, are highly dependent on the specific combination of the $\{\gamma, \omega, \eta\}$ parameters. Through Principal Component Analysis (PCA) we aim to inspect the parameters space and see if there exist patterns of entropy values that are recurrent among this space. We carried this analysis separately for the two cases of within and between modality variability.

In the first case we computed, for each subject and for each combination of the $\{\gamma, \omega, \eta\}$ parameters, the entropy between the partitions of anatomical and functional networks. Then, after having derived the average across subjects, we aligned all those vectors in a matrix H_{sf} of dimension $N \times N_{par}$ (100×2794), and we subjected it to Singular Value Decomposition (SVD). The SVD decomposes the matrix H_{sf} into singular vectors $U_{sf} \in [N \times N]$ and $V_{sf} \in [N_{par} \times N]$, and singular values $\Sigma_{sf} \in [N_{par} \times N]$, so that:

$$H_{sf} = U_{sf} \Sigma_{sf} V_{sf}^T \quad (\text{Eq. 7})$$

The matrices U_{sf} and V_{sf} are orthonormal by definition and contain the principal component scores and coefficients respectively. The columns of U_{sf} can be interpreted as the modes of variability between SC and FC partitions, while the values in the rows in V_{sf} indicate where these modes are likely to appear in the parameter space. The diagonal elements of Σ_{sf} instead contain the variance with which each component explains the variability across SC and FC.

We performed a similar analysis for the second case, i.e. variability across subjects. We built a matrix H_{sbj} of dimension $N \times N_{rep}$ containing in each column the vector of the entropy h computed among subjects within modality each modality (structural/functional connectivity). Again, we executed the SVD to decompose H_{sbj} in the singular vectors $U_{sbj} \in [N \times N]$ and $V_{sbj} \in [N_{par} \times N]$, and singular values $\Sigma_{sbj} \in [N_{par} \times N]$:

$$H_{sbj} = U_{sbj} \Sigma_{sbj} V_{sbj}^T \quad (\text{Eq. 8})$$

Again, the matrices U_{sbj} and V_{sbj} are orthonormal and contain the principal component scores and coefficients. Here, we interpret the columns of U_{sbj} as the modes of variability of the partitions across subjects. The values in the rows in V_{sbj} still indicate where these modes are likely to appear in the parameters space, while the diagonal elements of Σ_{sbj} contain the variance with which each component explains the variability across subjects.

In both cases, we observed the first four components in order to describe the most common patterns of inter-modality / inter-subject variability over the parameters space.

3.2.3.3. Variations of the community structure across modality and across subjects

After having looked at the modes with which partitions vary in the parameters space, we depicted how the relationships between modalities and between subjects evolve across different scales.

Regarding the relationship between structural and functional networks, we built our model so that their modular organization maximally varies across the η -values. For this reason, we fixed one ω -value and observed how the community structure of the functional networks is related to the one of structural networks across all the η -range at three spatial scales. We quantified this relationship in terms of node's flexibility (Bassett et al., 2011b). For each η we built a flexibility matrix of dimension $N \times N_{sbj}$ filled with ones and zeros basing on whether the node i in subject s changes cluster's assignment between SC and FC partitions or not. We then averaged these matrices over the rows (i.e. across subjects) and we aligned the resulting vectors to obtain a flexibility matrix of dimension $N \times N_\eta$. Through this matrix, we can observe which brain regions are coupled in SC and FC across all the η -range.

In a similar fashion, we studied the flexibility of the network's organization across subjects, within functional networks and within structural ones, knowing that it maximally varies along different ω -values. Thus, for each acquisition modality, we fixed one η -value and three γ -values, and we considered the flexibility of the partitions across subjects over the entire ω -range. For each ω , we built a flexibility matrix of dimension $N \times N_{sbj}$ filled with ones and zeros basing on whether the node i changes cluster's assignment between subject s and r . Again, we averaged these matrices over the rows and aligned the resulting vectors in order to obtain a flexibility matrix of dimension $N \times N_\omega$. This matrix captures all along the ω -range which brain regions contribute to stable modules across subjects and which ones do not.

3.2.4. Correlation with behavioral assessments

There exist an increasing body of literature pointing out the influence of the brain network architecture on cognition and behavior (Bressler and Menon, 2010; McIntosh, 1999; Mišić and Sporns, 2016). Here we investigate how patterns of variability between

connection modality and among subjects are related to clinical assessments of the subjects. Besides imaging data, the NKI-RS projects also collected from the participants several clinical, behavioral, and cognitive measures conducted through a common protocol covering a wide array of psychiatric, cognitive and behavioral functions. Here we selected measures falling within the assessment of the domain of cognitive and executive functioning, the Wechsler Abbreviate Scale of Intelligence (WASI-II) (Wechsler, 1999) and the Wechsler Individual Achievement Test – Second Edition Abbreviated (WIAT-IIA) (Wechsler, 2005). The former scale measures general intelligence, with IQ tests based on vocabulary, block design, similarities and matrix reasoning. The FSIQ (Full Scale IQ) is the index taking into account all the sub-tests, the VIQ (Verbal IQ) only considers the vocabulary, while the PIQ (Performance IQ) the block design and matrix reasoning. The latter scale (WIAT-IIA) is an analogous set of tests to evaluate word reading, numerical operations and spelling. It results in a score that, from now on, we call COMP. Both tests can be administered to participants aged from 6 to 85 years old.

We investigated the correlation between those measures and the patterns of coupling between structural and functional partitions. In order to do that we had to extrapolate a subject-level measure associated of the patterns of SC-FC variability. The scheme in Figure 3.2 summarize this procedure. Basically, we built a $N \times NS$ matrix, *mat_corr_scfc*, in which each column is referred to an individual, and is obtained by averaging the vectors of entropies computed between the SC-FC partitions laying in the parameters space where components are most expressed. At this point, for each node we could calculate the Pearson correlation between the relative row of the matrix ($1 \times NS$) indicating how much this node's assignment varies between SC and FC for each subject, and the four cognitive assessment vectors.

We also investigated the correlation between the same clinical scales and the patterns of communities' variability across subjects. In an analogous way (Figure 3.3) we built a $N \times NS$ matrix, *mat_corr_sbj*, where each column is referred to an individual, and is obtained by averaging the vectors of entropy between that subject's partition and each partition of the other subjects, relative to the parameters space where components are

most expressed. Again, we computed for each node the Pearson correlation between the correspondent row and the vectors containing clinical assessments.

3.3. Results

In this work, we introduced an extension of the multilayer modularity maximization optimization, developed to analyze multi-subject multi-modal datasets. Our approach is meant to map brain communities into subjects and acquisition modalities at different scales. The results of the application of our new framework to anatomical and functional networks of the NKI dataset will be illustrated in this section.

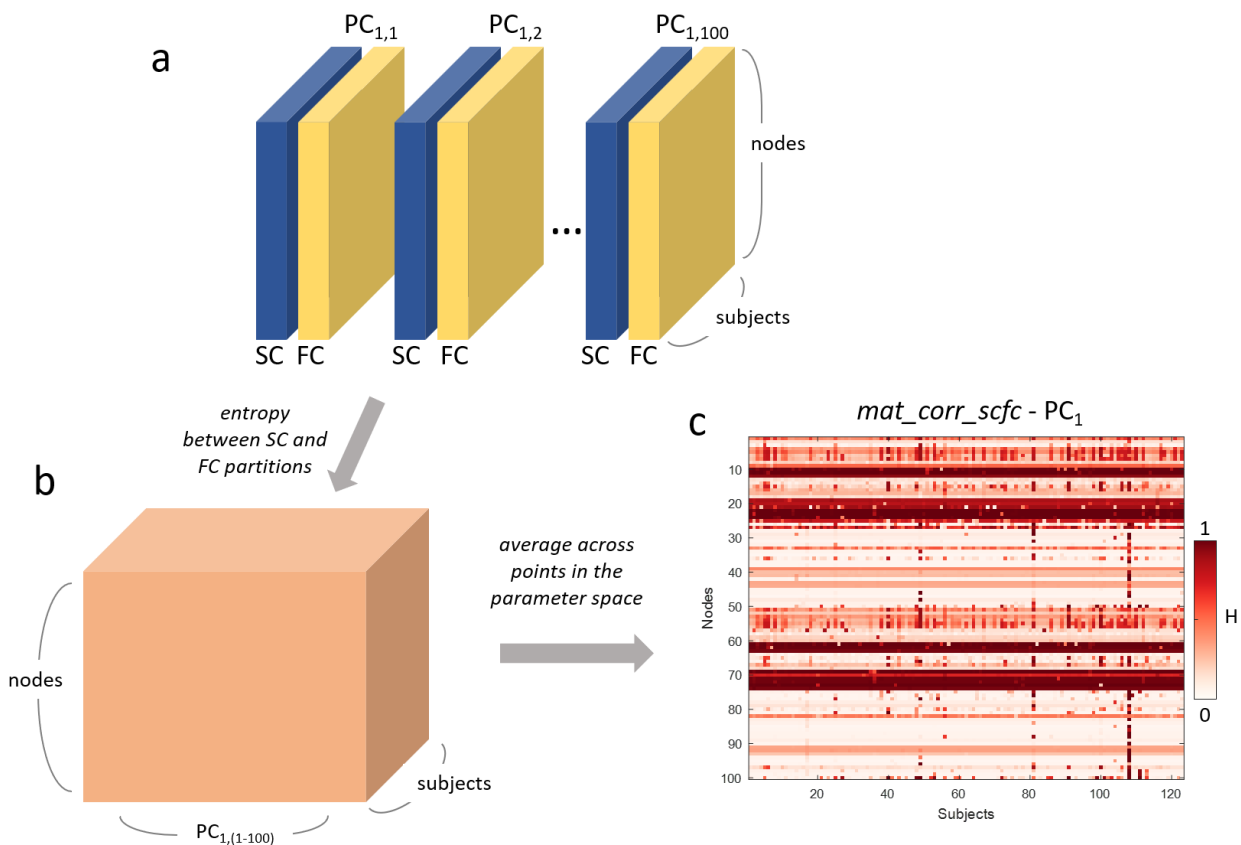


Figure 3.2. Schematic representation of how we built the subject-level matrix associated a pattern of variability between functional and structural partitions. This scheme refers to the first component; we applied it in the same way to the first four. Panel a: partitions of the structural and functional connectivity matrices for each subject correspondent to the 100 points in the parameters space where the first component is more expressed. Panel b: 3D matrix that we obtained after computing the entropy between FC and SC partitions for each subject in each of the 100 points of the parameter space. Panel c: 2D subject-level matrix we obtained averaging the matrix in panel b across the selected 100 points of the parameter space

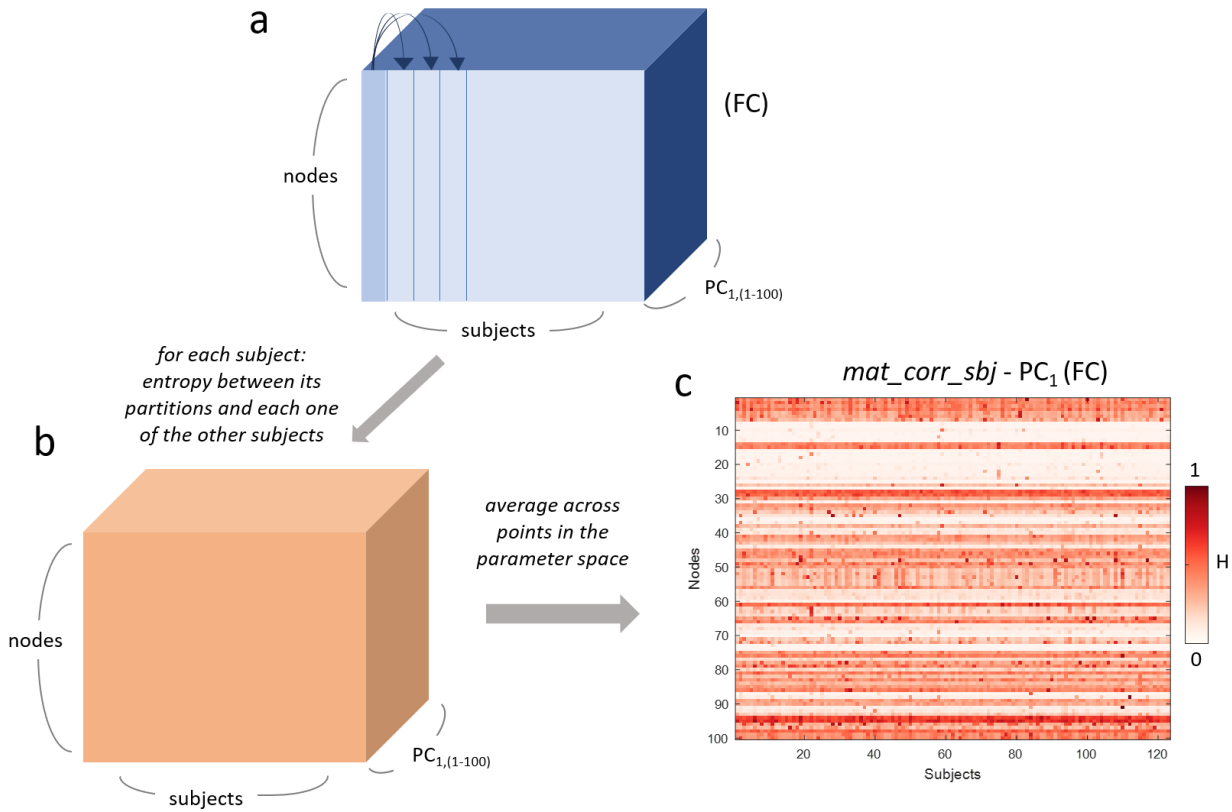


Figure 3.3. Schematic representation of how we built the subject-level matrix associated a pattern of inter-subject variability. This scheme refers to the first component of the functional connectivity partitions; we applied it in the same way to the first three components for both structural and functional partitions. Panel a: partitions of the functional connectivity matrices for each subject correspondent to the 100 points in the parameters space where the first component is more expressed. Panel b: 3D matrix that we obtained after computing for each subject the entropy between its partitions an the partition of every of the other subjects, in each of the 100 points of the parameter space. Panel c: 2D subject-level matrix we obtained averaging the matrix in panel b across the selected 100 points of the parameter space

3.3.1. Preliminary analysis of the communities

The output of the multilayer modularity maximization, as we formulated it, depends on three resolution parameters, whose values affect the number and the coupling of the communities across subjects and acquisition modality. The structural resolution parameter, γ , influences the number of the communities and, in turn, their size, so that setting it to high (low) values leads to many small (few big) clusters. The subject resolution parameter, ω , and the modality resolution parameter, η , impact the homogeneity of the partitions across subjects and acquisition modality, respectively, being higher for increasing values of these parameters. While several studies focus on specific combinations of such parameters, in this work we explored the modules at different

scales, tuning all the parameters in the range $[0, 1]$ sampled with 50 values, and obtaining an ensemble of 250.000 partitions for each subject. Among all of them we were interested in finding those physiologically interesting and meaningful. Thus, we represented on the 3D space defined by the resolution parameters the clusters number and entropy of the partitions averaged across subjects (Figure 3.4). We centered our analysis on the subspace of parameters where brain networks were parsed with 5 to 20 clusters, and where the average of the entropy of the partitions computed across the subjects (within modality) was > 0 . This resulted in considering 2742 combinations of $\{\gamma, \omega, \eta\}$, in the ranges $\gamma \in [0.0404, 0.2424]$, $\omega \in [2.12 \times 10^{-6}, 0.1616]$, $\eta \in [2.12 \times 10^{-6}, 0.9899]$.

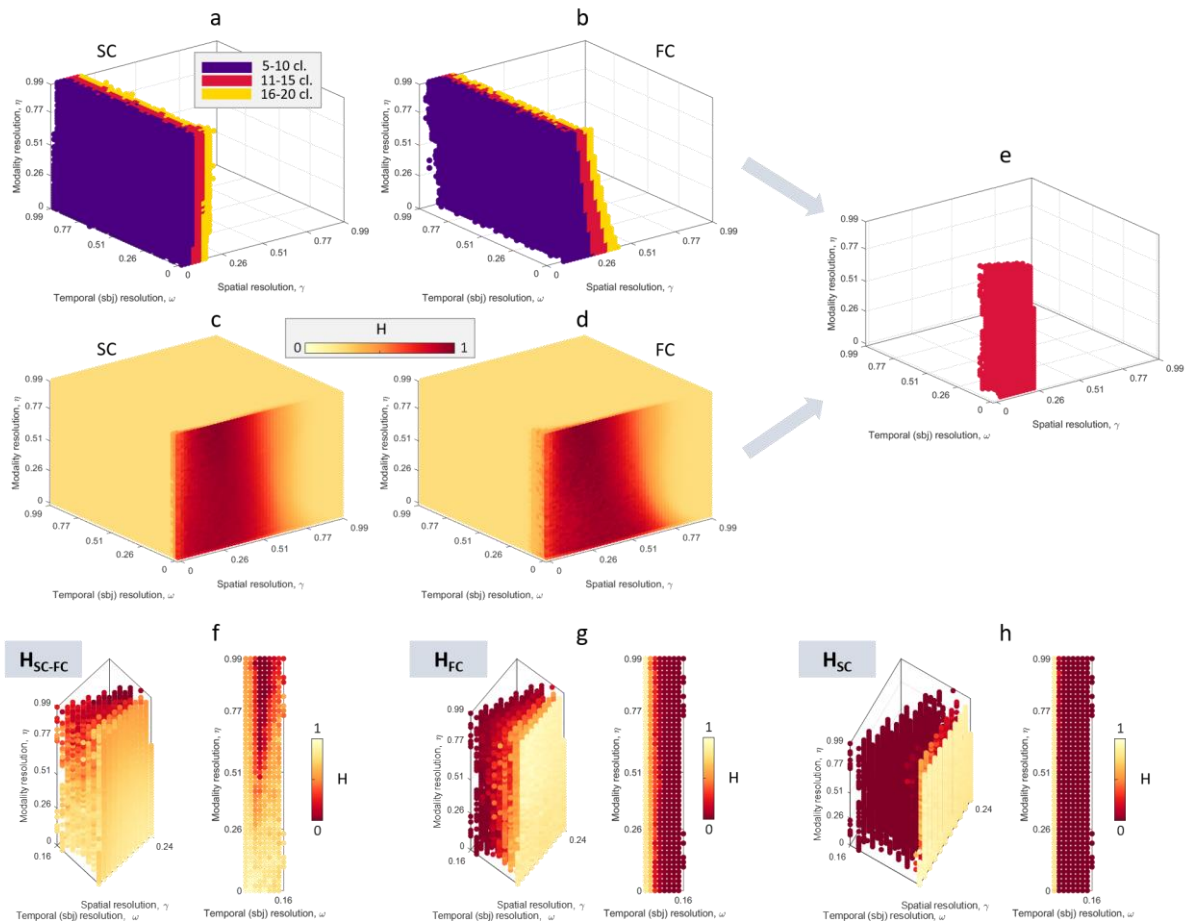


Figure 3.4. Panel a: number of modules identified for each point of the parameter space (only cases of 5 to 20 clusters are reported). Panel b) each point of the parameter space is colored proportionally to the value of the partitions' entropy across subjects. Panel c) in red we indicated the points of the parameter space in which we obtained meaningful partitions, basing on the criteria listed in section 3.2.3.1. Panel f) entropy between functional and structural communities represented in the sub-sampled parameter space. Panels g-h) inter-subject functional and structural (respectively) communities' entropy reported in the sub-sampled parameter space.

In this subspace we evaluated the variability of the sampled partitions between modalities (Figure 3.4f) and among subjects (Figure 3.4g-h) in terms of normalized nodes' entropy. As expected, we found that the magnitude of the variability of the nodes' assignment between SC and FC networks varies maximally along the modality resolution parameter η , that regulates the coupling of nodes across SC and FC. Low η -values yield to a weak coupling between FC and SC partitions, while high η -values yield to a strong coupling between the same partitions. On the contrary, the magnitude of the variability of the nodes' assignment within modality, across subjects varies monotonically with the temporal resolution parameter ω , that indeed in our model controls the inter-subjects coupling. Small ω -values result in communities with high entropy across subjects, while as the ω increases the entropy rapidly diminishes.

In figure 3.5 we report an example of how the three resolution parameters influence the partitions of structural and functional connectivity matrices.

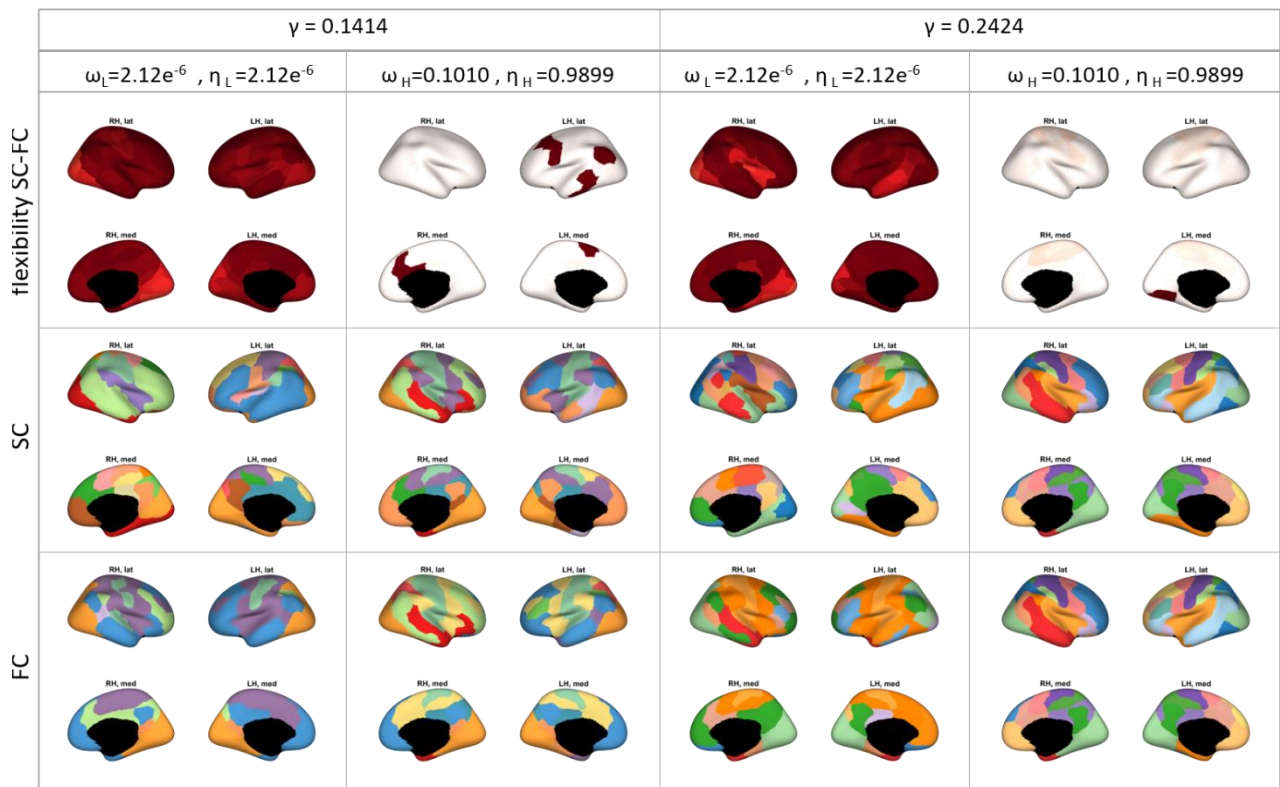


Figure 3.5. Representative partitions of the structural and functional brain networks under different combination of $\{\gamma, \omega, \eta\}$. The pedices H and L stand for high-value and low-value.

3.3.2. Modes of variability between and within modality

In the previous section we identified a subset of parameters where partitions could be considered physiologically interesting. Inside this subspace, we showed in which way the three resolution parameters affect the scale of the partitions and the magnitude of their variability between types of connectivity and among subjects. Then, in a way similar to (Betzel et al., 2019), we wanted to investigate if there exist recurrent patterns of variability which are encoded in this subspace in a meaningful way. For this purpose, we scored in a 100×2742 matrix the vectors containing the normalized nodes entropy (one for each point in the sampled parameter space) across modality or subjects and we executed the Principal Component Analysis (PCA) on it. Through the PCA we obtained 99 principal component scores (in the form orthonormal vectors of length equal to the number of nodes), and the relative coefficients, informative of their contribution of each of the 2742 samples points. Thus, we identified the modes of variability projecting the scores and the coefficients on the cortex surface and on the parameter space, respectively.

3.3.2.1. Principal component analysis – patterns of inter-modality variations

To investigate the modes of variability between SC and FC partitions we built the H_{sf} matrix (100×2742) concatenating the 2742 vectors (one for each point in the parameter space) containing the normalized entropy values between FC and SC partitions averaged across all the 123 subjects. We report in Figure 3.6 results relative to the first four components, that, out of the 99, explained most of the variance and globally occupy different zones in the parameter surface.

PC_1 is more expressed at high η and ω values, so in a subspace in which inter-subject variability is reduced and inter-modality variability is low. PC_1 scores represented on the cortex showed that in this region of the parameter space the nodes that are more likely to change cluster's assignment between FC and SC networks belong to the Dorsal Attention Network (DAN), the salience network and the somato-motor area. On the contrary, other regions like the control network and the DMN show high consistency between the two connectivity measures. The other principal components are more expressed in other regions of the parameters space and showed different patterns of inter-modality

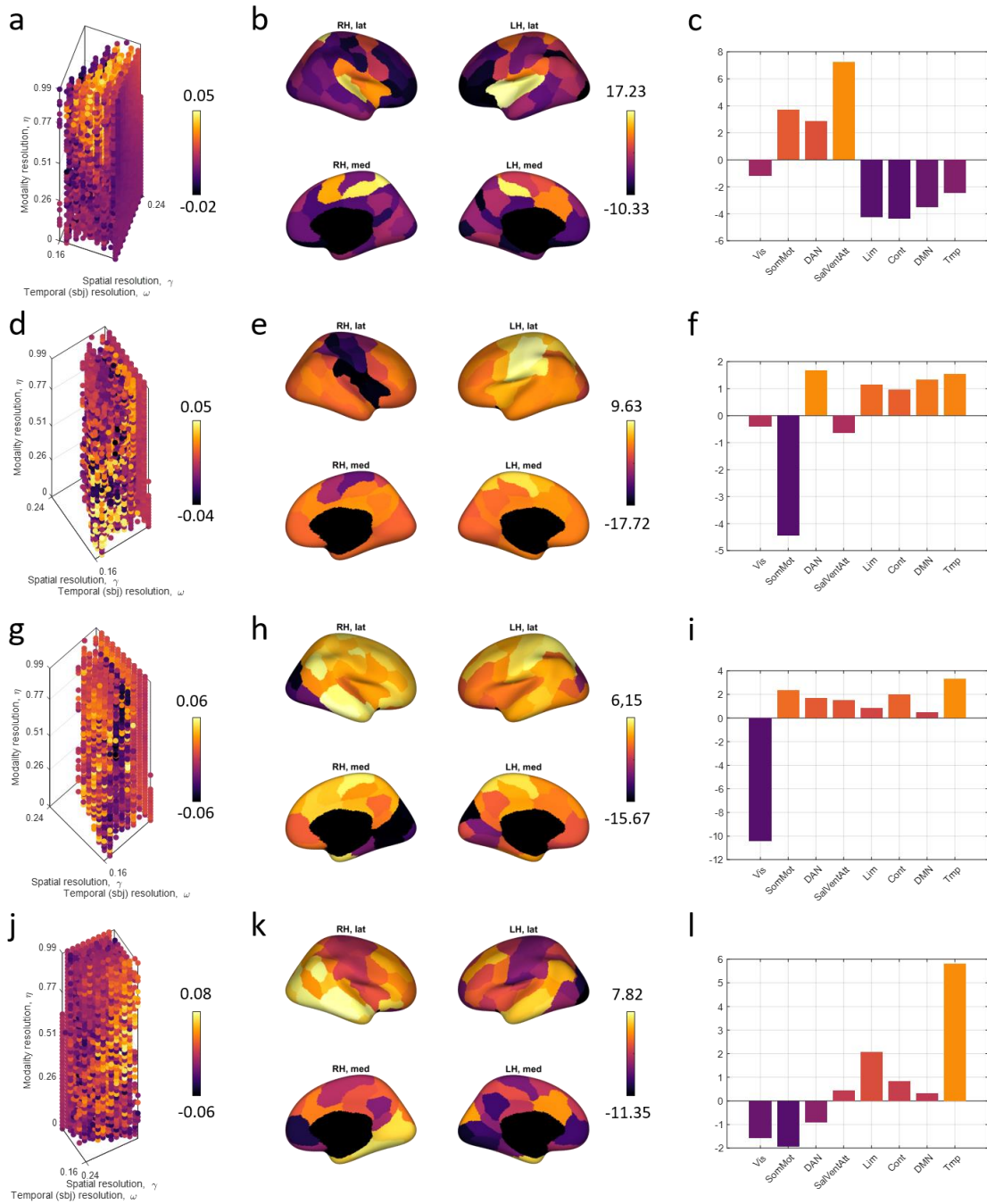


Figure 3.6. Principal component analysis on the entropy matrix incorporating the information about variability between SC and FC modules. The rows correspond to the analysis of each of the first four principal components. In the first column we show where, in the parameter space, each component is more expressed (information given by the pca's coefficients). In the second column we show the how much nodes are likely to change clusters between structural and functional partitions, through the pca's scores projected in the cortex. In the third column we averaged within the canonical functional networks the nodes' variability shown in the second column.

variability, suggesting that these patterns of variability of the SC and FC modular structure are scale-dependent. For example, PC₂ coefficients assume higher values in the subspace where γ and η are low and ω is high, that is networks have few clusters, are

highly coupled across subjects and barely coupled between modality. Here the regions whose modules' assignment is more variable between FC and SC networks are those involved in the DAN and in the DMN and those located in the medial side of the cortex. The regions belonging to the Salience network instead, showed high consistency between modalities. In PC₄ coefficient are more expressed at low γ , high ω , and medium η , where partitions have few clusters, high correspondence among subjects and a good level of overlap between modalities. In this subspace the DAN, somatomotor and visual areas tend to maintain the same modules allegiance in SC and FC networks, while the temporal, limbic and control networks are more likely to change passing from SC to FC networks.

3.3.2.2. *Principal component analysis – patterns of inter-subject variations*

To investigate the modes of variability across subjects (within modality) we built the H_{sbj} matrix (100×2742) concatenating the 2742 vectors (one for each point in the parameter space) containing the normalized entropy values between of the FC (or SC) partitions across the 123 subjects. We report here results relative to the first three components (Figure 3.7), that, out of the 99 explained most of the variance.

The coefficients of PC₁ observed in the parameter space are relative to value of ω equal to num where partitions across subjects are already fairly consistent. In both SC and FC patterns, the correspondent PC₁ scores show that the regions most variable across subjects belong to the visual and temporal areas, while the somatomotor area is the most consistent. With respect to SC pattern, the FC one indicates that partitions are slightly more variable across subjects, above all in the medial part of the cortex, and in the areas of the DAN. Other pattern of variability can be observed across the other considered independent components. In PC₂ for example, the coefficients are more expressed in the parameter space where the ω is the lowest, meaning where partitions across subjects are variable. As expected, the PC₂ scores indicate regions globally more variable with respect to PC₁ scores. Results suggest that, in both SC and FC networks, DMN and control networks are highly subject-specific, while the visual and the somatomotor area are more consistent across individuals. The SC scores with higher values are more spread all over the cortex.

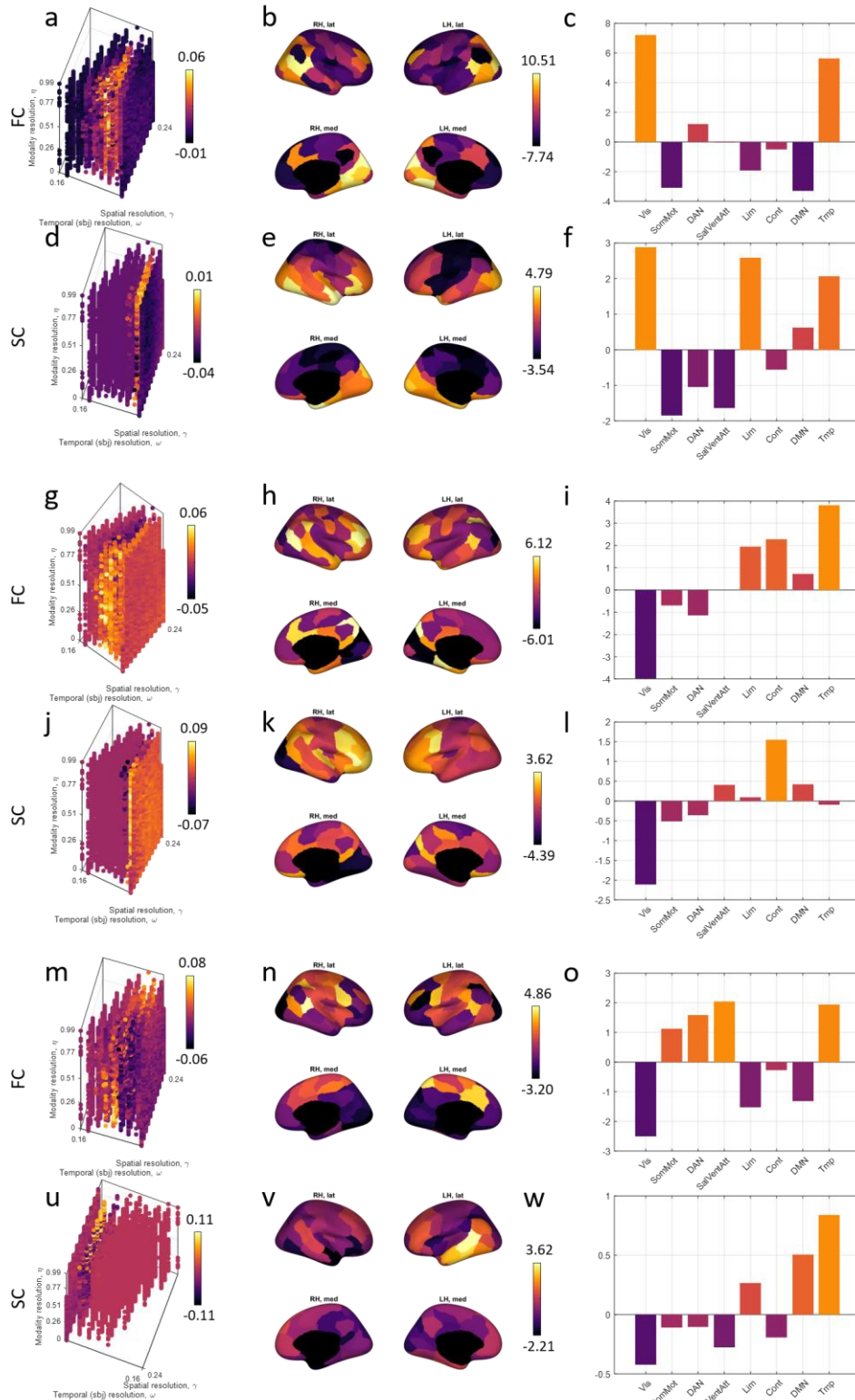


Figure 3.7. Principal component analysis on the entropy matrix incorporating the information about variability of the partitions across subjects. Each couple of rows correspond to the analysis of each of the first three principal components, for functional and structural connectivity matrices respectively. In the first column we show where, in the parameter space, each component is more expressed (information given by the pca's coefficients). In the second column we show the how much nodes are likely to change clusters across subjects, through the pca's scores projected in the cortex. In the third column we averaged within the canonical functional networks the nodes' variability shown in the second column.

3.3.3. Variability between and within modalities at specific scales

Through the novel multilayer modularity formulation, we have been able to identify partitions of the brain networks at different spatial scales, and differently coupled across subjects and type of connectivity. Through PCA we then detected recurrent pattern of variability on the cortex and in the parameter space. Here we deepen our study analyzing communities' properties at specific spatial and temporal scales. Indeed, focusing on a restricted combination of $\{\gamma, \omega, \eta\}$ allowed to provide a deeper characterization of communities, at interesting scales.

3.3.3.1. Inter-modality variations across η

Basing on our model, the coupling between partitions of FC and SC networks is mostly affected by the values of η . Here we explored how these partitions vary across η , focusing our analysis on a subset of the parameters $\{\gamma, \omega\}$. We choose $\omega = 0.0606$ and $\gamma = \{0.0808, 0.1414, 0.222\}$ (Figure 3.8a-b). Indeed, at this temporal scale we observed a progressive coupling of SC and FC partitions across η (Figure 3.4f and 3.8b), while the three γ -values ensure to look at the communities at different spatial scales, from a coarser to a finer

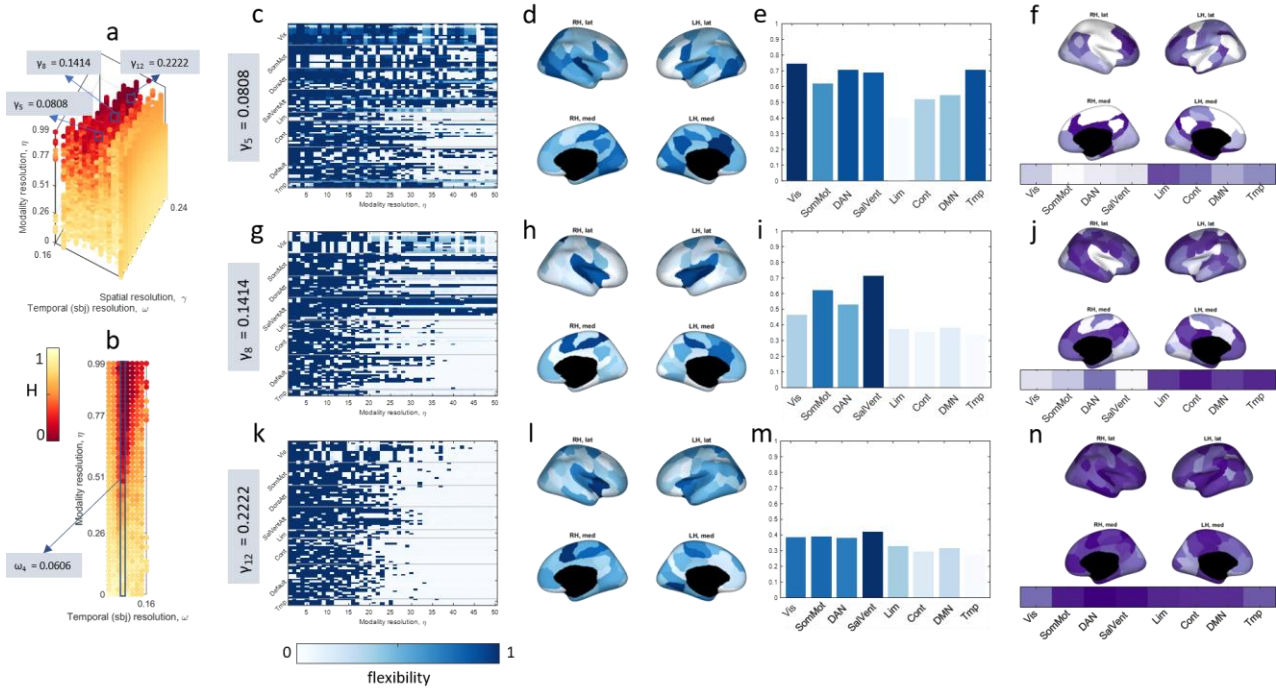


Figure 3.8. Analysis of the variability between FC and SC communities across η . Panels a-b: entropy between SC and FC partitions in the parameter space. Panels c-g-k: entropy between SC and FC partitions across η (averaged over the subjects) for three specific γ -values. Panels d-n: average of the entropy values for each node, canonical areas, and correlation between these values and η for each node.

spectrum of communities. For these combinations of $\{\gamma, \omega\}$ we observed how the flexibility between SC and FC partitions (averaged for all the subjects) varies across η (Figure 3.8c, 3.8g, 3.8k). In order to identify the more (less) flexible brain areas, we also represented the mean flexibility value across η on the cortex surface (Figure 3.8d, 3.8h, 3.8l), and within the ICNs (Figure 3.8e, 3.8i, 3.8m). Finally, we computed the correlation between flexibility and η , reporting significant values ($p < 0.05$) (Figure 3.8f, 3.8j, 3.8n).

According to these results, different brain regions exhibit different patterns of flexibility across η and γ . Increasing values of η results in low flexibility between FC and SC partitions. At the same time, also setting the γ to finer partitions results in high coupling between FC and SC partitions even at medium η -values. On the contrary, at coarser scales (obtained with $\gamma = [0.0808; 0.1414]$) we could observe how some regions keep different module's assignment even with high η -values. In particular, when $\gamma = 0.0808$, the nodes involved in the visual area, the temporal area, the DAN and salience network show low coupling between FC and SC partitions all over the η -range and, in turn, they do not correlate with the η -values. At the scale defined by $\gamma = 0.1414$ we can observe similar patterns, with the only difference that here the temporal area shows high consistence between the two modalities. When $\gamma = 0.2222$ instead, all the brain regions show high modules consistence between FC and SC networks for increasing η -values, so that all the nodes positively correlate with η . Globally, in every considered spatial scale, the nodes belonging to the salience network are those whose cluster's assignment remain more variable across modality.

In Figure 3.9 we reported representative partitions obtained with the just mentioned combinations of $\{\gamma, \omega, \eta\}$, which confirm what just inferred. Increasing η -values result in highly coupled partitions at the modality level. This coupling turns into a perfect match for high γ -values. For lower γ s instead, the nodes involved above all in the medial area and the salience network belong to different clusters in the two acquisition modalities.

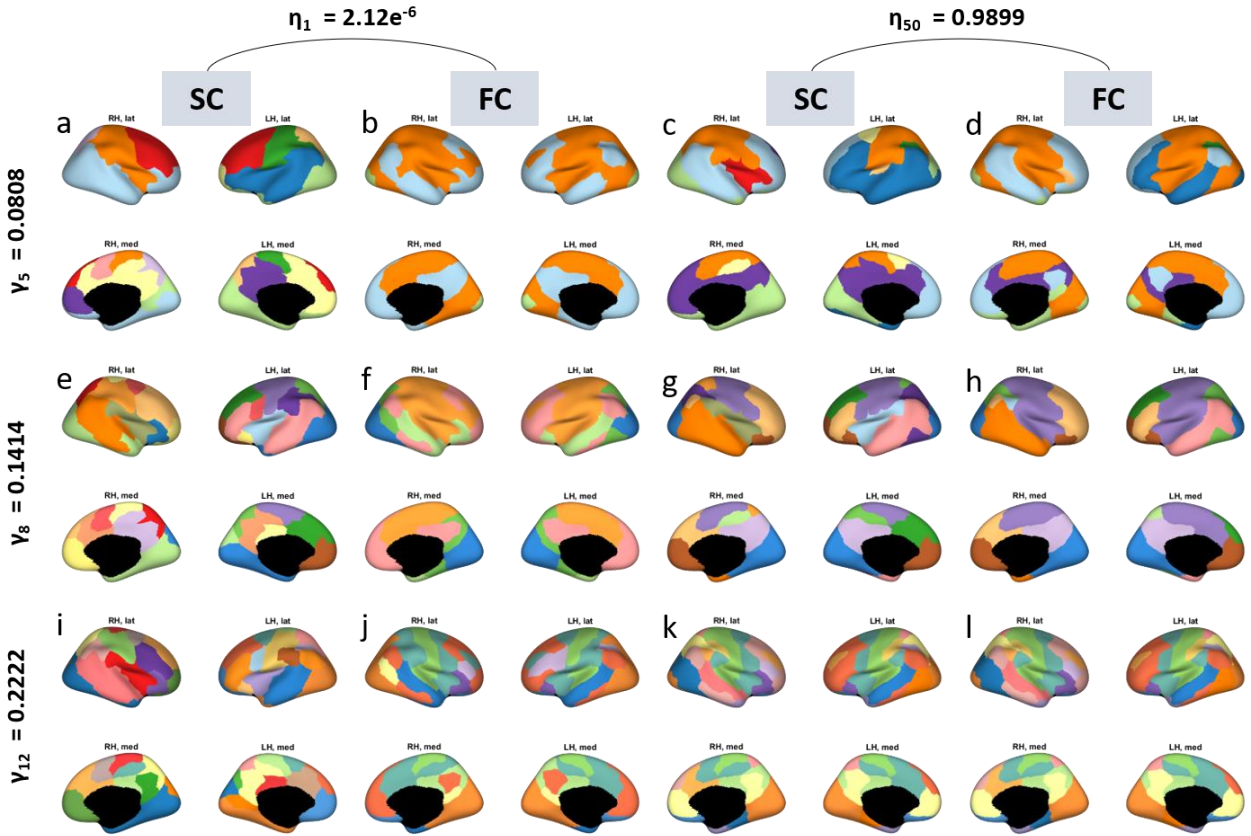


Figure 3.9. representative partitions for the specific combinations of $\{\gamma, \omega, \eta\}$ explored in figure 3.6

3.3.3.2. Inter-subject variations across ω

We evaluated how the partitions vary across subjects focusing on a restricted number of $\{\gamma, \omega, \eta\}$. We choose $\gamma = \{0.0808, 0.1414, 0.222\}$, $\omega = 0.0202$ and $\eta = 0.4848$ (Figure 3.10a-d). At this ω and η scales SC and FC partitions are at an intermediate level of coupling, and the partitions across subjects are not totally disjoint nor totally matched, as would it be by choosing lower and higher ω -values respectively. The values of γ have been chosen with the same criteria explained in the previous section. For these combinations of $\{\gamma, \omega, \eta\}$ we reported for each subject the mean value of the flexibility computed between its partition and the partitions of all the other subjects (Figure 3.10e-h). In order to identify the more (less) flexible brain areas across subjects, we also reported the mean flexibility value on the cortex surface, and within the ICNs. Finally, we reported a representative partition for each one of the considered combinations of $\{\gamma, \omega, \eta\}$ for both FC and SC networks.

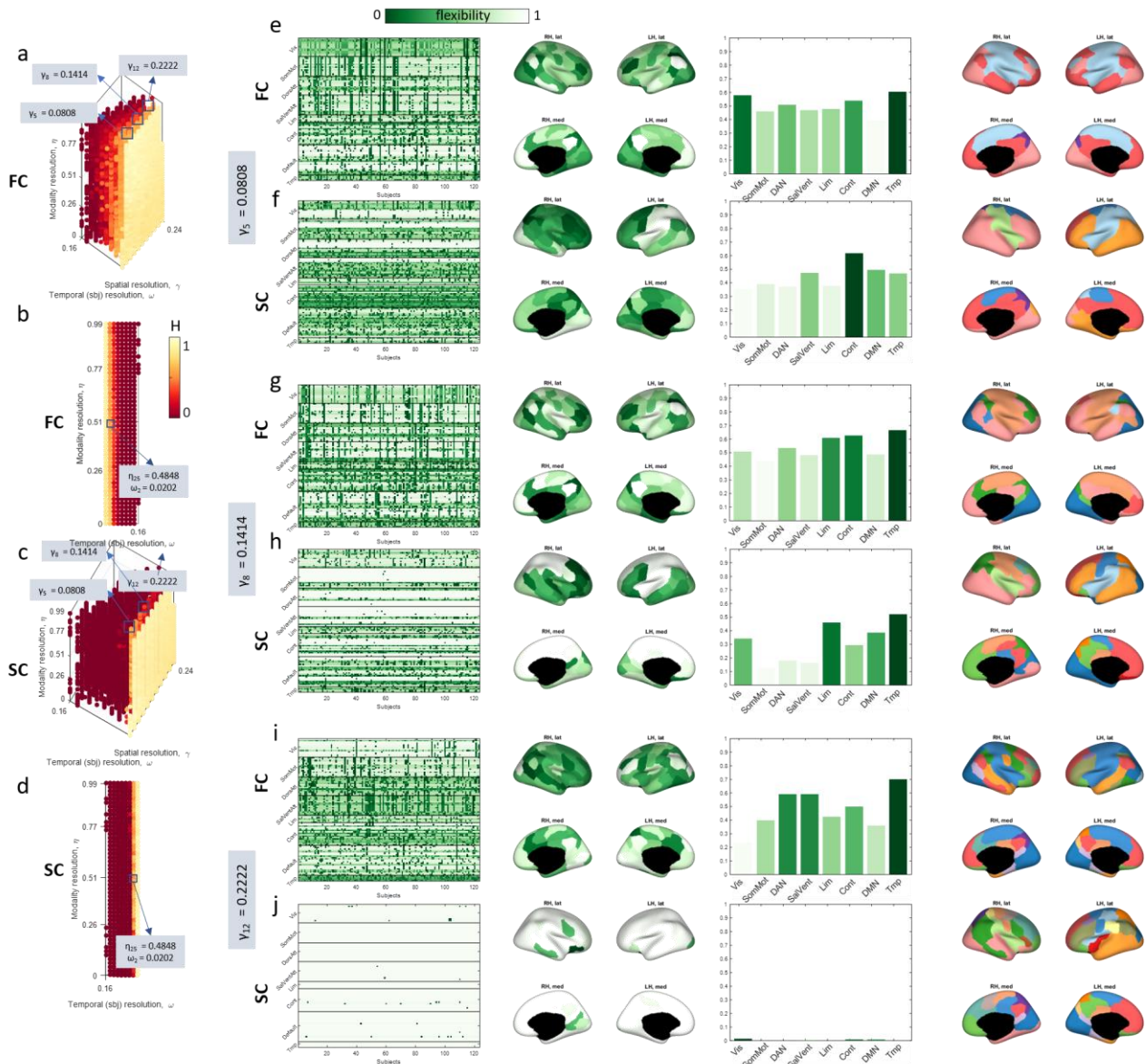


Figure 3.10. Analysis of the variability of the partitions across subjects. Panels a-d: entropy of the inter-subject partitions in the parameter space. Panels e-j: entropy of partitions across subjects across ω for three specific γ -values; average of these entropy values for each node represented in the cortex surface; average of these values within the functional canonical areas; representative partitions.

Results suggest that the flexibility and coupling of the partitions across subjects is dependent not only by the chosen temporal scale (ω) but also by the spatial scale (γ) at which we are looking communities. It is also evident that SC networks are globally more stable at the subject-level with respect to FC networks, which are more subject-specific. When $\gamma = 0.0808$ the temporal and visual areas, and the nodes pertaining to the control network are highly variable across subjects in the FC networks, while the DMN remains quite consistent. The anatomical networks of the same subjects instead, show high

variability in the clusters' assignment of the nodes of the control network, DMN, salience network and the temporal areas. Increasing γ to 0.1414 we observe different pattern of variability. In FC networks the temporal and limbic areas and the DAN and control networks constitute the clusters less consistent across subjects, while in the SC networks these clusters have been localized mostly in temporal, limbic and visual areas and in the DMN. At a finer scale ($\gamma = 0.222$) the SC networks have been partitioned with strong correspondence among subjects. The FC networks instead, still show a variability of the modules, primarily localized in the nodes of the temporal areas, and in those of the DAN and salience networks. Over all the scales, the part of the cortex that is more subject-specific at the modular structure level, for both kind of connectivity is the temporal area.

3.3.4. Correlation with behavioral assessments

The last passage of the current study was made to investigate the presence of any relations between behavioral assessments of the cognitive functions and the variability/coupling of the modular structure between type of connectivity. For this aim, we built a matrices of dimension $N \times N$ s (100x123) for each one of the first four principal components, in which each column is a measure of the entropy between SC and FC partitions of the i -th subject in the subspace identified by the component (see methods). Thus, we could compute the correlation between each row of the matrix (representing the entropy of a specific node for each subject) and each one of the vectors containing the different cognitive assessments introduced in section 2, here indicated with the acronyms *viq*, *piq*, *fsiq* and *comp*.

Results are reported in Figure 3.11. Here we show where the 100 more expressed coefficients of the first four components lay in the parameter space (panel *a*). As already mentioned, these four components barely overlap, covering almost all the 3D space identified by the parameters $\{\gamma, \omega, \eta\}$. We represented on the cortex surface the correlation coefficient obtained considering the *fsiq* index (panels *c-f*). We have chosen to report this index out of the four because it is the one that most correlate with all the others (panel *b*). These results suggest that while the entropy associated to some brain regions correlate similarly across different scales (identified by the components), some other brain areas

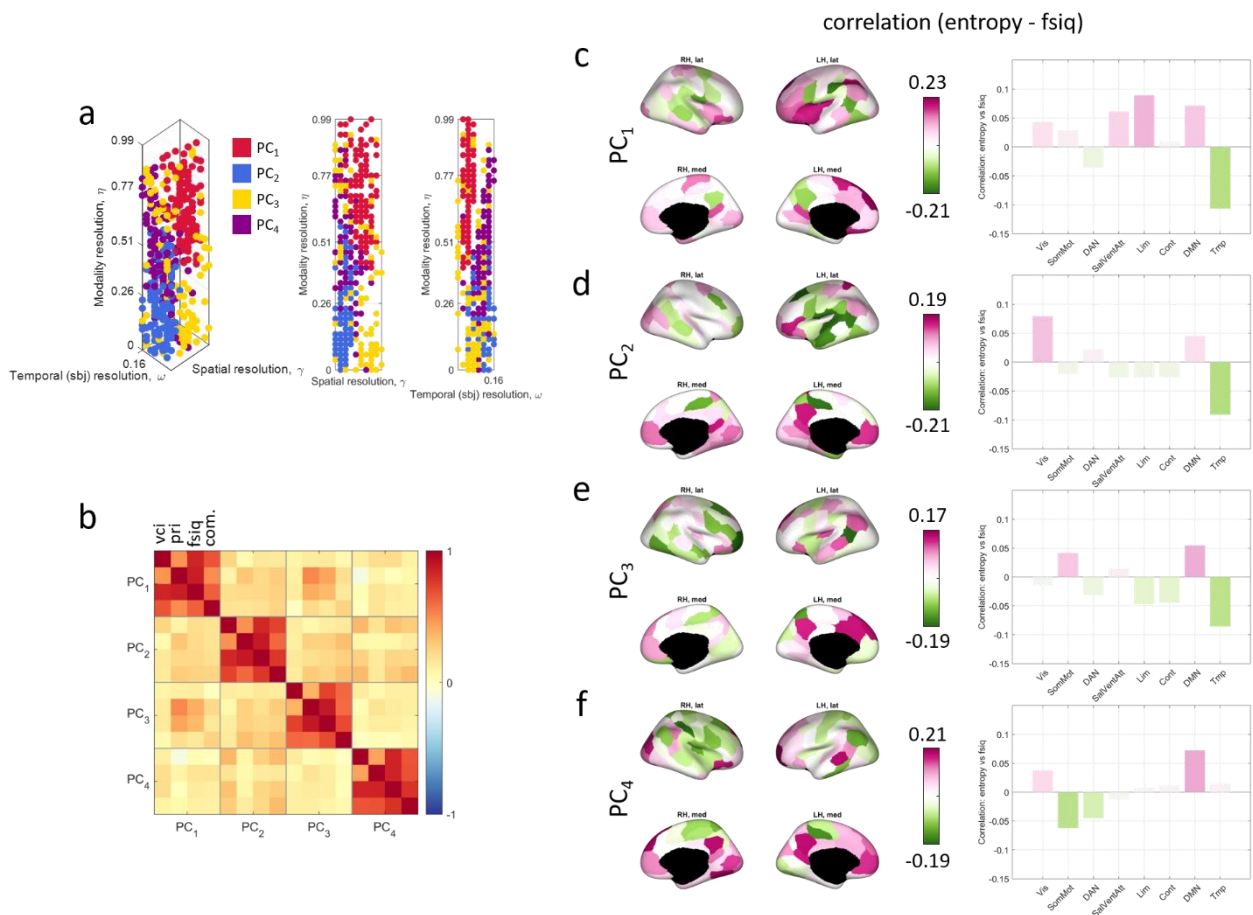


Figure 3.11. Correlation between inter-modality variability and behavioral assessments. Panel a: Plot on the parameter space of the highest 100 values of the first four components. Panels c-f: correlation between the average inter-modality variability relative to each component and the *fsiq* (plotted on the cortex and observed for the canonical functional networks). Panel b: correlation between the obtained correlation values for each clinical index and each component.

display a coupling between FC and SC partitions that correlate with *fsiq* in a different manner dependent on the scale we focus on. In the first case fall the nodes involved in the DMN, which showed a positive correlation coefficient for every principal component. This means that in a subject the higher is the entropy between FC and SC partitions in this area, the better is the cognitive score achieved by the subject. The opposite thing is verified in the nodes belonging to the temporal system, whose entropy negatively correlate with *fsiq*, meaning that in this area the more the communities are matched between SC and FC, the better results the cognitive assessment. Other regions present a positive or a negative correlation passing from a portion of the parameter space to another one. For example, the entropy associated to the somatomotor system positively correlate with *fsiq* in the first and third components, which identify a space with good coupling of the partitions across

subjects (high ω), and a good/bad SC-FC coupling respectively (high/low η). On the contrary the somatomotor entropy is negatively correlated with *fsiq* in the spaces identified by second and fourth components, relative to partitions more variable across subjects (low ω) and highly/slightly variable across modality respectively (low/high η). Other systems show a correlation only at certain scales, like the salience network that in the PC₁ positively correlate with *fsiq*, while in the other PCs its correlation coefficient is close to 0.

We carried a similar analysis to investigate the relations between the same cognitive scales and the variability/coupling of the modular structure across subjects in both cases of functional and structural networks. For this purpose, we considered the first three components and we built two matrices (one for each type of connectivity) of dimension $N \times N$ in which each column is strictly related to the entropy between that subject's partition and the partitions of all the other subjects (details in the methods section). Then, we computed the correlation between each row of the matrix and the same cognitive behavioral scales above introduced.

Results are presented in Figure 3.12. In panels *a-b* we show that also in this case the components are barely overlapped in the parameter space, and are mainly ω -specific. Interestingly, we noticed that while the correlations between functional communities and intelligence scores are still scale dependent (such correlation are more similar across the different assessment scores than across principal components, panel *d*), the structural connectivity do not show this scale-dependence (panel *c*). In particular, the inter-subject modular variation of the regions involved in the temporal area, the DMN, control network, limbic and visual areas is positively correlated to clinical scale, while the inter-subjects variation observed in the somato-motor area together with the DAN and salience networks are shows an opposite trend (panels *e,g,i*). As in the previous paragraph, the DMN presents an inter-subject variability that is always positively correlated to the considered behavioral scales, regardless of the scale and the type of connectivity. Other areas instead, like the visual and temporal areas, present an inter-subject functional communities' variability which positively or negatively correlates with iq according to the scale at which we observe such communities.

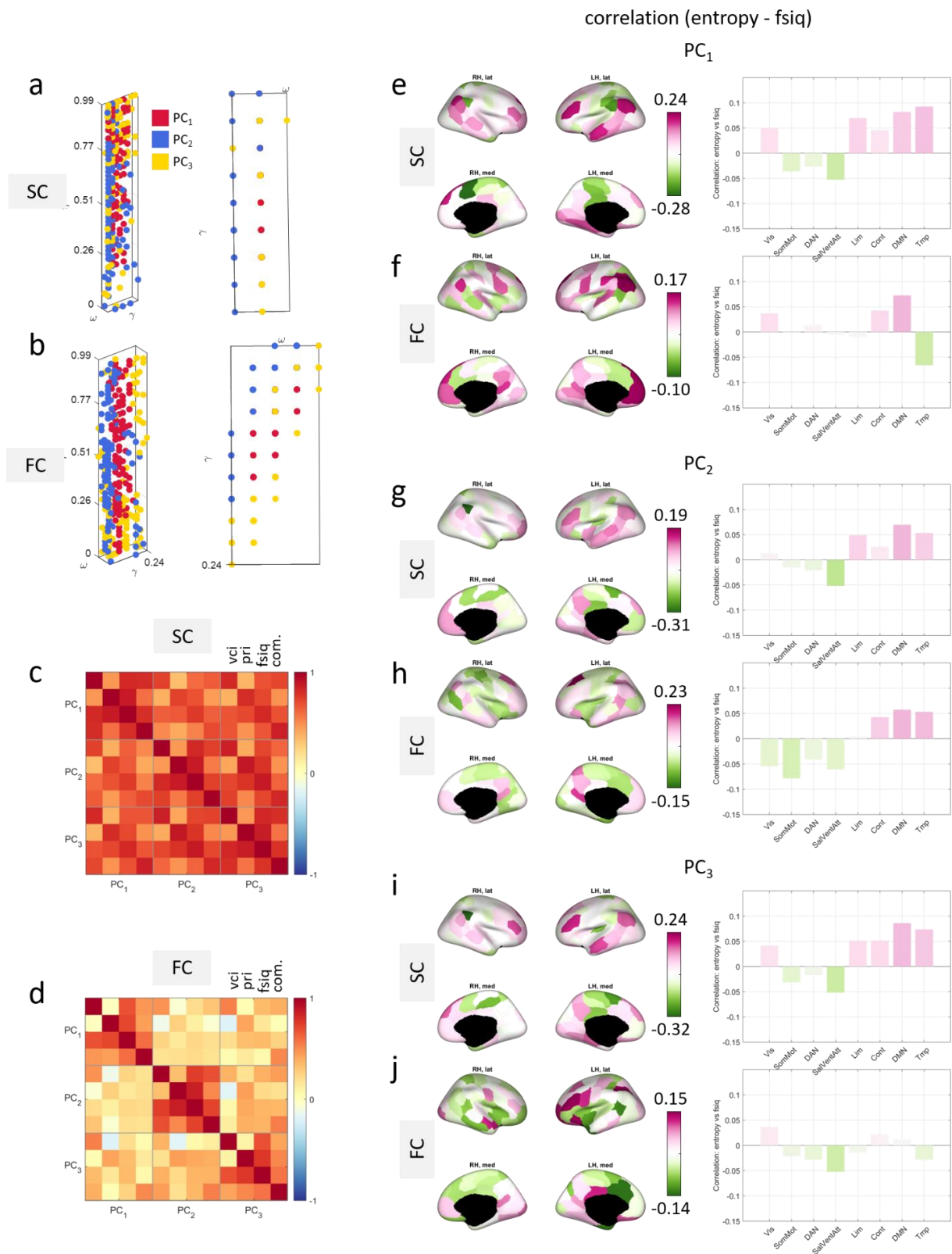


Figure 3.12. Correlation between inter-subject variability and behavioral assessments. Panels a-b: Plot on the parameter space of the highest 100 values of the first three components. Panels e-j: correlation between the average inter-subject variability relative to each component and the fsiq (plotted on the cortex and observed for the canonical functional networks, both for functional and structural networks). Panels c-d: correlation between the obtained correlation values for each clinical index and each component (for both structural and functional networks).

3.4. Discussion

In this section we explored how the modular structure of the human brain networks is organized across subjects and across structural and functional connectivity metrics. In doing this we proposed a novel multilayer framework, developed on top of the popular multilayer modular optimization (Mucha et al., 2010). Through this extension we could observe the coupling of the partitions across structural and functional connectivity metrics and across subjects, simultaneously, independently, and at different scales.

3.4.1. Relationship between structural and functional modular structure across subjects

The principal aim of this work was to characterize how community organization of the brain varies between types of connectivity. Our results suggest that the way structural and functional connectivity's modules are coupled is not ubiquitous. Rather, having the possibility to explore this coupling across spatial scales, subjects and different levels of coupling between SC and FC links, we could notice that it depends on all these mentioned factors. Trivially, the strength with which nodes are coupled across modality is proportional to strength of coupling between structural and functional partitions. Regarding the dependence from the spatial scale, previous studies have shown how brain networks display multiscale community organization (Betzel and Bassett, 2017), so that it is intuitive thinking that also the relationship of this organization between different metrics will be multiscale in turn. In particular, this relationship goes in the direction of a high coupling in fine partitions and vice versa. This is intuitive too, as partitions made of many small clusters are more likely to be more similar each other, with respect to partitions made of larger clusters. The strength of the coupling between SC and FC partitions is also dependent from the coupling of the partitions across subjects. A higher coupling between structure-function partitions was also more evident when considering partitions highly coupled across subjects.

Besides these empirical observations, we quantitatively found, through principal component analysis, modes of coupling between anatomical and functional partitions. Occupying different zones in the parameter space, these modes are independent each other. We described in detail the structure-function relationship explained by the first four

components where located in the parameter space as follows: PC₁ {high- η high- ω high- γ }, PC₂ {low- η medium- ω low- γ }, PC₃ {low- η low- ω high- γ }, PC₄ {medium- η high- ω low- γ }. These results confirmed that the structure-function coupling, at the modular level, is highly dependent on the resolution parameters. In the best possible condition from the SC-FC coupling point of view, represented by PC₁, the regions whose community assignment is more variable across modality are mainly associated to the salience ventral attention network. Interestingly, this might align with the results in (Vázquez-Rodríguez et al., 2019), where the relationship between structure and function in this area has shown to be lower than chance. The DMN instead is the area whose behavior is more variable across the components. This is intuitive given the high number of circuits in which these regions participate and the dynamics they exhibit (Buckner and DiNicola, 2019; Vatansever et al., 2015; Zhang et al., 2016). In PC₂ and PC₃, high entropy values between structural and functional communities are widespread and cover almost all the cortex surface. This is intuitive as these principal components are expressed also at low- ω , that is when subjects' partitions are uncoupled. As functional brain networks have been proven to be subject-specific (Finn et al., 2015; Gordon et al., 2017; Laumann et al., 2015), so will also be their relationship with the underlying structural network. Thus, when the coupling among subjects is low (first ω values in our case), is reasonable to expect a different (un)coupling among different regions of the brain.

Previous studies have shown that structure-function relationship and human behavior are related (Medaglia et al., 2018). Inspired by the observation in (Betzel et al., 2019), where also the correlation between the modular organization of the functional brain networks and clinical scores has been proven to be scale-dependent, we explored how measures associated to the iq test are associated to the different modes of variability between structural and functional modular organization. We could observe that this relationship is actually scale-dependent. Indeed, across the four principal components, most of the brain regions showed completely different patterns of correlation between SC-FC communities' entropy and the iq-based measures. Notably, the default mode networks is the subsystem whose patterns of correlations vary the least, maintaining always a

positive correlation by iq and its flexibility across structure and function. This result could be partially related with what mentioned above.

All these findings suggest that the coupling between anatomical and functional organization is neither well summarized by a single spatial/temporal scale, nor is ubiquitously associated to human cognition and behavior. Different studies have been carried out focusing on a single-scale community structure and its relationship with cognitive output and provided important insight into brain functions. However, our work, together with (Betzel et al., 2019; Betzel and Bassett, 2017), suggest that more multi-scale analysis are needed in order to gain a more comprehensive understanding of the brain structure, function and cognition.

On the heels of the structure-function investigation, we replicated each step of the analysis to gain also insights into the inter-subjects' variability of the modular structure. We proved that patterns of variability can be recapitulated in modes, covering distinct zones of the parameter space. Interestingly, these patterns were similar to those in (Betzel et al., 2019). In particular, the pattern observed in the subspace where the PC_1 is more expressed, highly overlaps with the one of PC_2 in. In our study this PC correspond to a region where inter-subjects' partitions are quite coupled, and the most variable regions (within the two cases of functional and structural connectivity) are associated to the default mode network and the visual area, while the less flexible regions across subjects are involved in the somatomotor area and the control network. When the inter-subjects coupling increases the primary sensory (visual) area become one of the less flexible.

Moreover, the inter-subjects investigation proved that cognition and behavior are associated to brain networks' organization features in a scale-dependent way, paving the way to more comprehensive analysis.

3.4.2. Methodological innovations of the multilayer framework

In this work we extended the classical multilayer modularity maximization framework to address a long-standing neuroscience question: what is the relationship between anatomical and functional modular organization? And how this relationship is expressed

across different individuals? Through our novel approach we could track modules across the two connection modalities and across subjects contemporaneously. The main advantage of this method consists in having communities matched across layers (represented by both individuals and type of connectivity), facilitating their comparison. Once obtained the communities we then characterized their variability both statistically (paragraph 3.3.2) and qualitatively (paragraph 3.3.3).

Previous studies already used the multilayer framework (De Domenico, 2017; Vaiana and Muldoon, 2018) to track communities across subjects (Betzel et al., 2019), time (Baum et al., 2017; Betzel et al., 2017b; Braun et al., 2015; Shine et al., 2016), learning paradigms (Bassett et al., 2011b; Gerraty et al., 2018), tasks (Cole et al., 2014) clinical cohorts (He et al., 2018), or to model brain dynamics (Khambhati et al., 2018). Through our model we could observe how the modular structure reorganizes according to two factors from which it depends, that are subjects and connections modality. This framework opens the door to new studies in which we can take into account that the human brain functioning is shaped by many co-occurrent factors. In general, more multilayer schemes are needed to incorporate multiple channels of connectivity, without aggregating or discarding useful information, to obtain a more comprehensive knowledge on the brain functioning.

3.4.3. Limitation and future advancements

Despite the innovation presented through a novel multilayer framework, our work presents some limitations. First of all we focused on a very specific kind on communities, the modules, that are defined upon an assortative criterium (Girvan and Newman, 2002). Despite it is well established that the brain shows an assortative organization that promotes states of segregation and integration (Fukushima et al., 2018), necessary for an efficient brain functioning (Tononi et al., 1994; Wig, 2017), brain networks could also present different kind of organizations, based for example on core-periphery structure, disassortative communities or diffusion models (Betzel et al., 2018b; Newman, 2012b). Recent studies started to explore different brain networks organization (Faskowitz et al., 2018) and future advancements could be done extending these efforts toward the multilayer modeling.

Another limitation consists in testing our model on a single dataset and a single parcellation of the brain networks. Further analysis could validate our results on other datasets (like the Human Connectome Project (Van Essen et al., 2013)), or finer parcellations (Gordon et al., 2016).

Finally, we focused on a restricted sample of participants, the adults. Future works could exploit the proposed methods and extend the study to lifespan studies or clinical cohorts, to investigate if and how the relationship between structure and function evolves across ages or diseases.

3.5. Conclusion

In conclusion, we investigated the relationship between structural and functional brain networks organization, and how it is shaped across subjects. In doing this we developed a novel multilayer framework able to incorporate multiple channels of connectivity, so that we could consider how the network modular structure varies across connection modality and across subjects simultaneously. While confirming previous findings on specific brain areas, our results provide also evidence that these relationships are scale-dependent, that can be recapitulated by “modes” of variability. As a consequence, we also showed that the way behavior is linked to the brain networks organization features is also scale-dependent. Overall, this work not only increases the state-of-the-art knowledge about structure-function linkage but also planted the seed for new analysis that can be done to comprehensively map the human brain networks organization.

Conclusion

The increasing evidences that the brain networks are organized in modules of strongly interconnected brain areas, that shape mechanisms of brain functioning and cognition, inspired this three-years project. The research activity here described has been carried out with the primary purpose of broadening the state-of-the-art knowledge on brain structural and functional organization across multiple domains. In attempting this, we tackled a number of methodological challenges. We steered our efforts to develop multilayer networks models that allow the analysis of the evolution of the brain modular organization across time, years, subjects and connection modalities.

In the first section we performed a simulation study to assess which algorithm is more suitable to detect modules in multilayer brain networks. We tested different algorithms through an ad-hoc implemented generator of multilayer networks with assortative communities. The main advantage of this generator is its flexibility, so that we could investigate the algorithms' performance on a wide range of conditions (regarding graph's density, number of clusters, noise level, intensity of the variation of the modular structure, ecc...) commonly found in brain networks. We found that the more appropriate algorithm is the well-known *genlouvain* (based on modularity maximization), widely used in the neuroscience field but whose performance has never been really assessed. We also tested the different algorithms on time-varying EEG-based brain networks, obtaining results in agreement with those of the simulation study. In fact, not only *genlouvain* was the algorithm more capable of recovering the underlying evolving community organization, but it also returned partitions physiologically interesting.

Genlouvain is a multiscale community detection algorithm, able to recover communities of different size and diversely coupled across layers, basing on the setting of its spatial and temporal resolution parameters. Common approaches consist of setting those parameters in a data driven way, or exploring the community organization at multiple scales, as previous studies has proven the multiscale nature of the human brain networks

organization. As an aside of the first work, we also provided some guidelines on the choice of these parameters basing on the network's properties.

In the second section we developed a robust multilayer framework, based on multilayer modularity maximization, to investigate the evolution of anatomical brain networks across the lifespan. Our strategy relies on a resampling-based method implemented to track statistically meaningful changes of variables of interest (in our case the properties of the modular structure) in multilayer networks. In this case focused on specific spatial and temporal resolution scales empirically selected. We found that the human brain exhibits an age-dependent modular organization, whose properties vary with age according to linear and non-linear (U-shaped) trends. The number of communities increases with age, as well as the strength with which they reconfigure. Modularity instead, is higher in the early and in the late lifespan, and we track the origins of this high modularity to two different substrates in brain connectivity, linked to the number and the weights of the intra-clusters' edges. We also proved that age impacts the way in which clusters are distributed across the cortex surface, as they became more and more hemispheric-specific with age. Finally, we also identify which brain regions mostly contribute to the network reconfiguration and those who remain more stable across years. These findings strengthen our knowledge on the connectome organization across lifespan, while the methods developed can be used to monitor variables of interest in structural and functional brain networks across other datasets.

Finally, in the third section, we studied the relationship between anatomical and functional brain networks organization, and its inter-subject's variation. We extended the multilayer modularity maximization framework in order to simultaneously capture variations across subjects and connection modalities, by adding a third resolution parameter. This time we performed this analysis with a multiscale approach, observing how the modular organization varies across these two domains depending on the spatial resolution and the inter- and intra-subjects coupling. We found that the nodes more responsible of a different modular organization between anatomical and functional networks are those involved in the default mode network. However, more in general, the

variability of the community structure across modality and subjects is highly depend on the scale at which we observe the modules. Thus, we characterized patterns of variability and recapitulated them into scale-dependent “modes”. We also proved that the multi-scale nature of the modular structure leads to correlation patterns with measures of cognitive performance are still scale-dependent. This result suggests that deeper investigation at multiple scales are needed not to miss potentially relevant brain-behavior associations.

In conclusion, the results of this thesis increased the current knowledge on brain structure and function through the development and the validation of new methods at the intersection of computational neuroscience and network science. Future studies could employ the proposed frameworks to extend our analysis to clinical cohorts and explore how brain diseases impact on the relationship between brain anatomy and activity, or how they affect the normal aging from the structural organization point of view. Overall, this work means to open the door toward comprehensive and statistically robust investigation, taking into account the multilayer nature of brain structure functioning.

Bibliography

- Adachi, Y., Osada, T., Sporns, O., Watanabe, T., Matsui, T., Miyamoto, K., Miyashita, Y., 2012. Functional Connectivity between Anatomically Unconnected Areas Is Shaped by Collective Network-Level Effects in the Macaque Cortex. *Cereb Cortex* 22, 1586–1592. <https://doi.org/10.1093/cercor/bhr234>
- Andrews-Hanna, J.R., Snyder, A.Z., Vincent, J.L., Lustig, C., Head, D., Raichle, M.E., Buckner, R.L., 2007. Disruption of Large-Scale Brain Systems in Advanced Aging. *Neuron* 56, 924–935. <https://doi.org/10.1016/j.neuron.2007.10.038>
- Andric, M., Hasson, U., 2015. Global features of functional brain networks change with contextual disorder. *NeuroImage* 117, 103–113. <https://doi.org/10.1016/j.neuroimage.2015.05.025>
- Astolfi, L., Cincotti, F., Mattia, D., Marciani, M.G., Baccala, L.A., Fallani, F. de V., Salinari, S., Ursino, M., Zavaglia, M., Ding, L., Edgar, J.C., Miller, G.A., He, B., Babiloni, F., 2007. Comparison of different cortical connectivity estimators for high-resolution EEG recordings. *Human Brain Mapping* 28, 143–157. <https://doi.org/10.1002/hbm.20263>
- Astolfi, L., Cincotti, F., Mattia, D., Marciani, M.G., Baccala, L.A., Fallani, F.D.V., Salinari, S., Ursino, M., Zavaglia, M., Babiloni, F., 2006. Assessing cortical functional connectivity by partial directed coherence: simulations and application to real data. *IEEE Transactions on Biomedical Engineering* 53, 1802–1812. <https://doi.org/10.1109/TBME.2006.873692>
- Avants, B.B., Epstein, C.L., Grossman, M., Gee, J.C., 2008. Symmetric diffeomorphic image registration with cross-correlation: Evaluating automated labeling of elderly and neurodegenerative brain. *Medical Image Analysis, Special Issue on The Third International Workshop on Biomedical Image Registration – WBIR 2006* 12, 26–41. <https://doi.org/10.1016/j.media.2007.06.004>
- Baccalá, L.A., Sameshima, K., 2001. Partial directed coherence: a new concept in neural structure determination. *Biol Cybern* 84, 463–474. <https://doi.org/10.1007/PL00007990>
- Basser, P.J., Pajevic, S., Pierpaoli, C., Duda, J., Aldroubi, A., 2000. In vivo fiber tractography using DT-MRI data. *Magnetic Resonance in Medicine* 44, 625–632. [https://doi.org/10.1002/1522-2594\(200010\)44:4<625::AID-MRM17>3.0.CO;2-O](https://doi.org/10.1002/1522-2594(200010)44:4<625::AID-MRM17>3.0.CO;2-O)
- Bassett, D.S., Brown, J.A., Deshpande, V., Carlson, J.M., Grafton, S.T., 2011a. Conserved and variable architecture of human white matter connectivity. *NeuroImage* 54, 1262–1279. <https://doi.org/10.1016/j.neuroimage.2010.09.006>
- Bassett, D.S., Sporns, O., 2017. Network neuroscience. *Nature Neuroscience* 20, 353–364. <https://doi.org/10.1038/nn.4502>
- Bassett, D.S., Wymbs, N.F., Porter, M.A., Mucha, P.J., Carlson, J.M., Grafton, S.T., 2011b. Dynamic reconfiguration of human brain networks during learning. *PNAS* 108, 7641–7646. <https://doi.org/10.1073/pnas.1018985108>
- Baum, G.L., Ciric, R., Roalf, D.R., Betzel, R.F., Moore, T.M., Shinohara, R.T., Kahn, A.E., Vandekar, S.N., Rupert, P.E., Quarmley, M., Cook, P.A., Elliott, M.A., Ruparel, K., Gur, R.E., Gur, R.C., Bassett, D.S., Satterthwaite, T.D., 2017. Modular Segregation of

- Structural Brain Networks Supports the Development of Executive Function in Youth. *Current Biology* 27, 1561-1572.e8. <https://doi.org/10.1016/j.cub.2017.04.051>
- Bazzi, M., Jeub, L.G.S., Arenas, A., Howison, S.D., Porter, M.A., 2019. A Framework for the Construction of Generative Models for Mesoscale Structure in Multilayer Networks. arXiv:1608.06196 [cond-mat, physics:nlin, physics:physics, stat].
- Bertolero, M.A., Yeo, B.T.T., D'Esposito, M., 2015. The modular and integrative functional architecture of the human brain. *PNAS* 112, E6798–E6807. <https://doi.org/10.1073/pnas.1510619112>
- Betzell, R.F., Bassett, D.S., 2018. Specificity and robustness of long-distance connections in weighted, interareal connectomes. *PNAS* 115, E4880–E4889. <https://doi.org/10.1073/pnas.1720186115>
- Betzell, R.F., Bassett, D.S., 2017. Multi-scale brain networks. *NeuroImage, Functional Architecture of the Brain* 160, 73–83. <https://doi.org/10.1016/j.neuroimage.2016.11.006>
- Betzell, R.F., Bertolero, M.A., Gordon, E.M., Gratton, C., Dosenbach, N.U.F., Bassett, D.S., 2019. The community structure of functional brain networks exhibits scale-specific patterns of inter- and intra-subject variability. *NeuroImage*. <https://doi.org/10.1016/j.neuroimage.2019.07.003>
- Betzell, R.F., Byrge, L., He, Y., Goñi, J., Zuo, X.-N., Sporns, O., 2014. Changes in structural and functional connectivity among resting-state networks across the human lifespan. *NeuroImage* 102, 345–357. <https://doi.org/10.1016/j.neuroimage.2014.07.067>
- Betzell, R.F., Griffa, A., Avena-Koenigsberger, A., Goñi, J., Thiran, J.-P., Hagmann, P., Sporns, O., 2013. Multi-scale community organization of the human structural connectome and its relationship with resting-state functional connectivity. *Network Science* 1, 353–373. <https://doi.org/10.1017/nws.2013.19>
- Betzell, R.F., Griffa, A., Hagmann, P., Mišić, B., 2018a. Distance-dependent consensus thresholds for generating group-representative structural brain networks. *Network Neuroscience* 3, 475–496. https://doi.org/10.1162/netn_a_00075
- Betzell, R.F., Medaglia, J.D., Bassett, D.S., 2018b. Diversity of meso-scale architecture in human and non-human connectomes. *Nat Commun* 9, 1–14. <https://doi.org/10.1038/s41467-017-02681-z>
- Betzell, R.F., Medaglia, J.D., Papadopoulos, L., Baum, G.L., Gur, Ruben, Gur, Raquel, Roalf, D., Satterthwaite, T.D., Bassett, D.S., 2017a. The modular organization of human anatomical brain networks: Accounting for the cost of wiring. *Network Neuroscience* 1, 42–68. https://doi.org/10.1162/NETN_a_00002
- Betzell, R.F., Mišić, B., He, Y., Rumschlag, J., Zuo, X.-N., Sporns, O., 2015. Functional brain modules reconfigure at multiple scales across the human lifespan. arXiv:1510.08045 [q-bio].
- Betzell, R.F., Satterthwaite, T.D., Gold, J.I., Bassett, D.S., 2017b. Positive affect, surprise, and fatigue are correlates of network flexibility. *Sci Rep* 7, 1–10. <https://doi.org/10.1038/s41598-017-00425-z>

- Blondel, V.D., Guillaume, J.-L., Lambiotte, R., Lefebvre, E., 2008. Fast unfolding of communities in large networks. *Journal of Statistical Mechanics: Theory and Experiment* 2008, P10008. <https://doi.org/10.1088/1742-5468/2008/10/P10008>
- Boccaletti, S., Latora, V., Moreno, Y., Chavez, M., Hwang, D.-U., 2006. Complex networks: Structure and dynamics. *Physics Reports* 424, 175–308. <https://doi.org/10.1016/j.physrep.2005.10.009>
- Börner, K., Sanyal, S., Vespignani, A., 2007. Network science. *Annual Review of Information Science and Technology* 41, 537–607. <https://doi.org/10.1002/aris.2007.1440410119>
- Braun, U., Schäfer, A., Walter, H., Erk, S., Romanczuk-Seiferth, N., Haddad, L., Schweiger, J.I., Grimm, O., Heinz, A., Tost, H., Meyer-Lindenberg, A., Bassett, D.S., 2015. Dynamic reconfiguration of frontal brain networks during executive cognition in humans. *PNAS* 112, 11678–11683. <https://doi.org/10.1073/pnas.1422487112>
- Breakspear, M., 2017. Dynamic models of large-scale brain activity. *Nature Neuroscience* 20, 340–352. <https://doi.org/10.1038/nn.4497>
- Bressler, S.L., Menon, V., 2010. Large-scale brain networks in cognition: emerging methods and principles. *Trends in Cognitive Sciences* 14, 277–290. <https://doi.org/10.1016/j.tics.2010.04.004>
- Buckner, R.L., 2004. Memory and Executive Function in Aging and AD: Multiple Factors that Cause Decline and Reserve Factors that Compensate. *Neuron* 44, 195–208. <https://doi.org/10.1016/j.neuron.2004.09.006>
- Buckner, R.L., DiNicola, L.M., 2019. The brain's default network: updated anatomy, physiology and evolving insights. *Nat Rev Neurosci* 20, 593–608. <https://doi.org/10.1038/s41583-019-0212-7>
- Buckner, R.L., Sepulcre, J., Talukdar, T., Krienen, F.M., Liu, H., Hedden, T., Andrews-Hanna, J.R., Sperling, R.A., Johnson, K.A., 2009. Cortical Hubs Revealed by Intrinsic Functional Connectivity: Mapping, Assessment of Stability, and Relation to Alzheimer's Disease. *J. Neurosci.* 29, 1860–1873. <https://doi.org/10.1523/JNEUROSCI.5062-08.2009>
- Bullmore, E., Sporns, O., 2009. Complex brain networks: graph theoretical analysis of structural and functional systems. *Nature Reviews Neuroscience* 10, 186–198. <https://doi.org/10.1038/nrn2575>
- Bullmore, E.T., Bassett, D.S., 2011. Brain Graphs: Graphical Models of the Human Brain Connectome. *Annual Review of Clinical Psychology* 7, 113–140. <https://doi.org/10.1146/annurev-clinpsy-040510-143934>
- Byrge, L., Sporns, O., Smith, L.B., 2014. Developmental process emerges from extended brain–body–behavior networks. *Trends in Cognitive Sciences* 18, 395–403. <https://doi.org/10.1016/j.tics.2014.04.010>
- Cao, M., Wang, J.-H., Dai, Z.-J., Cao, X.-Y., Jiang, L.-L., Fan, F.-M., Song, X.-W., Xia, M.-R., Shu, N., Dong, Q., Milham, M.P., Castellanos, F.X., Zuo, X.-N., He, Y., 2014. Topological organization of the human brain functional connectome across the lifespan. *Developmental Cognitive Neuroscience* 7, 76–93. <https://doi.org/10.1016/j.dcn.2013.11.004>

- Chakrabarti, D., Kumar, R., Tomkins, A., 2006. Evolutionary Clustering, in: Proceedings of the 12th ACM SIGKDD International Conference on Knowledge Discovery and Data Mining, KDD '06. ACM, New York, NY, USA, pp. 554–560. <https://doi.org/10.1145/1150402.1150467>
- Chan, M.Y., Park, D.C., Savalia, N.K., Petersen, S.E., Wig, G.S., 2014. Decreased segregation of brain systems across the healthy adult lifespan. *PNAS* 111, E4997–E5006. <https://doi.org/10.1073/pnas.1415122111>
- Chavez, M., Valencia, M., Navarro, V., Latora, V., Martinerie, J., 2010. Functional Modularity of Background Activities in Normal and Epileptic Brain Networks. *Phys. Rev. Lett.* 104, 118701. <https://doi.org/10.1103/PhysRevLett.104.118701>
- Chen, Z., Liu, M., Gross, D.W., Beaulieu, C., 2013. Graph theoretical analysis of developmental patterns of the white matter network. *Front. Hum. Neurosci.* 7. <https://doi.org/10.3389/fnhum.2013.00716>
- Chen, Z.J., He, Y., Rosa-Neto, P., Gong, G., Evans, A.C., 2011. Age-related alterations in the modular organization of structural cortical network by using cortical thickness from MRI. *NeuroImage* 56, 235–245. <https://doi.org/10.1016/j.neuroimage.2011.01.010>
- Cole, M.W., Bassett, D.S., Power, J.D., Braver, T.S., Petersen, S.E., 2014. Intrinsic and Task-Evoked Network Architectures of the Human Brain. *Neuron* 83, 238–251. <https://doi.org/10.1016/j.neuron.2014.05.014>
- Compston, A., 2010. The Berger rhythm: potential changes from the occipital lobes in man, by E.D. Adrian and B.H.C. Matthews (From the Physiological Laboratory, Cambridge). *Brain* 1934: 57; 355-385. *Brain* 133, 3–6. <https://doi.org/10.1093/brain/awp324>
- Crofts, J.J., Higham, D.J., 2009. A weighted communicability measure applied to complex brain networks. *Journal of The Royal Society Interface* 6, 411–414. <https://doi.org/10.1098/rsif.2008.0484>
- Dale, A.M., Fischl, B., Sereno, M.I., 1999. Cortical Surface-Based Analysis: I. Segmentation and Surface Reconstruction. *NeuroImage* 9, 179–194. <https://doi.org/10.1006/nimg.1998.0395>
- Damoiseaux, J.S., Rombouts, S. a. R.B., Barkhof, F., Scheltens, P., Stam, C.J., Smith, S.M., Beckmann, C.F., 2006. Consistent resting-state networks across healthy subjects. *PNAS* 103, 13848–13853. <https://doi.org/10.1073/pnas.0601417103>
- Danon, L., Díaz-Guilera, A., Duch, J., Arenas, A., 2005. Comparing community structure identification. *J. Stat. Mech.* 2005, P09008–P09008. <https://doi.org/10.1088/1742-5468/2005/09/P09008>
- De Domenico, M., 2017. Multilayer modeling and analysis of human brain networks. *Gigascience* 6. <https://doi.org/10.1093/gigascience/gix004>
- Deco, G., Jirsa, V., McIntosh, A.R., Sporns, O., Kötter, R., 2009. Key role of coupling, delay, and noise in resting brain fluctuations. *PNAS* 106, 10302–10307. <https://doi.org/10.1073/pnas.0901831106>
- Dennis, E.L., Jahanshad, N., McMahon, K.L., de Zubicaray, G.I., Martin, N.G., Hickie, I.B., Toga, A.W., Wright, M.J., Thompson, P.M., 2013. Development of brain structural connectivity between ages 12 and 30: A 4-Tesla diffusion imaging study in 439

- adolescents and adults. *NeuroImage* 64, 671–684. <https://doi.org/10.1016/j.neuroimage.2012.09.004>
- Destrieux, C., Fischl, B., Dale, A., Halgren, E., 2010. Automatic parcellation of human cortical gyri and sulci using standard anatomical nomenclature. *NeuroImage* 53, 1–15. <https://doi.org/10.1016/j.neuroimage.2010.06.010>
- Di Martino, A., Fair, D.A., Kelly, C., Satterthwaite, T.D., Castellanos, F.X., Thomason, M.E., Craddock, R.C., Luna, B., Leventhal, B.L., Zuo, X.-N., Milham, M.P., 2014. Unraveling the Miswired Connectome: A Developmental Perspective. *Neuron* 83, 1335–1353. <https://doi.org/10.1016/j.neuron.2014.08.050>
- Dong, W., Lepri, B., Pentland, A. (Sandy), 2011. Modeling the Co-evolution of Behaviors and Social Relationships Using Mobile Phone Data, in: *Proceedings of the 10th International Conference on Mobile and Ubiquitous Multimedia, MUM '11*. ACM, New York, NY, USA, pp. 134–143. <https://doi.org/10.1145/2107596.2107613>
- Duffau, H., 2014. The huge plastic potential of adult brain and the role of connectomics: New insights provided by serial mappings in glioma surgery. *Cortex* 58, 325–337. <https://doi.org/10.1016/j.cortex.2013.08.005>
- Efron, B., Tibshirani, R.J., 1993. *An Introduction to the Bootstrap*. Springer US, Boston, MA. <https://doi.org/10.1007/978-1-4899-4541-9>
- Eickhoff, S.B., Paus, T., Caspers, S., Grosbras, M.-H., Evans, A.C., Zilles, K., Amunts, K., 2007. Assignment of functional activations to probabilistic cytoarchitectonic areas revisited. *NeuroImage* 36, 511–521. <https://doi.org/10.1016/j.neuroimage.2007.03.060>
- Esteban, O., Birman, D., Schaer, M., Koyejo, O.O., Poldrack, R.A., Gorgolewski, K.J., 2017. MRIQC: Advancing the automatic prediction of image quality in MRI from unseen sites. *PLOS ONE* 12, e0184661. <https://doi.org/10.1371/journal.pone.0184661>
- Esteban, O., Markiewicz, C.J., Blair, R.W., Moodie, C.A., Isik, A.I., Erramuzpe, A., Kent, J.D., Goncalves, M., DuPre, E., Snyder, M., Oya, H., Ghosh, S.S., Wright, J., Durnez, J., Poldrack, R.A., Gorgolewski, K.J., 2019. fMRIPrep: a robust preprocessing pipeline for functional MRI. *Nat Methods* 16, 111–116. <https://doi.org/10.1038/s41592-018-0235-4>
- Fallani, F.D.V., Costa, L. da F., Rodriguez, F.A., Astolfi, L., Vecchiato, G., Toppi, J., Borghini, G., Cincotti, F., Mattia, D., Salinari, S., Isabella, R., Babiloni, F., 2010. A graph-theoretical approach in brain functional networks. Possible implications in EEG studies. *Nonlinear Biomed Phys* 4, S8. <https://doi.org/10.1186/1753-4631-4-S1-S8>
- Faskowitz, J., Yan, X., Zuo, X.-N., Sporns, O., 2018. Weighted Stochastic Block Models of the Human Connectome across the Life Span. *Scientific Reports* 8, 12997. <https://doi.org/10.1038/s41598-018-31202-1>
- Filippi, M., van den Heuvel, M.P., Fornito, A., He, Y., Hulshoff Pol, H.E., Agosta, F., Comi, G., Rocca, M.A., 2013. Assessment of system dysfunction in the brain through MRI-based connectomics. *The Lancet Neurology* 12, 1189–1199. [https://doi.org/10.1016/S1474-4422\(13\)70144-3](https://doi.org/10.1016/S1474-4422(13)70144-3)
- Finn, E.S., Shen, X., Scheinost, D., Rosenberg, M.D., Huang, J., Chun, M.M., Papademetris, X., Constable, R.T., 2015. Functional connectome fingerprinting: identifying

- individuals using patterns of brain connectivity. *neuro* 18, 1664–1671. <https://doi.org/10.1038/nn.4135>
- Folino, F., Pizzuti, C., 2014. An Evolutionary Multiobjective Approach for Community Discovery in Dynamic Networks. *IEEE Transactions on Knowledge and Data Engineering* 26, 1838–1852. <https://doi.org/10.1109/TKDE.2013.131>
- Fonov, V., Evans, A., McKinstry, R., Almlí, C., Collins, D., 2009. Unbiased nonlinear average age-appropriate brain templates from birth to adulthood. *NeuroImage, Organization for Human Brain Mapping 2009 Annual Meeting* 47, S102. [https://doi.org/10.1016/S1053-8119\(09\)70884-5](https://doi.org/10.1016/S1053-8119(09)70884-5)
- Fornito, A., Zalesky, A., Breakspear, M., 2013. Graph analysis of the human connectome: Promise, progress, and pitfalls. *NeuroImage, Mapping the Connectome* 80, 426–444. <https://doi.org/10.1016/j.neuroimage.2013.04.087>
- Fornito, A., Zalesky, A., Bullmore, E., 2016. *Fundamentals of Brain Network Analysis*. Academic Press.
- Fornito, A., Zalesky, A., Bullmore, E.T., 2010. Network Scaling Effects in Graph Analytic Studies of Human Resting-State fMRI Data. *Front Syst Neurosci* 4. <https://doi.org/10.3389/fnsys.2010.00022>
- Fortunato, S., 2010. Community detection in graphs. *Physics Reports* 486, 75–174. <https://doi.org/10.1016/j.physrep.2009.11.002>
- Fox, M.D., Snyder, A.Z., Vincent, J.L., Corbetta, M., Essen, D.C.V., Raichle, M.E., 2005. The human brain is intrinsically organized into dynamic, anticorrelated functional networks. *PNAS* 102, 9673–9678. <https://doi.org/10.1073/pnas.0504136102>
- Fox, P.T., Friston, K.J., 2012. Distributed processing; distributed functions? *NeuroImage, NEUROIMAGING: THEN, NOW AND THE FUTURE* 61, 407–426. <https://doi.org/10.1016/j.neuroimage.2011.12.051>
- Friston, K.J., 2011. Functional and Effective Connectivity: A Review. *Brain Connectivity* 1, 13–36. <https://doi.org/10.1089/brain.2011.0008>
- Friston, K.J., 1994. Functional and effective connectivity in neuroimaging: A synthesis. *Human Brain Mapping* 2, 56–78. <https://doi.org/10.1002/hbm.460020107>
- Fukushima, M., Betzel, R.F., He, Y., van den Heuvel, M.P., Zuo, X.-N., Sporns, O., 2018. Structure–function relationships during segregated and integrated network states of human brain functional connectivity. *Brain Struct Funct* 223, 1091–1106. <https://doi.org/10.1007/s00429-017-1539-3>
- Garyfallidis, E., Brett, M., Amirbekian, B., Rokem, A., Van Der Walt, S., Descoteaux, M., Nimmo-Smith, I., 2014. Dipy, a library for the analysis of diffusion MRI data. *Front. Neuroinform.* 8. <https://doi.org/10.3389/fninf.2014.00008>
- Gerraty, R.T., Davidow, J.Y., Foerde, K., Galvan, A., Bassett, D.S., Shohamy, D., 2018. Dynamic Flexibility in Striatal-Cortical Circuits Supports Reinforcement Learning. *J. Neurosci.* 38, 2442–2453. <https://doi.org/10.1523/JNEUROSCI.2084-17.2018>
- Girvan, M., Newman, M.E.J., 2002. Community structure in social and biological networks. *Proc Natl Acad Sci U S A* 99, 7821–7826. <https://doi.org/10.1073/pnas.122653799>
- Godwin, D., Barry, R.L., Marois, R., 2015. Breakdown of the brain’s functional network modularity with awareness. *PNAS* 112, 3799–3804. <https://doi.org/10.1073/pnas.1414466112>

- Gong, G., Rosa-Neto, P., Carbonell, F., Chen, Z.J., He, Y., Evans, A.C., 2009. Age- and Gender-Related Differences in the Cortical Anatomical Network. *J. Neurosci.* 29, 15684–15693. <https://doi.org/10.1523/JNEUROSCI.2308-09.2009>
- Goñi, J., Heuvel, M.P. van den, Avena-Koenigsberger, A., Mendizabal, N.V. de, Betzel, R.F., Griffa, A., Hagmann, P., Corominas-Murtra, B., Thiran, J.-P., Sporns, O., 2014a. Resting-brain functional connectivity predicted by analytic measures of network communication. *PNAS* 111, 833–838. <https://doi.org/10.1073/pnas.1315529111>
- Goñi, J., Heuvel, M.P. van den, Avena-Koenigsberger, A., Mendizabal, N.V. de, Betzel, R.F., Griffa, A., Hagmann, P., Corominas-Murtra, B., Thiran, J.-P., Sporns, O., 2014b. Resting-brain functional connectivity predicted by analytic measures of network communication. *PNAS* 111, 833–838. <https://doi.org/10.1073/pnas.1315529111>
- Good, B.H., de Montjoye, Y.-A., Clauset, A., 2010. Performance of modularity maximization in practical contexts. *Phys. Rev. E* 81, 046106. <https://doi.org/10.1103/PhysRevE.81.046106>
- Gordon, E.M., Laumann, T.O., Adeyemo, B., Huckins, J.F., Kelley, W.M., Petersen, S.E., 2016. Generation and Evaluation of a Cortical Area Parcellation from Resting-State Correlations. *Cereb Cortex* 26, 288–303. <https://doi.org/10.1093/cercor/bhu239>
- Gordon, E.M., Laumann, T.O., Gilmore, A.W., Newbold, D.J., Greene, D.J., Berg, J.J., Ortega, M., Hoyt-Drazen, C., Gratton, C., Sun, H., Hampton, J.M., Coalson, R.S., Nguyen, A.L., McDermott, K.B., Shimony, J.S., Snyder, A.Z., Schlaggar, B.L., Petersen, S.E., Nelson, S.M., Dosenbach, N.U.F., 2017. Precision Functional Mapping of Individual Human Brains. *Neuron* 95, 791-807.e7. <https://doi.org/10.1016/j.neuron.2017.07.011>
- Gorgolewski, K., Burns, C.D., Madison, C., Clark, D., Halchenko, Y.O., Waskom, M.L., Ghosh, S.S., 2011. Nipype: A Flexible, Lightweight and Extensible Neuroimaging Data Processing Framework in Python. *Front. Neuroinform.* 5. <https://doi.org/10.3389/fninf.2011.00013>
- Granell, C., Darst, R.K., Arenas, A., Fortunato, S., Gómez, S., 2015. Benchmark model to assess community structure in evolving networks. *Phys. Rev. E* 92, 012805. <https://doi.org/10.1103/PhysRevE.92.012805>
- Granger, C.W.J., 1969. Investigating Causal Relations by Econometric Models and Cross-spectral Methods. *Econometrica* 37, 424–438. <https://doi.org/10.2307/1912791>
- Greve, D.N., Fischl, B., 2009. Accurate and robust brain image alignment using boundary-based registration. *NeuroImage* 48, 63–72. <https://doi.org/10.1016/j.neuroimage.2009.06.060>
- Guimerà, R., Amaral, L.A.N., 2005. Functional cartography of complex metabolic networks. *Nature* 433, 895. <https://doi.org/10.1038/nature03288>
- Hagmann, P., Cammoun, L., Gigandet, X., Meuli, R., Honey, C.J., Wedeen, V.J., Sporns, O., 2008. Mapping the Structural Core of Human Cerebral Cortex. *PLOS Biology* 6, e159. <https://doi.org/10.1371/journal.pbio.0060159>
- Hagmann, P., Kurant, M., Gigandet, X., Thiran, P., Wedeen, V.J., Meuli, R., Thiran, J.-P., 2007. Mapping Human Whole-Brain Structural Networks with Diffusion MRI. *PLOS ONE* 2, e597. <https://doi.org/10.1371/journal.pone.0000597>

- Hagmann, P., Sporns, O., Madan, N., Cammoun, L., Pienaar, R., Wedeen, V.J., Meuli, R., Thiran, J.-P., Grant, P.E., 2010. White matter maturation reshapes structural connectivity in the late developing human brain. *PNAS* 107, 19067–19072. <https://doi.org/10.1073/pnas.1009073107>
- He, B., Astolfi, L., Valdés-Sosa, P.A., Marinazzo, D., Palva, S.O., Bénar, C., Michel, C.M., Koenig, T., 2019. Electrophysiological Brain Connectivity: Theory and Implementation. *IEEE Transactions on Biomedical Engineering* 66, 2115–2137. <https://doi.org/10.1109/TBME.2019.2913928>
- He, Y., Lim, S., Fortunato, S., Sporns, O., Zhang, L., Qiu, J., Xie, P., Zuo, X.-N., 2018. Reconfiguration of Cortical Networks in MDD Uncovered by Multiscale Community Detection with fMRI. *Cereb Cortex* 28, 1383–1395. <https://doi.org/10.1093/cercor/bhx335>
- Heuvel, M.P. van den, Sporns, O., 2013. An Anatomical Substrate for Integration among Functional Networks in Human Cortex. *J. Neurosci.* 33, 14489–14500. <https://doi.org/10.1523/JNEUROSCI.2128-13.2013>
- Heuvel, M.P. van den, Sporns, O., 2011. Rich-Club Organization of the Human Connectome. *J. Neurosci.* 31, 15775–15786. <https://doi.org/10.1523/JNEUROSCI.3539-11.2011>
- Honey, C.J., Kötter, R., Breakspear, M., Sporns, O., 2007. Network structure of cerebral cortex shapes functional connectivity on multiple time scales. *PNAS* 104, 10240–10245. <https://doi.org/10.1073/pnas.0701519104>
- Honey, C.J., Thivierge, J.-P., Sporns, O., 2010. Can structure predict function in the human brain? *NeuroImage, Computational Models of the Brain* 52, 766–776. <https://doi.org/10.1016/j.neuroimage.2010.01.071>
- Huang, H., Shu, N., Mishra, V., Jeon, T., Chalak, L., Wang, Z.J., Rollins, N., Gong, G., Cheng, H., Peng, Y., Dong, Q., He, Y., 2015. Development of Human Brain Structural Networks Through Infancy and Childhood. *Cereb Cortex* 25, 1389–1404. <https://doi.org/10.1093/cercor/bht335>
- Hutchison, R.M., Womelsdorf, T., Allen, E.A., Bandettini, P.A., Calhoun, V.D., Corbetta, M., Della Penna, S., Duyn, J.H., Glover, G.H., Gonzalez-Castillo, J., Handwerker, D.A., Keilholz, S., Kiviniemi, V., Leopold, D.A., de Pasquale, F., Sporns, O., Walter, M., Chang, C., 2013. Dynamic functional connectivity: Promise, issues, and interpretations. *NeuroImage, Mapping the Connectome* 80, 360–378. <https://doi.org/10.1016/j.neuroimage.2013.05.079>
- Imperati, D., Colcombe, S., Kelly, C., Martino, A.D., Zhou, J., Castellanos, F.X., Milham, M.P., 2011. Differential Development of Human Brain White Matter Tracts. *PLOS ONE* 6, e23437. <https://doi.org/10.1371/journal.pone.0023437>
- Jenkinson, M., Bannister, P., Brady, M., Smith, S., 2002. Improved Optimization for the Robust and Accurate Linear Registration and Motion Correction of Brain Images. *NeuroImage* 17, 825–841. <https://doi.org/10.1006/nimg.2002.1132>
- Jirsa, V.K., McIntosh, A.R. (Eds.), 2007. *Handbook of Brain Connectivity, Understanding Complex Systems*. Springer-Verlag, Berlin Heidelberg.
- Jutla, I.S., Jeub, L.G.S., Mucha, P.J., n.d. A generalized Louvain method for community detection implemented in Matlab 2.

- Kaminski, M.J., Blinowska, K.J., 1991. A new method of the description of the information flow in the brain structures. *Biol. Cybern.* 65, 203–210. <https://doi.org/10.1007/BF00198091>
- Karbowski, K., 1990. Sixty Years of Clinical Electroencephalography. *ENE* 30, 170–175. <https://doi.org/10.1159/000117338>
- Kelly, C., Biswal, B.B., Craddock, R.C., Castellanos, F.X., Milham, M.P., 2012. Characterizing variation in the functional connectome: promise and pitfalls. *Trends in Cognitive Sciences* 16, 181–188. <https://doi.org/10.1016/j.tics.2012.02.001>
- Khambhati, A.N., Sizemore, A.E., Betzel, R.F., Bassett, D.S., 2018. Modeling and interpreting mesoscale network dynamics. *NeuroImage, Brain Connectivity Dynamics* 180, 337–349. <https://doi.org/10.1016/j.neuroimage.2017.06.029>
- Kim, M.-S., Han, J., 2009. A particle-and-density based evolutionary clustering method for dynamic networks. *Proceedings of the VLDB Endowment* 2, 622–633. <https://doi.org/10.14778/1687627.1687698>
- Kivelä, M., Arenas, A., Barthelemy, M., Gleeson, J.P., Moreno, Y., Porter, M.A., 2014. Multilayer networks. *J Complex Netw* 2, 203–271. <https://doi.org/10.1093/comnet/cnu016>
- Klein, A., Ghosh, S.S., Bao, F.S., Giard, J., Häme, Y., Stavsky, E., Lee, N., Rossa, B., Reuter, M., Neto, E.C., Keshavan, A., 2017. Mindboggling morphometry of human brains. *PLOS Computational Biology* 13, e1005350. <https://doi.org/10.1371/journal.pcbi.1005350>
- Klimesch, W., 1999. EEG alpha and theta oscillations reflect cognitive and memory performance: a review and analysis. *Brain Research Reviews* 29, 169–195. [https://doi.org/10.1016/S0165-0173\(98\)00056-3](https://doi.org/10.1016/S0165-0173(98)00056-3)
- Lancichinetti, A., Fortunato, S., 2012. Consensus clustering in complex networks. *Scientific Reports* 2, 336. <https://doi.org/10.1038/srep00336>
- Lancichinetti, A., Fortunato, S., 2009. Community detection algorithms: A comparative analysis. *Phys. Rev. E* 80, 056117. <https://doi.org/10.1103/PhysRevE.80.056117>
- Laumann, T.O., Gordon, E.M., Adeyemo, B., Snyder, A.Z., Joo, S.J., Chen, M.-Y., Gilmore, A.W., McDermott, K.B., Nelson, S.M., Dosenbach, N.U.F., Schlaggar, B.L., Mumford, J.A., Poldrack, R.A., Petersen, S.E., 2015. Functional System and Areal Organization of a Highly Sampled Individual Human Brain. *Neuron* 87, 657–670. <https://doi.org/10.1016/j.neuron.2015.06.037>
- Lebel, C., Gee, M., Camicioli, R., Wieler, M., Martin, W., Beaulieu, C., 2012. Diffusion tensor imaging of white matter tract evolution over the lifespan. *NeuroImage* 60, 340–352. <https://doi.org/10.1016/j.neuroimage.2011.11.094>
- Leicht, E.A., Newman, M.E.J., 2008. Community Structure in Directed Networks. *Phys. Rev. Lett.* 100, 118703. <https://doi.org/10.1103/PhysRevLett.100.118703>
- Lim, S., Han, C.E., Uhlhaas, P.J., Kaiser, M., 2015. Preferential Detachment During Human Brain Development: Age- and Sex-Specific Structural Connectivity in Diffusion Tensor Imaging (DTI) Data. *Cereb Cortex* 25, 1477–1489. <https://doi.org/10.1093/cercor/bht333>

- Lin, Y.-R., Chi, Y., Zhu, S., Sundaram, H., Tseng, B.L., 2009. Analyzing Communities and Their Evolutions in Dynamic Social Networks. *ACM Trans. Knowl. Discov. Data* 3, 8:1–8:31. <https://doi.org/10.1145/1514888.1514891>
- Lin, Y.-R., Chi, Y., Zhu, S., Sundaram, H., Tseng, B.L., 2008. Facetnet: a framework for analyzing communities and their evolutions in dynamic networks, in: *Proceeding of the 17th International Conference on World Wide Web - WWW '08*. Presented at the Proceeding of the 17th international conference, ACM Press, Beijing, China, p. 685. <https://doi.org/10.1145/1367497.1367590>
- Lindquist, M.A., Geuter, S., Wager, T.D., Caffo, B.S., 2019. Modular preprocessing pipelines can reintroduce artifacts into fMRI data. *Human Brain Mapping* 40, 2358–2376. <https://doi.org/10.1002/hbm.24528>
- Logothetis, N.K., Pauls, J., Augath, M., Trinath, T., Oeltermann, A., 2001. Neurophysiological investigation of the basis of the fMRI signal. *Nature* 412, 150–157. <https://doi.org/10.1038/35084005>
- Lohse, C., Bassett, D.S., Lim, K.O., Carlson, J.M., 2014. Resolving Anatomical and Functional Structure in Human Brain Organization: Identifying Mesoscale Organization in Weighted Network Representations. *PLOS Computational Biology* 10, e1003712. <https://doi.org/10.1371/journal.pcbi.1003712>
- McIntosh, A.R., 2000. Towards a network theory of cognition. *Neural Networks* 13, 861–870. [https://doi.org/10.1016/S0893-6080\(00\)00059-9](https://doi.org/10.1016/S0893-6080(00)00059-9)
- Mcintosh, A.R., 1999. Mapping Cognition to the Brain Through Neural Interactions. *Memory* 7, 523–548. <https://doi.org/10.1080/096582199387733>
- McIntosh, A.R., Mišić, B., 2013. Multivariate Statistical Analyses for Neuroimaging Data. *Annual Review of Psychology* 64, 499–525. <https://doi.org/10.1146/annurev-psych-113011-143804>
- Medaglia, J.D., Huang, W., Karuza, E.A., Kelkar, A., Thompson-Schill, S.L., Ribeiro, A., Bassett, D.S., 2018. Functional alignment with anatomical networks is associated with cognitive flexibility. *Nat Hum Behav* 2, 156–164. <https://doi.org/10.1038/s41562-017-0260-9>
- Meilă, M., 2007. Comparing clusterings—an information based distance. *Journal of Multivariate Analysis* 98, 873–895. <https://doi.org/10.1016/j.jmva.2006.11.013>
- Messé, A., Rudrauf, D., Giron, A., Marrelec, G., 2015. Predicting functional connectivity from structural connectivity via computational models using MRI: An extensive comparison study. *NeuroImage* 111, 65–75. <https://doi.org/10.1016/j.neuroimage.2015.02.001>
- Meunier, D., Lambiotte, R., Bullmore, E.T., 2010. Modular and Hierarchically Modular Organization of Brain Networks. *Front. Neurosci.* 4. <https://doi.org/10.3389/fnins.2010.00200>
- Meunier, D., Lambiotte, R., Fornito, A., Ersche, K., Bullmore, E.T., 2009. Hierarchical modularity in human brain functional networks. *Front. Neuroinform.* 3. <https://doi.org/10.3389/neuro.11.037.2009>
- Micheloyannis, S., Pachou, E., Stam, C.J., Vourkas, M., Erimaki, S., Tsirka, V., 2006. Using graph theoretical analysis of multi channel EEG to evaluate the neural efficiency

- hypothesis. *Neuroscience Letters* 402, 273–277. <https://doi.org/10.1016/j.neulet.2006.04.006>
- Mišić, B., Betzel, R.F., de Reus, M.A., van den Heuvel, M.P., Berman, M.G., McIntosh, A.R., Sporns, O., 2016. Network-Level Structure-Function Relationships in Human Neocortex. *Cereb Cortex* 26, 3285–3296. <https://doi.org/10.1093/cercor/bhw089>
- Mišić, B., Betzel, R.F., Nematzadeh, A., Goñi, J., Griffa, A., Hagmann, P., Flammini, A., Ahn, Y.-Y., Sporns, O., 2015. Cooperative and Competitive Spreading Dynamics on the Human Connectome. *Neuron* 86, 1518–1529. <https://doi.org/10.1016/j.neuron.2015.05.035>
- Mišić, B., Sporns, O., 2016. From regions to connections and networks: new bridges between brain and behavior. *Current Opinion in Neurobiology, Systems neuroscience* 40, 1–7. <https://doi.org/10.1016/j.conb.2016.05.003>
- Mori, S., Zhang, J., 2006. Principles of Diffusion Tensor Imaging and Its Applications to Basic Neuroscience Research. *Neuron* 51, 527–539. <https://doi.org/10.1016/j.neuron.2006.08.012>
- Mucha, P.J., Richardson, T., Macon, K., Porter, M.A., Onnela, J.-P., 2010. Community Structure in Time-Dependent, Multiscale, and Multiplex Networks. *Science* 328, 876–878. <https://doi.org/10.1126/science.1184819>
- Muldoon, S.F., Bassett, D.S., 2016. Network and Multilayer Network Approaches to Understanding Human Brain Dynamics. <https://doi.org/10.1086/687857>
- Newman, M., 2010. *Networks: An Introduction*. Oxford University Press.
- Newman, M., 2003. The Structure and Function of Complex Networks. *SIAM Rev.* 45, 167–256. <https://doi.org/10.1137/S003614450342480>
- Newman, M.E.J., 2012a. Communities, modules and large-scale structure in networks. *Nature Physics* 8, 25–31. <https://doi.org/10.1038/nphys2162>
- Newman, M.E.J., 2012b. Communities, modules and large-scale structure in networks. *Nature Physics* 8, 25–31. <https://doi.org/10.1038/nphys2162>
- Newman, M.E.J., 2006. Modularity and community structure in networks. *Proc Natl Acad Sci U S A* 103, 8577–8582. <https://doi.org/10.1073/pnas.0601602103>
- Newman, M.E.J., Girvan, M., 2004. Finding and evaluating community structure in networks. *Physical Review E* 69. <https://doi.org/10.1103/PhysRevE.69.026113>
- Niedermeyer, E., 1997. Alpha rhythms as physiological and abnormal phenomena. *International Journal of Psychophysiology* 26, 31–49. [https://doi.org/10.1016/S0167-8760\(97\)00754-X](https://doi.org/10.1016/S0167-8760(97)00754-X)
- Nolte, G., Mueller, K.R., 2010. Localizing and Estimating Causal Relations of Interacting Brain Rhythms. *Front. Hum. Neurosci.* 4. <https://doi.org/10.3389/fnhum.2010.00209>
- Nooner, K.B., Colcombe, S., Tobe, R., Mennes, M., Benedict, M., Moreno, A., Panek, L., Brown, S., Zavitz, S., Li, Q., Sikka, S., Gutman, D., Bangaru, S., Schlachter, R.T., Kamiel, S., Anwar, A., Hinz, C., Kaplan, M., Rachlin, A., Adelsberg, S., Cheung, B., Khanuja, R., Yan, C., Craddock, C., Calhoun, V., Courtney, W., King, M., Wood, D., Cox, C., Kelly, C., DiMartino, A., Petkova, E., Reiss, P., Duan, N., Thompsen, D., Biswal, B., Coffey, B., Hoptman, M., Javitt, D.C., Pomara, N., Sidtis, J., Koplewicz, H., Castellanos, F.X., Leventhal, B., Milham, M., 2012. The NKI-Rockland Sample: A

- Model for Accelerating the Pace of Discovery Science in Psychiatry. *Front. Neurosci.* 6. <https://doi.org/10.3389/fnins.2012.00152>
- Park, H.-J., Friston, K., 2013. Structural and Functional Brain Networks: From Connections to Cognition. *Science* 342, 1238411. <https://doi.org/10.1126/science.1238411>
- Parkes, L., Fulcher, B., Yücel, M., Fornito, A., 2018. An evaluation of the efficacy, reliability, and sensitivity of motion correction strategies for resting-state functional MRI. *NeuroImage* 171, 415–436. <https://doi.org/10.1016/j.neuroimage.2017.12.073>
- Persson, J., Nyberg, L., Lind, J., Larsson, A., Nilsson, L.-G., Ingvar, M., Buckner, R.L., 2006. Structure–Function Correlates of Cognitive Decline in Aging. *Cereb Cortex* 16, 907–915. <https://doi.org/10.1093/cercor/bhj036>
- Petti, M., Toppi, J., Babiloni, F., Cincotti, F., Mattia, D., Astolfi, L., 2016. EEG Resting-State Brain Topological Reorganization as a Function of Age [WWW Document]. *Computational Intelligence and Neuroscience*. <https://doi.org/10.1155/2016/6243694>
- Pichiorri, F., Petti, M., Caschera, S., Astolfi, L., Cincotti, F., Mattia, D., 2018. An EEG index of sensorimotor interhemispheric coupling after unilateral stroke: clinical and neurophysiological study. *European Journal of Neuroscience* 47, 158–163. <https://doi.org/10.1111/ejn.13797>
- Porter, M.A., Onnela, J.-P., Mucha, P.J., 2009. *Communities in Networks* (SSRN Scholarly Paper No. ID 1357925). Social Science Research Network, Rochester, NY.
- Power, J.D., Cohen, A.L., Nelson, S.M., Wig, G.S., Barnes, K.A., Church, J.A., Vogel, A.C., Laumann, T.O., Miezin, F.M., Schlaggar, B.L., Petersen, S.E., 2011. Functional Network Organization of the Human Brain. *Neuron* 72, 665–678. <https://doi.org/10.1016/j.neuron.2011.09.006>
- Puxeddu, M.G., Petti, M., Mattia, D., Astolfi, L., 2019. The Optimal Setting for Multilayer Modularity Optimization in Multilayer Brain Networks*, in: 2019 41st Annual International Conference of the IEEE Engineering in Medicine and Biology Society (EMBC). Presented at the 2019 41st Annual International Conference of the IEEE Engineering in Medicine and Biology Society (EMBC), pp. 624–627. <https://doi.org/10.1109/EMBC.2019.8856674>
- Puxeddu, M.G., Petti, M., Pichiorri, F., Cincotti, F., Mattia, D., Astolfi, L., 2017. Community detection: Comparison among clustering algorithms and application to EEG-based brain networks, in: 2017 39th Annual International Conference of the IEEE Engineering in Medicine and Biology Society (EMBC). Presented at the 2017 39th Annual International Conference of the IEEE Engineering in Medicine and Biology Society (EMBC), pp. 3965–3968. <https://doi.org/10.1109/EMBC.2017.8037724>
- Raz, N., Ghisletta, P., Rodrigue, K.M., Kennedy, K.M., Lindenberger, U., 2010. Trajectories of brain aging in middle-aged and older adults: Regional and individual differences. *NeuroImage* 51, 501–511. <https://doi.org/10.1016/j.neuroimage.2010.03.020>
- Riitta Hari, M.D., Aina Puce, P., n.d. *MEG-EEG Primer*. Oxford University Press.
- Rosenthal, G., Sporns, O., Avidan, G., 2017. Stimulus Dependent Dynamic Reorganization of the Human Face Processing Network. *Cereb Cortex* 27, 4823–4834. <https://doi.org/10.1093/cercor/bhw279>

- Rubinov, M., Sporns, O., 2010. Complex network measures of brain connectivity: Uses and interpretations. *NeuroImage, Computational Models of the Brain* 52, 1059–1069. <https://doi.org/10.1016/j.neuroimage.2009.10.003>
- Sambataro, F., Murty, V.P., Callicott, J.H., Tan, H.-Y., Das, S., Weinberger, D.R., Mattay, V.S., 2010. Age-related alterations in default mode network: Impact on working memory performance. *Neurobiology of Aging* 31, 839–852. <https://doi.org/10.1016/j.neurobiolaging.2008.05.022>
- Satterthwaite, T.D., Elliott, M.A., Gerraty, R.T., Ruparel, K., Loughhead, J., Calkins, M.E., Eickhoff, S.B., Hakonarson, H., Gur, R.C., Gur, R.E., Wolf, D.H., 2013. An improved framework for confound regression and filtering for control of motion artifact in the preprocessing of resting-state functional connectivity data. *NeuroImage* 64, 240–256. <https://doi.org/10.1016/j.neuroimage.2012.08.052>
- Schaefer, A., Kong, R., Gordon, E.M., Laumann, T.O., Zuo, X.-N., Holmes, A.J., Eickhoff, S.B., Yeo, B.T.T., 2018. Local-Global Parcellation of the Human Cerebral Cortex from Intrinsic Functional Connectivity MRI. *Cereb Cortex* 28, 3095–3114. <https://doi.org/10.1093/cercor/bhx179>
- Schaub, M.T., Delvenne, J.-C., Rosvall, M., Lambiotte, R., 2017. The many facets of community detection in complex networks. *Appl Netw Sci* 2, 1–13. <https://doi.org/10.1007/s41109-017-0023-6>
- Schmidt, C., Piper, D., Pester, B., Mierau, A., Witte, H., 2018. Tracking the Reorganization of Module Structure in Time-Varying Weighted Brain Functional Connectivity Networks. *International Journal of Neural Systems* 28, 1750051. <https://doi.org/10.1142/S0129065717500514>
- Shine, J.M., Bissett, P.G., Bell, P.T., Koyejo, O., Balsters, J.H., Gorgolewski, K.J., Moodie, C.A., Poldrack, R.A., 2016. The Dynamics of Functional Brain Networks: Integrated Network States during Cognitive Task Performance. *Neuron* 92, 544–554. <https://doi.org/10.1016/j.neuron.2016.09.018>
- Silva, J.C., Bennett, L., Papageorgiou, L.G., Tsoka, S., 2016. A mathematical programming approach for sequential clustering of dynamic networks. *Eur. Phys. J. B* 89, 39. <https://doi.org/10.1140/epjb/e2015-60656-5>
- Sotiropoulos, S.N., Zalesky, A., 2019. Building connectomes using diffusion MRI: why, how and but. *NMR in Biomedicine* 32, e3752. <https://doi.org/10.1002/nbm.3752>
- Sporns, O., 2014. Contributions and challenges for network models in cognitive neuroscience. *Nature Neuroscience* 17, 652–660. <https://doi.org/10.1038/nn.3690>
- Sporns, O., 2013. Network attributes for segregation and integration in the human brain. *Current Opinion in Neurobiology, Macrocircuits* 23, 162–171. <https://doi.org/10.1016/j.conb.2012.11.015>
- Sporns, O., 2011. The human connectome: a complex network. *Ann. N. Y. Acad. Sci.* 1224, 109–125. <https://doi.org/10.1111/j.1749-6632.2010.05888.x>
- Sporns, O., Betzel, R.F., 2016. Modular Brain Networks. *Annu Rev Psychol* 67, 613–640. <https://doi.org/10.1146/annurev-psych-122414-033634>
- Stam, C.J., van Straaten, E.C.W., Van Dellen, E., Tewarie, P., Gong, G., Hillebrand, A., Meier, J., Van Mieghem, P., 2016. The relation between structural and functional connectivity patterns in complex brain networks. *International Journal of*

- Psychophysiology, Research on Brain Oscillations and Connectivity in A New Take-Off State 103, 149–160. <https://doi.org/10.1016/j.ijpsycho.2015.02.011>
- Takahashi, D.Y., Baccal, L.A., Sameshima, K., 2007. Connectivity Inference between Neural Structures via Partial Directed Coherence. *Journal of Applied Statistics* 34, 1259–1273. <https://doi.org/10.1080/02664760701593065>
- Thomas Yeo, B.T., Krienen, F.M., Sepulcre, J., Sabuncu, M.R., Lashkari, D., Hollinshead, M., Roffman, J.L., Smoller, J.W., Zöllei, L., Polimeni, J.R., Fischl, B., Liu, H., Buckner, R.L., 2011. The organization of the human cerebral cortex estimated by intrinsic functional connectivity. *J Neurophysiol* 106, 1125–1165. <https://doi.org/10.1152/jn.00338.2011>
- Tononi, G., Sporns, O., Edelman, G.M., 1994. A measure for brain complexity: relating functional segregation and integration in the nervous system. *PNAS* 91, 5033–5037. <https://doi.org/10.1073/pnas.91.11.5033>
- Toppi, J., Mattia, D., Risetti, M., Formisano, R., Babiloni, F., Astolfi, L., 2016. Testing the Significance of Connectivity Networks: Comparison of Different Assessing Procedures. *IEEE Transactions on Biomedical Engineering* 63, 2461–2473. <https://doi.org/10.1109/TBME.2016.2621668>
- Tustison, N.J., Avants, B.B., Cook, P.A., Zheng, Y., Egan, A., Yushkevich, P.A., Gee, J.C., 2010. N4ITK: Improved N3 Bias Correction. *IEEE Transactions on Medical Imaging* 29, 1310–1320. <https://doi.org/10.1109/TMI.2010.2046908>
- Vaiana, M., Muldoon, S.F., 2018. Multilayer Brain Networks. *J Nonlinear Sci.* <https://doi.org/10.1007/s00332-017-9436-8>
- Van Essen, D.C., Smith, S.M., Barch, D.M., Behrens, T.E.J., Yacoub, E., Ugurbil, K., 2013. The WU-Minn Human Connectome Project: An overview. *NeuroImage, Mapping the Connectome* 80, 62–79. <https://doi.org/10.1016/j.neuroimage.2013.05.041>
- Vatansever, D., Menon, D.K., Manktelow, A.E., Sahakian, B.J., Stamatakis, E.A., 2015. Default Mode Dynamics for Global Functional Integration. *J. Neurosci.* 35, 15254–15262. <https://doi.org/10.1523/JNEUROSCI.2135-15.2015>
- Vázquez-Rodríguez, B., Suárez, L.E., Markello, R.D., Shafiei, G., Paquola, C., Hagmann, P., Heuvel, M.P. van den, Bernhardt, B.C., Spreng, R.N., Misisic, B., 2019. Gradients of structure–function tethering across neocortex. *PNAS* 116, 21219–21227. <https://doi.org/10.1073/pnas.1903403116>
- Westlye, L.T., Walhovd, K.B., Dale, A.M., Bjørnerud, A., Due-Tønnessen, P., Engvig, A., Grydeland, H., Tamnes, C.K., Østby, Y., Fjell, A.M., 2010. Life-Span Changes of the Human Brain White Matter: Diffusion Tensor Imaging (DTI) and Volumetry. *Cereb Cortex* 20, 2055–2068. <https://doi.org/10.1093/cercor/bhp280>
- Wig, G.S., 2017. Segregated Systems of Human Brain Networks. *Trends in Cognitive Sciences* 21, 981–996. <https://doi.org/10.1016/j.tics.2017.09.006>
- Wijk, B.C.M. van, Stam, C.J., Daffertshofer, A., 2010. Comparing Brain Networks of Different Size and Connectivity Density Using Graph Theory. *PLOS ONE* 5, e13701. <https://doi.org/10.1371/journal.pone.0013701>
- Wu, K., Taki, Y., Sato, K., Kinomura, S., Goto, R., Okada, K., Kawashima, R., He, Y., Evans, A.C., Fukuda, H., 2012. Age-related changes in topological organization of

- structural brain networks in healthy individuals. *Human Brain Mapping* 33, 552–568. <https://doi.org/10.1002/hbm.21232>
- Yeatman, J.D., Wandell, B.A., Mezer, A.A., 2014. Lifespan maturation and degeneration of human brain white matter. *Nature Communications* 5, 4932. <https://doi.org/10.1038/ncomms5932>
- Zhang, J., Cheng, W., Liu, Z., Zhang, K., Lei, X., Yao, Y., Becker, B., Liu, Y., Kendrick, K.M., Lu, G., Feng, J., 2016. Neural, electrophysiological and anatomical basis of brain-network variability and its characteristic changes in mental disorders. *Brain* 139, 2307–2321. <https://doi.org/10.1093/brain/aww143>
- Zhang, Y., Brady, M., Smith, S., 2001. Segmentation of brain MR images through a hidden Markov random field model and the expectation-maximization algorithm. *IEEE Transactions on Medical Imaging* 20, 45–57. <https://doi.org/10.1109/42.906424>
- Zhou, J., Gennatas, E.D., Kramer, J.H., Miller, B.L., Seeley, W.W., 2012. Predicting Regional Neurodegeneration from the Healthy Brain Functional Connectome. *Neuron* 73, 1216–1227. <https://doi.org/10.1016/j.neuron.2012.03.004>
- Zuo, X.-N., He, Y., Betzel, R.F., Colcombe, S., Sporns, O., Milham, M.P., 2017. Human Connectomics across the Life Span. *Trends in Cognitive Sciences* 21, 32–45. <https://doi.org/10.1016/j.tics.2016.10.005>

List of publications

International Journal Papers:

- I. A. Paffi, F. Apollonio, **M.G. Puxeddu**, M. Parazzini, G. D’Inzeo, P. Ravazzani and M. Liberti: “A numerical study to compare stimulations by intraoperative microelectrodes and chronic macroelectrodes in the DBS technique”, *BioMed Research International*, Aug. 2013.

Papers in International Conferences indexed in ISI Web of Science:

- I. **M.G. Puxeddu**, M. Petti, D. Mattia, L. Astolfi, “The optimal setting for multilayer modularity optimization in multilayer brain networks”, in 41st Annual International Conference of the IEEE EMBS, Berlin, Germany, July 23-27, 2019.
- II. **M.G. Puxeddu**, M. Petti, F. Pichiorri, F. Cincotti, D. Mattia, L. Astolfi: “Community detection: comparison between clustering algorithms and application to EEG-based brain networks”, in 39th Annual International Conference of the IEEE EMBS, Jeju Island, Korea, Jul 11-15, 2017. (Selected for oral presentation).
- III. A. Paffi, F. Apollonio, **M.G. Puxeddu**, M. Parazzini, G. D’Inzeo, P. Ravazzani, F. Camera, M. Liberti: “A dosimetric study comparing intra-operative microelectrode and chronic macroelectrode in the DBS technique”, in 6th International IEEE EMBS Conference on Neural Engineering, San Diego, CA, Nov 6-8, 2013, pp. 1206 – 1209.

Abstract in National and International Conferences not indexed in ISI:

- I. **M.G. Puxeddu**, J. Toppi, D. Mattia, L. Astolfi, “Reduction of latency jitter in ERP through visibility graphs and community detection”, in 41st Annual International Conference of the IEEE EMBS, Berlin, Germany, July 23-27, 2019.
- II. **M.G. Puxeddu**, J. Faskowitz, M. Petti, L. Astolfi, O. Sporns, “Modular structure of anatomical brain networks across the human lifespan”, Organization for Human Brain Mapping, Rome, June 9-13, 2019
- III. **M.G. Puxeddu**, M. Petti, F. Pichiorri, F. Cincotti, D. Mattia, L. Astolfi, “Analysis of multilayer clustering algorithms for the application to brain functional connectivity”, VI Congresso Nazionale del GNB, Milano, June 25-27, 2018.
- IV. **M.G. Puxeddu**, M. Petti, L. Astolfi, “Multilayer analysis for community detection in evolving brain networks”, Mediterranean School of Complex Networks, Salina, Italy, Sep 4 – 8, 2017. (Selected for oral presentation).
- V. A. Paffi, **M.G. Puxeddu**, F. Apollonio, M. Parazzini, G. D’Inzeo, P. Ravazzani, M. Liberti: “A numerical dosimetric study to clarify different stimulations by intra-operative microelectrodes and chronic macroelectrodes in the DBS technique”, BioEM2013, Thessaloniki, Greece, Jun 10-14, 2013.

Scientific Curriculum

Maria Grazia Puxeddu, Ph.D. candidate

PERSONAL INFORMATIONS

Date of birth 31 October 1990
Nationality Italian
Email mariagrazia.puxeddu@gmail.com (personal email)
mariagrazia.puxeddu@uniroma1.it (university email)
Work address Department of Computer, Control and Management Engineering “Antonio Ruberti”, University of Rome Sapienza, Via Ariosto 25, 00185, Rome, Italy

EDUCATION AND TRAINING

Date	October 2016 – date
Position held	PhD Student in Bioengineering (ING-INF/06) at the University of Rome La Sapienza, Department of Computer, Control and Management Engineering “Antonio Ruberti”
Date	October 2016 – date
Conference	Visiting student at laboratory of Neuroelectrical Imaging and BCI at IRCCS Fondazione Santa Lucia, Rome
Date	April 2018 – October 2018
Position held	Visitor scholar at Indiana University, Bloomington (USA), Department of Psychological and Brain Science
Date	September 4-8, 2017
Position held	IV Mediterranean School of Complex Networks, Salina (ME)
Date	December 2015 – July 2016
Position held	Internship at laboratory of Neuroelectrical Imaging and BCI at IRCCS Fondazione Santa Lucia, Rome
Date	A.A. 2013/14 – 2015/16
Title of qualification	Master’s degree in Biomedical engineering (ING-INF/06),
Grade	110/110 Cum Laude
Institution	University of Rome La Sapienza
Thesis title	“Algoritmi di clustering per lo studio di reti stazionarie e tempo-varianti: studio di simulazione ed applicazione alla connettività cerebrale”
Date	A.A. 2009/10 – 2012/13
Title of qualification	Bachelor’s Degree in Clinical Engineering (ING-INF/06)
Institution	University of Rome La Sapienza
Thesis title	“Studio dosimetrico per il posizionamento del microelettrodo intraoperatorio nella stimolazione cerebrale profonda”

RESEARCH ACTIVITY

Research activity broadly includes methodological development in the field of complex brain network analysis. Specifically, the focus is on the analysis of electroencephalographic (EEG) and magnetic resonance imaging (f-MRI) based brain networks. In particular:

- Analysis of multilayer brain networks through advanced techniques of graph theory;
- Multilayer graphs and community detection;
- Definition of new indicators of brain patterns related to motor and cognitive functions;
- Analysis of EEG and MRI data.

PARTICIPATION IN RESEARCH GROUPS

- National groups:
 - *Bioengineering and Bioinformatic Laboratory (BiBiLab)*, at the Department of Computer, Control and Management Engineering, University of Rome Sapienza. Responsible: Laura Astolfi.
 - *Neuroelectrical Imaging and BCI Laboratory (NeiLab)*, at IRCCS Fondazione Santa Lucia, Rome. Responsible: Donatella Mattia.
- International groups:
 - *Computational Cognitive Neuroscience Laboratory*, at Department of Psychological and Brain Sciences, Indiana University, Bloomington. Responsible: Olaf Sporns.
 - *Brain Networks and Behavior Lab (BNBL)*, at Department of Psychological and Brain Sciences, Indiana University, Bloomington. Responsible: Richard Betzel.

ACADEMIC ACTIVITY

- Teaching activity (seminar and tutorials) in:
 - “*Neuroscience*” (Biomedical Engineering, ING-INF/06, 9CFU), A.A. 2016/17, 2017/18, 2018/19, 2019/20
 - “*Models of biological systems*” (Biomedical Engineering, ING-INF/06, 9CFU), A.A. 2017/18, 2018/19
 - “*Methods for the analysis of biomedical signals*” (Biomedical Engineering, ING-INF/06, 12CFU), A.A. 2016/17, 2017/18
 - “*Modelling and simulation of biomolecular dynamical systems*” (Bioinformatics, ING-INF/06, 6CFU), A.A. 2018/19
 - “*Bioinformatics*” (Data Science, ING-INF/06, 6CFU), A.A. 2019/2020
- Co-supervision to 3 master’s degree thesis in Biomedical Engineering:
 - “*Analysis of multilayer clustering algorithms for the study of dynamic brain networks*”, Dissertation on January 2016
 - “*The use of advanced methods of graph theory for the study of the evolution of brain connectivity patterns after post-stroke rehabilitation*”, Dissertation on October 2019
 - “*Development and validation of algorithms based on multilayer graphs for the study of the intra- and inter-frequencies dependencies in brain connectivity*”, Dissertation on October 2019

AWARDS AND ACHIEVEMENTS

- Grant for the project *Avvio alla Ricerca* (AR1181643680C682) titled “*A multilayer network based analysis to infer dependencies among frequencies in EEG signals*”, (Principal Investigator), received from Sapienza University of Rome, 01 Oct 2018.
- Grant for the mobility project reserved for PhD students of the XXXI and XXXII cycles, titled “*MoRe-Net, Motor Recovery supported by hybrid Brain-Computer Interface and complex network theory*”, received from Sapienza University of Rome, 07 Dec 2017.

- III. Best Thesis Award “Vincenzo Tagliasco” received from the Italian National Bioengineering Group in the occasion of the “XXXVIII Scuola Nazionale del Gruppo di Bioingegneria”, Bressanone, Italy, 18 – 22 Sept 2017.
- IV. Grant for the project *Avvio alla Ricerca*, (AR11715C821E23FC) titled “*Multilayer approaches for the detection of stable and dynamic communities in EEG-based brain networks*” (principal investigator), received from Sapienza University of Rome, 17 July 2017
- V. Prize “Excellent graduate” for the academic year 2015/16, received from *Fondazione Roma Sapienza* and promoted by *NoiSapienza Associazione Alumni*, in the occasion of the V edition of “Giornata del Laureato”, Rome, Italy, 15 May 2017.

PARTICIPATION IN RESEARCH PROJECTS

- I. Principal Investigator for the project *Avvio alla Ricerca* (AR1181643680C682) titled “*A multilayer network based analysis to infer dependencies among frequencies in EEG signals*”, funded by Sapienza University of Rome, 01 Oct 2018.
- II. Participant in the project “*Sviluppo di algoritmi per l’analisi di potenziali evento-correlati in presenza di jitter*” (RP11816436CDA44C), (Principal Investigator: Laura Astolfi), funded by Sapienza University of Rome – Progetto di Ateneo 2018.
- III. Participant in the mobility project reserved for PhD students of the XXXI and XXXII cycles, titled “*MoRe-Net, Motor Recovery supported by hybrid Brain-Computer Interface and complex network theory*”, funded by Sapienza University of Rome, 07 Dec 2017.
- IV. Participant in the project “*EMBRACING: Estimating Multiple-Brain connectivity in Autism during Cooperative Interaction: anew tool for real-time hyperscanning*” (RM11715C82606455), (Principal Investigator: Laura Astolfi), funded by Sapienza University of Rome – Progetto di Ateneo 2017.
- V. Principal Investigator in the project *Avvio alla Ricerca*, (AR11715C821E23FC) titled “*Multilayer approaches for the detection of stable and dynamic communities in EEG-based brain networks*”, funded by Sapienza University of Rome, 17 July 2017.
- VI. Participant in the project “*MIME-BCI: Mindfulness Meditation training supported by Brain-Computer Interfaces*”, (Principal Investigator: Febo Cincotti), funded by Sapienza University of Rome – Progetti di Ateneo 2016.

PARTICIPATION TO CONFERENCES AND SCIENTIFIC MEETINGS

Date	July 23-27, 2019
Event	41 st Annual International Conference of the IEEE EMBS, Berlin, Germany
Date	June 9-13, 2019
Event	2019 OHBM Annual Meeting, Rome, Italy
Date	June 6-8, 2019
Event	OHBM Hackathon in Rome 2019, Rome, Italy
Date	May 2-4, 2018
Event	BrainHack Global, Indiana Univeristy, Bloomington, USA
Date	September 4-8, 2017
Event	IV Mediterranean School of Complex Networks, Salina (ME), Italy

EDITORIAL ACTIVITY

Reviewer for the international journals:

- Biomedical Signal Processing and Control, Elsevier
- Computer Methods and Programs in Biomedicine, Elsevier

Reviewer for conference papers of the the 41st Annual International Conference of the IEEE EMBS, Berlin, Germany.

PERSONAL SKILLS AND COMPETENCES

Mother tongue	ITALIAN
	ENGLISH
Reading	Excellent
Writing	Excellent
Speaking	Excellent
Certificate	FCE
Abroad Experience	- 6 months as visitor student in the laboratory led by Olaf Sporns (Bloomington, Indiana, USA) - Intensive course of 2-week general English, organized by MLA courses in Bristol (UK)
	FRENCH
Reading	Excellent
Writing	Good
Speaking	Good
Computer skills	Excellent knowledge of MATLAB ENVIRONMENT (daily use), good knowledge of PYTHON and R (occasional use, attendee of online tutorials and the course organized by LUG Sapienza). Competent with most programs of the MICROSOFT OFFICE SUITE .
Technical skills	Competent with EEG acquisition devices such as BrainAmp, gTech. Good knowledge of software for the analysis of brain signals, such as EEGLAB and BRAINVISION ANALYZER .

I hereby authorize you to use my personal details contained in this document (D. lgs. n.196/2003).

Rome, 31 Ottobre 2019

